Entanglement and Entropy Engineering of Atomic Two-Qubit Mixed States

Stephen Clark

A thesis
submitted in partial fulfilment
of the requirements for the degree
of
Master of Science
at the
University of Auckland

University of Auckland
2002

Acknowledgements

My greatest thanks go to my supervisor, Scott Parkins, who could not have been more helpful (and patient). In particular, I appreciate his willingness to spend time with his students even when busy with teaching duties or his own research.

It has been a pleasure to share an office with Stojan Rebić during the year I have spent writing this thesis. We have had many interesting discussions (he might prefer the term "interrogations") on many subjects, not necessarily restricted to physics. This thesis, and my general understanding of quantum optics, have benefitted greatly from the steady stream of information and ideas he has cheerfully provided.

Finally, I would like to thank my friends, family, and particularly my parents, for the encouragement they have given me during the past three years of my resumed higher education. Without their support this thesis would not exist.

Stephen Clark,
February, 2002.

Abstract

We propose and analyze a number of schemes to deterministically entangle pairs of atoms through their interaction with quantum-correlated reservoirs. These reservoirs are created using sources of squeezed light, such as the degenerate or non-degenerate parametric amplifier, or by means of quantum-reservoir engineering [1]. The atoms become entangled when the phase-sensitive correlations present in the reservoir transfer to the atoms [2].

In a succession of models, we consider pairs of atoms that are either in free space, or trapped in one or more high-finesse optical micro-cavities. For atoms in a cavity QED situation, a variety of possible atomic level schemes are investigated, in which coherent driving lasers and the quantized cavity mode are used to initiate Raman transitions between two meta-stable atomic ground states. In particular, we find a 4-level atomic configuration for an atom in a cavity, which, in the appropriate limits, is shown to interact with a single squeezed cavity mode in a manner that is entirely analogous to the interaction of a single atom in free space with a broadband squeezed vacuum.

For each system we find the reduced master equation for the atomic ground states and investigate the dynamics of this master equation using the entropy-entanglement plane. Under appropriate conditions, we find that the atoms may be modelled as a pair of two-level systems (qubits) for which the amplitude and phase coupling to the quantum reservoir are independently adjustable. Using local unitary transformations and appropriate manipulation of the amplitude and phase decay rates, we can then generate non-maximally entangled mixed states covering the full range of the Linear Entropy-Entanglement of Formation plane.

The most promising scheme we have developed uses quantum-reservoir engineering to entangle two 5-level atoms trapped in a single optical cavity. An effective squeezed reservoir is created without the need for non-classical sources of light. The deleterious effects of spontaneous emission from the excited atomic states during the Raman transition are investigated for this model. Even in the presence of spontaneous emission we can generate states covering a broad region of the Linear Entropy-Entanglement of Formation plane, including areas above the line corresponding to the Werner states.

Contents

List of Figures

Chapter 1

Introduction

In this introductory Chapter we explain the motivation behind attempts to entangle separated atoms. This is done by means of a general discussion about quantum information and entanglement, and of the recent drive to understand and manipulate them.

Contents

1.1 Quantum information

The historic paper presented by Deutsch in 1985 [3] is credited with awakening the scientific community to the unique possibilities offered by *quantum computing*. Deutsch showed that the inherent parallelism of quantum computation enables certain problems to be tackled efficiently by a quantum computer in a manner which classical computers can not hope to emulate.

Deutsch's ideas triggered an explosion of interest in the differences between quantum and classical information that continues unabated to the current day. Quantum algorithms have been developed that are of considerable commercial interest, particularly the polynomial-time factorization algorithm of Shor [4] and the improved linear database search due to Grover [5]. However, the experimental implementation of quantum logic gates and quantum computers has generally lagged far behind the theoretical developments.

Quantum information may be distinguished from classical information by the differing ways that the two types of information may be manipulated. These differences may be summarized as follows:

1. Quantum states may not be copied. This is a statement of the *no-cloning theorem* [6]. Classically it is always assumed that information can be accurately and cheaply copied.

2. Quantum states exist in superpositions. It is the ability to perform calculations on superpositions of states that give quantum computers their power.

3. Quantum states are generally non-orthogonal and cannot be reliably distinguished. Classically we assume that distinct states can be distinguished with certainty.

4. Quantum states can have a non-local aspect, as exemplified by the Einstein-Podolsky-Rosen paradox and Bell's inequalities [7].

1.1.1 The qubit

The simplest known system capable of storing information is the *qubit* [8]. It is the direct quantum-mechanical analog of the classical bit. A qubit is a quantum-mechanical state in a two-dimensional Hilbert space. It has the form

$$|\psi\rangle = \alpha\,|0\rangle + \beta\,|1\rangle\,, \tag{1.1a}$$

where normalization of the state requires

$$|\alpha|^2 + |\beta|^2 = 1. \tag{1.1b}$$

The concept of quantum information is based on the qubit in the same way that classical information is based on the bit.

1.2 Entanglement

Entanglement is a property of composite quantum systems in which the correlations between the subsystems cannot be explained classically. Entanglement is now appreciated as a resource that is necessary for the implementation of all specifically quantum information protocols such as *quantum computing*, *quantum teleportation* and *quantum cryptography*.

The main difficulty in generating and manipulating entanglement is decoherence, the process in which the quantum correlations that lead to entanglement are destroyed by interactions with the environment. One solution to the problem of decoherence is to generate an environment in which the quantum correlations are generated rather than destroyed. This can be achieved for atoms by strongly coupling them to a source of broadband squeezed light or some other similar quantum reservoir. This concept is the central idea behind the systems studied in this thesis.

1.2.1 Creating entanglement

There have been many different proposals for entangling objects. The majority of the experiments on entanglement performed to date involve photons, since they are readily produced and manipulated [9]. Thus far, the experimental entanglement of up to four photons has been demonstrated [10]. However, photons are not easy to store, and have only a weak interaction with each other (although see [11]), making them unsuitable for many proposed experiments in the manipulation of quantum information.

In this Thesis we consider systems with the following characteristics:

1. The entangled objects are atoms and we entangle their electronic states (rather than their motional or nuclear states).

2. Pairs of atoms are entangled rather than larger ensembles.

3. The atoms are trapped and therefore well-localized.

4. The atoms are separated sufficiently far from each other that they have no direct interaction between them (e.g., no dipole interaction). The interaction between the atoms is indirect, in that it is mediated by one or more light fields.

There have been significant recent advances in the trapping of single atoms in free space [12, 13] and in high-finesse optical cavities [14, 15, 16, 17, 18]. Atoms in such cavities can exhibit *strong coupling* to the light field and, for the atomic transitions of interest, only a single mode of the cavity

plays a significant role in the dynamics of the atom. An atom in such an environment can be precisely controlled and it is a sufficiently simple system that the theoretical techniques of quantum optics may be used to accurately model its interaction with the incident light fields.

The work in this Thesis complements other theoretical proposals employing optical cavity QED to entangle atoms [19, 20]. To date, the experimental entanglement of atoms in an optical cavity QED has not been achieved. However, experiments have been performed that entangle Rydberg atoms in microwave cavities [21, 22, 23] and that entangle trapped ions [24, 25, 26].

1.2.2 Using entanglement

In this Thesis we explore certain experimental possibilities for generating entanglement between trapped, individually addressable atoms. Such systems would enable exciting new experiments to be performed. Their uses include the following:

1. Entangled atoms may be used as constituents of quantum computers, such as quantum gates and quantum memories [27].

2. Entangled atoms are, at least in principle, long-lived objects (unlike photons). They may be used to store and manipulate entanglement over long time periods.

3. Entangled atoms may be used to perform tests on the fundamentals of quantum mechanics, in particular to demonstrate violations of *Bell's inequalities* [7].

4. Investigations of the recently developed techniques for manipulating entanglement. A controllable source of states of arbitrary entropy and entanglement would allow protocols such as *quantum teleportation* [28] and *entanglement distillation* [29] to be explored for mixed states.

When the electronic states of separated atoms are entangled the combined system has a nonlocal aspect, describable as a *quantum channel*. This quantum channel cannot be used to transmit information on its own, but it can be used to demonstrate non-classical behaviour such as is seen in violations of Bell's inequalities.

1.2.3 Quantifying entanglement

Entanglement in general multi-partite quantum systems is still poorly understood. It is only in some special cases that methods of quantifying entanglement have been developed. In particular, there is a method to quantify

the entanglement in mixed two-qubit systems [30]. Chapter 2 is devoted to the question of mixed-state entanglement.

1.2.4 Bell states

A qubit has only one subsystem; it is too simple to demonstrate entanglement. The simplest system in which an entangled state can exist is a pair of qubits, i.e., a state in the Hilbert space $2 \otimes 2$. Throughout this Thesis we will be concerned with states in this space.

The *Bell states* are maximally entangled pairs of qubits, normally denoted

$$\left|\phi^{\pm}\right\rangle = \frac{1}{\sqrt{2}}\left(|00\rangle \pm |11\rangle\right), \tag{1.2a}$$

$$\left|\psi^{\pm}\right\rangle = \frac{1}{\sqrt{2}}\left(|01\rangle \pm |10\rangle\right). \tag{1.2b}$$

We shall call the states $|\phi^{\pm}\rangle$ *correlated Bell states*, and the states $|\psi^{\pm}\rangle$ *anti-correlated Bell states*. The Bell states form a basis for the space of two qubits.

As maximally entangled states of the simplest possible system exhibiting entanglement, the Bell states are considered, in some sense, to be fundamental units of entanglement. The *ebit* is a name coined for this fundamental quantity of entanglement present in a single Bell state.

1.3 Outline of Thesis

This rest of this Thesis is structured as follows:

Chapter 2 introduces the concepts of separability and entanglement for quantum systems in a mixed state. Necessary conditions for a system to be separable and the varieties of entanglement and methods for their quantification are discussed. The relationship between entanglement and the Bell inequalities is explored. The entropy-entanglement plane is introduced as a convenient visualization tool for states of two qubit systems.

Chapter 3 provides a short background on selected topics in quantum optics.

Chapter 4 investigates the effect of squeezed light on two separated two-level atoms, under a number of simplifying assumptions. Two methods of generating the necessary spatially entangled light beams are considered. The steady state of the atoms is solved, and their degree of entanglement is quantified. Their relevance for investigating violations of Bell inequalities is ex-

amined. Finally the dynamics of their evolution are investigated using the entropy-entanglement plane.

Chapter 5 considers a single three-level atom trapped in a high-finesse optical cavity with a view to determining whether it has the same effective interaction with squeezed light as does a free two-level atom interacting with broadband squeezed light. It is found that a 3-level configuration does not have the desired interaction but, in the appropriate limit, a more complex 4-level system has the required interaction.

Chapter 6 investigates a scheme based on two atoms that each have the 4-level Λ-configuration developed in Chapter 5. This pair of 4-level atoms are trapped in a high finesse optical cavity which is driven by quadrature-squeezed light from a degenerate parametric amplifier. In another scenario, two 4-level atoms are trapped in individual optical cavities each driven by a different output field from a non-degenerate parametric amplifier. In both cases we show that the correlations in the light fields are transferred to the atoms and how atomic two-qubit states of arbitrary entanglement and entropy may be generated.

Chapter 7 introduces quantum reservoir engineering and shows how it can be used to entangle atoms. The scheme investigated in this Chapter is considerably easier to implement experimentally than the scheme in Chapter 6 because non-classical light fields are not required. The effects of spontaneous emission during the Raman transitions are also investigated.

The final Chapter of conclusions summarizes the results obtained in this thesis and suggests some areas that might be of interest in future research.

1.4 Notation

Throughout this thesis the following notation is used.

- Acute marks are not usually added to indicate operators, except in the rare situations when confusion may arise between an operator and it's eigenvalue.
- The Dirac ket-bra notation is used for elements of a Hilbert space and their dual transformations.
- Tilde marks are occasionally used to indicate an operator that is in the interaction picture, e.g. $\tilde{\rho}$.
- The complex conjugate is indicated with a superscript asterisk, e.g. z^*.
- The adjoint operator is indicated with a superscript dagger, e.g. $a^\dagger$.

- The transpose of a matrix is indicated with a superscript T, e.g. A^T.
- Vector quantities are denoted in bold type, e.g. $\mathbf{x}$.
- In an equation, H.c. is used to represent the Hermitian conjugate operator of the previous term.

In Chapter 3, which presents some background material on Quantum Optics, we retain the constant $\hbar$ in our equations. However, elsewhere in this Thesis we always use units such that $\hbar = 1$.

This Thesis has been typeset using LaTeX©. All numerical simulations were performed using the quantum toolbox designed by Sze Tan of the University of Auckland [31] running on the mathematics package MATLAB©. Some analytical work was performed using the symbolic mathematics package Mathematica©.

Chapter 2

Mixed-State Entanglement

This Chapter introduces the concepts of separability and entanglement in mixed quantum systems. Necessary conditions for a system to be separable are discussed, as are the varieties of entanglement and methods for their quantification. The relationship between entanglement and the Bell inequalities is explored. Finally, the entropy-entanglement plane is introduced as a convenient visualization tool for mixed states of two-qubit systems.

Contents

2.1 Introduction

Entanglement is a property of composite quantum systems in which the correlations between the subsystems cannot be explained classically. The essence of entanglement is obtained from the statement: *If two systems interacted in the past it is, in general, not possible to assign a single state vector to either of the subsystems.* In other words, maximal knowledge of the entire system does not necessarily include maximal knowledge of its parts.

All experimentally realistic systems produce mixed states due to the unavoidable effects of environmentally induced noise. Therefore, we do not even have maximal knowledge of the entire system. In this Chapter, we are interested in understanding the meaning of entanglement for such mixed states.

In recent times, the entanglement of mixed states has been investigated vigorously, and it is now much better understood (for an excellent review see [32]). Some surprising discoveries have been made, such as the difference between the entanglement required to create a given state, and that which may be obtained from a given state (see Section 2.3.3). This may lead to a description of entanglement that is analogous to the principles of thermodynamics [33, 34, 35, 36].

2.2 Separability

A general mixed quantum system consisting of two subsystems A and B is defined to be *separable* if the density operator describing it can be written in the form

$$\rho = \sum_i P_i \; \rho_A^i \otimes \rho_B^i, \tag{2.1a}$$

where the P_i are real and positive and satisfy

$$\sum_i P_i = 1. \tag{2.1b}$$

This definition was given by Werner in 1989 [37] who called it a *classically-correlated state.* A state is called *entangled* if it is not separable. In general, the decomposition of a separable state into a mixture of product states is not unique. A good review paper on separability is [38].

A test for separability in general multi-dimensional Hilbert spaces has not yet been found. However, some progress has been made. Peres has shown [39] that a necessary condition for separability of a bipartite state is

that the *partial transposition* of ρ has only non-negative eigenvalues. The partial transposition of a state may be defined using its matrix elements in a basis created from the tensor product of an orthonormal basis for each subsystem

$$\rho_{m\mu,n\nu} = \langle m| \otimes \langle \mu| \, \rho \, |n\rangle \otimes |\nu\rangle \, . \tag{2.2}$$

The partial transposition of ρ, with respect to the first subsystem A, is then

$$\rho^{T_A}_{m\mu,n\nu} = \rho_{n\mu,m\nu}. \tag{2.3}$$

Horodecki *et al.* [40] have shown that non-negativity of the eigenvalues of the partial transpose is also a sufficient condition for separability in $2 \otimes 2$ and $2 \otimes 3$ systems, but not for higher dimensions.

Other necessary criteria are known to exist [32]. For instance, a separable system always satisfies any Bell inequality, but not vice versa (see Section 2.4).

2.3 Entanglement

In this section we consider some numerical measures of entanglement. At the present time these can only be calculated for a few special cases such as bipartite qubit systems - not for the general case of a mixed multi-partite system of arbitrary dimension.

2.3.1 Entropy of entanglement

A unique measure of the entanglement exists for pure bipartite systems [35]. This is the *entropy of entanglement* [29], denoted by $E(\psi_{AB})$. It is the von Neumann entropy of the reduced density matrix

$$E(\psi_{AB}) \equiv -\mathrm{Tr}\left(\rho_A \log_2 \rho_A\right), \tag{2.4a}$$

where

$$\rho_A \equiv \mathrm{Tr}_B \left\{|\psi_{AB}\rangle \langle \psi_{AB}|\right\}. \tag{2.4b}$$

For mixed-state entanglement the situation is less clear and several entanglement monotones have been proposed. The most important of these are:

1. The *entanglement of formation*, $E_F(\rho)$.

2. The *distillable entanglement*, $E_D(\rho)$.

3. The *relative entropy of entanglement*, $E_R(\rho)$.

4. The *negativity*, $\mathcal{N}(\rho)$.

It is not known how to calculate E_F, E_D or E_R for general mixed states of systems of arbitrary dimensions, because they are all defined variationally. The negativity is a measure that is designed to be computable. These entanglement measures are described in the following Subsections.

2.3.2 Entanglement of formation

The entanglement of formation, $E_F(\rho)$, quantifies the asymptotic pure-state entanglement required to produce ρ. The entanglement of formation is defined as the minimum entanglement of any ensemble of pure states realizing ρ [41]. Recall that the unique entanglement measure for a pure state is the entropy of entanglement as defined in Equation (2.4a). Using that result, the entanglement of formation for a mixed state is

$$E_F(\rho) = \min \sum_i P_i E(\psi_i), \tag{2.5a}$$

where the minimization is over all decompositions

$$\rho = \sum_i P_i \left|\psi_i\right\rangle \left\langle\psi_i\right|. \tag{2.5b}$$

Two qubits

An analytic expression found by Wootters for the entanglement of formation of two qubits [30] was an important advance. It may be calculated as follows:

Define the *spin-flipped state* for two qubits to be

$$\tilde{\rho} = (\sigma_y \otimes \sigma_y)\, \rho^* \,(\sigma_y \otimes \sigma_y)\,, \tag{2.6a}$$

where the conjugation of ρ is taken in the computational basis and

$$\sigma_y = \begin{pmatrix} 0 & -i \\ i & 0 \end{pmatrix}. \tag{2.6b}$$

The *concurrence* is defined to be

$$\mathcal{C}(\rho) = \max\left\{0, \lambda_1 - \lambda_2 - \lambda_3 - \lambda_4\right\}, \tag{2.7a}$$

where λ_i are the eigenvalues in decreasing order of

$$R = \sqrt{\sqrt{\rho}\tilde{\rho}\sqrt{\rho}}. \tag{2.7b}$$

The *tangle*, denoted $\tau(\rho)$, is related to the concurrence by

$$\tau(\rho) = \mathcal{C}(\rho)^2. \tag{2.8}$$

Finally, the entanglement of formation is calculated as

$$E_F(\rho) = h\left(\frac{1+\sqrt{1-\tau(\rho)}}{2}\right), \tag{2.9}$$

where

$$h(x) = -x\log_2 x - (1-x)\log_2(1-x) \tag{2.10}$$

is the *Shannon entropy*.

We may note that if $\rho = |\psi\rangle\langle\psi|$ is a pure state, then a simpler formula applies for the concurrence,

$$\mathcal{C}(\psi) = \left|\left\langle\psi|\tilde{\psi}\right\rangle\right|. \tag{2.11}$$

In this Thesis we commonly calculate the degree of entanglement for the two-qubit states we produce. Since the entanglement of formation, the tangle, and the concurrence are monotonically related to each other, we are free to choose whichever measure is more convenient. We normally use the tangle or the concurrence since they are easier to calculate analytically.

2.3.3 Entanglement of distillation

The *distillable entanglement*, $E_D(\rho)$, quantifies the asymptotic pure state entanglement that can be distilled from ρ by means of local operations and classical communication (LOCC) only [42]. A state ρ is said to be *distillable* if two parties sharing ρ can obtain singlets (pure Bell states of two qubits) from the initial state $\rho^{\otimes n}$.

It is known that all pure entangled states [29], and all entangled states of two qubits [43], can be distilled. Nevertheless, there are entangled states that cannot be distilled; these states are said to have *bound entanglement* [42]. In this Thesis we will only be concerned with two-qubit states, which do not exhibit bound entanglement. It is not known how to calculate the entanglement of distillation for any mixed system.

2.3.4 Relative entropy of entanglement

The relative entropy of entanglement of a mixed state is defined as

$$E_R(\rho) = \min_{\sigma\in\mathcal{D}} S(\rho||\sigma), \tag{2.12a}$$

where

$$S(\rho||\sigma) = \mathrm{Tr}(\rho\ln\rho - \rho\ln\sigma) \tag{2.12b}$$

is the *quantum relative entropy* [44]. The minimum is taken over the set $\mathcal{D}$ of separable states. The relative entropy of entanglement is known to be bounded above by $E_F(\rho)$ and below by $E_D(\rho)$ [45], i.e.,

$$E_D(\rho) \leq E_R(\rho) \leq E_F(\rho). \tag{2.13}$$

2.3.5 Negativity

Vidal *et al.* introduced a measure of entanglement, designed specifically to be computable, called the *negativity* [46]. This is defined in terms of the trace norm (sum of the absolute values of the eigenvalues) of the partial transpose of a bipartite mixed state,

$$\mathcal{N}(\rho) \equiv \frac{\left\|\rho^{T_A}\right\|_1 - 1}{2}. \tag{2.14}$$

The negativity corresponds to the absolute value of the sum of the negative eigenvalues of ρ^{T_A}, and it vanishes for separable states.

The quantity $\mathcal{N}(\rho)$ does not increase under LOCC and hence is an entanglement monotone. It is also known that, for an entangled mixed state of two qubits, the negativity never exceeds the concurrence [47].

2.4 Bell inequalities

It was Bell [7] who first realized that local realism gives rise to inequalities that can be violated by quantum mechanical systems. Many different Bell inequalities have now been proposed [48, 49, 50, 51] and experiments have been performed that demonstrate the violation of these inequalities [52, 53, 9].

The strongest known Bell inequality for two qubits [32] is due to Clauser, Horne, Shimony and Holt (the CHSH inequality) [48],

$$B = \mathrm{Tr}(\rho\mathcal{B}) \leq 2, \tag{2.15}$$

where the Bell-CHSH observable $\mathcal{B}$ is given by

$$\mathcal{B} = \mathbf{a}\cdot\boldsymbol{\sigma}\otimes(\mathbf{b}+\mathbf{b}')\cdot\boldsymbol{\sigma} + \mathbf{a}'\cdot\boldsymbol{\sigma}\otimes(\mathbf{b}-\mathbf{b}')\cdot\boldsymbol{\sigma}. \tag{2.16}$$

Here $\mathbf{a}$, $\mathbf{a}'$, $\mathbf{b}$ and $\mathbf{b}'$ are unit vectors in $\mathbb{R}^3$ and $\boldsymbol{\sigma}$ is the standard vector of Pauli matrices,

$$\boldsymbol{\sigma} = \begin{pmatrix} \sigma_1 \\ \sigma_2 \\ \sigma_3 \end{pmatrix}, \tag{2.17a}$$

where

$$\sigma^1 = \begin{pmatrix} 0 & 1 \\ 1 & 0 \end{pmatrix},\ \sigma^2 = \begin{pmatrix} 0 & -i \\ i & 0 \end{pmatrix},\ \sigma^3 = \begin{pmatrix} 1 & 0 \\ 0 & -1 \end{pmatrix}. \tag{2.17b}$$

A convenient expression for the maximum value of B (2.15) allowed by quantum mechanics for any given two-qubit state ρ, was found by Horodecki *et al.* in 1995 [54]. It amounts to maximising the CHSH inequality (2.15) over all possible vectors $\mathbf{a}$, $\mathbf{a}'$, $\mathbf{b}$ and $\mathbf{b}'$. To calculate the maximum value of B the density matrix ρ should be first expressed in the Hilbert-Schmidt basis by finding $\mathbf{r}$, $\mathbf{s}$ and T such that

$$\rho = \frac{1}{4}\left(\mathbf{1}_2\otimes\mathbf{1}_2 + \mathbf{r}\cdot\boldsymbol{\sigma}\otimes\mathbf{1}_2 + \mathbf{1}_2\otimes\mathbf{s}\cdot\boldsymbol{\sigma} + \sum_{n,m=1}^{3} T_{nm}\sigma_n\otimes\sigma_m\right). \tag{2.18}$$

Then the maximum violation is

$$B_{max}(\rho) \;=\; 2\sqrt{M(\rho)}, \tag{2.19a}$$

where $M(\rho)$ is the sum of the two largest eigenvalues of $T^\dagger T$, and where T is the 3×3 matrix whose (n,m)-element is

$$T_{nm} \;=\; \mathrm{Tr}\left\{\rho\,(\sigma_n\otimes\sigma_m)\right\}. \tag{2.19b}$$

The condition $M(\rho)\leq 1$ is equivalent to satisfying all possible CHSH inequalities simultaneously and its violation is thus a sufficient condition for entanglement. It is known that any entangled pure state of two qubits violates some Bell inequality.

In a surprising result, Popescu showed in 1994 [55] that there are entangled states that do not violate any standard Bell inequality. Thus, violation of a Bell inequality is a sufficient condition for entanglement, but not a necessary condition (see also recent results in [56]). Popescu further showed in 1995 [57] that there are states for which a single measurement satisfies the standard Bell inequalities, but for which a sequence of measurements violates the Bell inequality. Further information on Bell inequalities may be found in [58, 32].

2.5 The entropy-entanglement plane

The *entropy-entanglement plane* [59] is a useful tool for representing the state of an entangled mixed system. Entanglement is invariant under local unitary transformations and entropy is invariant under all unitary transformations. Therefore, plotting sequences of states in this plane emphasizes changes due to global non-unitary transformations such as dissipative damping into a reservoir.

There is flexibility in the choice of measures we use for the entropy and entanglement. We commonly use the *linear entropy*,

$$S_L = \frac{4}{3}\left\{1 - \mathrm{Tr}\left(\rho^2\right)\right\},$$

as our measure of the purity of the system [60], because it is easier to apply analytically. Alternatively, the von-Neumann entropy may be used,

$$S_v = -\mathrm{Tr}\left(\rho \log_2 \rho\right). \tag{2.20}$$

As our measure of entanglement, we usually plot the concurrence or tangle (defined in Section 2.3.2), since these are calculable for mixed two-qubit systems. We use a minor variation of the concurrence (2.7a) and call it the *free concurrence*,

$$\mathcal{C}_{free} = \lambda_1 - \lambda_2 - \lambda_3 - \lambda_4, \tag{2.21}$$

with λ_i as defined in Section 2.3.2. The free concurrence reduces to the concurrence for entangled states. For separable states the concurrence is always 0, whereas the free concurrence can take on negative values. In some sense, the more negative the free concurrence, the further the state is from being non-classical. Thus, using the free concurrence allows us to better distinguish separable states. Also, using the definition of the free concurrence we can define the equivalent variation of the tangle (2.8), calling it the *free tangle*,

$$\tau_{free} = |\mathcal{C}_{free}|\,\mathcal{C}_{free}. \tag{2.22}$$

2.5.1 Structure of the LEFT plane

The structure of the linear entropy-free tangle (LEFT) plane for a two-qubit system is shown in Figure 2.1. All physically possible two-qubit states are believed to lie in the shaded region, but the boundaries of this area have not been proved analytically when $\tau_{free} < 0$.

Three ranges of states are plotted:

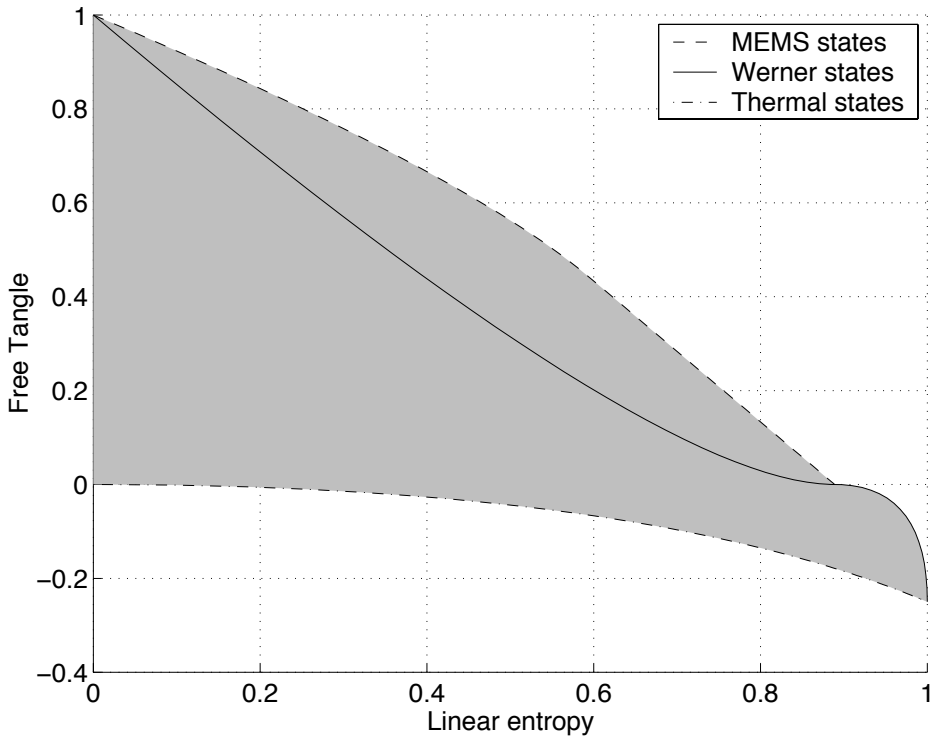

Figure 2.1: The structure of the linear entropy-free tangle (LEFT) plane for a two-qubit system. All entangled states lie on or below the line of MEMS states. All physically possible two-qubit states are believed to lie in the shaded area, but the boundaries of this area have not been proved analytically when $\tau_{free} < 0$.

1. The *maximally entangled mixed states* (MEMS), as recently characterized in [59]. These are the states having the maximum possible entanglement for any given entropy (as measured by the tangle and linear entropy respectively). They are defined by

$$\rho_{MEMS}(q) = \begin{pmatrix} g(q) & 0 & 0 & q/2 \\ 0 & 1-2g(q) & 0 & 0 \\ 0 & 0 & 0 & 0 \\ q/2 & 0 & 0 & g(q) \end{pmatrix}, \tag{2.23a}$$

where

$$g(q) = \begin{cases} 1/3, & 0 \le q < 2/3 \\ q/2, & 2/3 \le q \le 1 \end{cases}. \tag{2.23b}$$

All valid two-qubit states lie on or below the MEMS line.

2. The *Werner states* [37]. For two qubits, these very important states are mixtures of a maximally entangled Bell state (1.2) and the totally mixed state, e.g.,

$$\rho_W(q) = (1-q)\left|\phi^+\right\rangle + \frac{q}{4}\left(\mathbf{1}_2 \otimes \mathbf{1}_2\right), \ 0 \le q \le 1. \tag{2.24}$$

3. The *thermal states* given by

$$\rho_{TH}(\bar{n}) = \frac{1}{(1+2\bar{n})^2} \begin{pmatrix} \bar{n}^2 & 0 & 0 & 0 \\ 0 & \bar{n}(1+\bar{n}) & 0 & 0 \\ 0 & 0 & \bar{n}(1+\bar{n}) & 0 \\ 0 & 0 & 0 & (1+\bar{n})^2 \end{pmatrix}, \quad 0 \le \bar{n} < \infty. \tag{2.25}$$

These are states obtained when a two-qubit system is driven by thermal light characterized by a mean photon number of $\bar{n}$.

The point where the MEMS line and the Werner line meet (at $S_L = 8/9$) represents the maximally mixed state that has $\tau_{free} = 0$. There is a discontinuity of the structure of the MEMS states which occurs at $\tau_{free} = 4/9$, as seen from Equation (2.23). It should be noted that the lower boundaries of the LEFT plane for non-separable states are only a conjecture.

2.5.2 Various mixtures

In Figure 2.2 we use the LEFT plane to show a variety of other interesting mixed two-qubit states. The following mixtures are plotted:

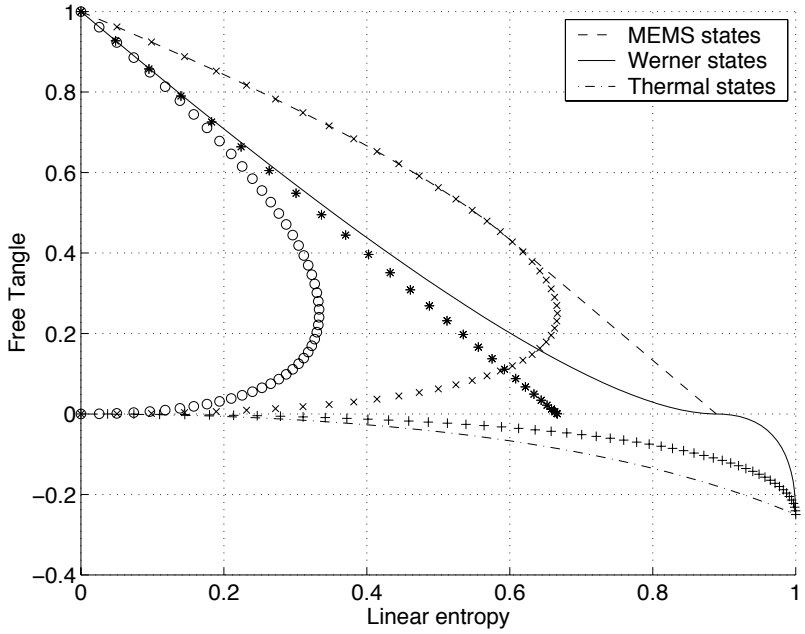

Figure 2.2: Various incoherent mixtures of two-qubit states in the LEFT plane. See the text for a description of the states plotted in this Figure.

1. The crosses are mixtures of a correlated Bell state (i.e. $|\phi^+\rangle$ or $|\phi^-\rangle$) and the ground state $|00\rangle$.

2. The pluses are mixtures of an anti-correlated Bell state (i.e. $|\psi^+\rangle$ or $|\psi^-\rangle$) and the ground state $|00\rangle$.

3. The asterisks are mixtures of the ground state $|00\rangle$ and the totally mixed state $\frac{1}{4}(\mathbf{1}_2 \otimes \mathbf{1}_2)$.

4. The dots are mixtures of any two different Bell states.

It should be noted that mixtures of $|00\rangle$ and one of the anti-correlated Bell states $|\psi^\pm\rangle$ coincide with a portion of the MEMS line. This observation becomes relevant in later Chapters where we try to generate states above the Werner line.

2.5.3 Other entropy-entanglement planes

It is informative to consider the structure of the entropy-entanglement plane for different combinations of entropy and entanglement measures. Six different combinations are plotted in Figure 2.3.

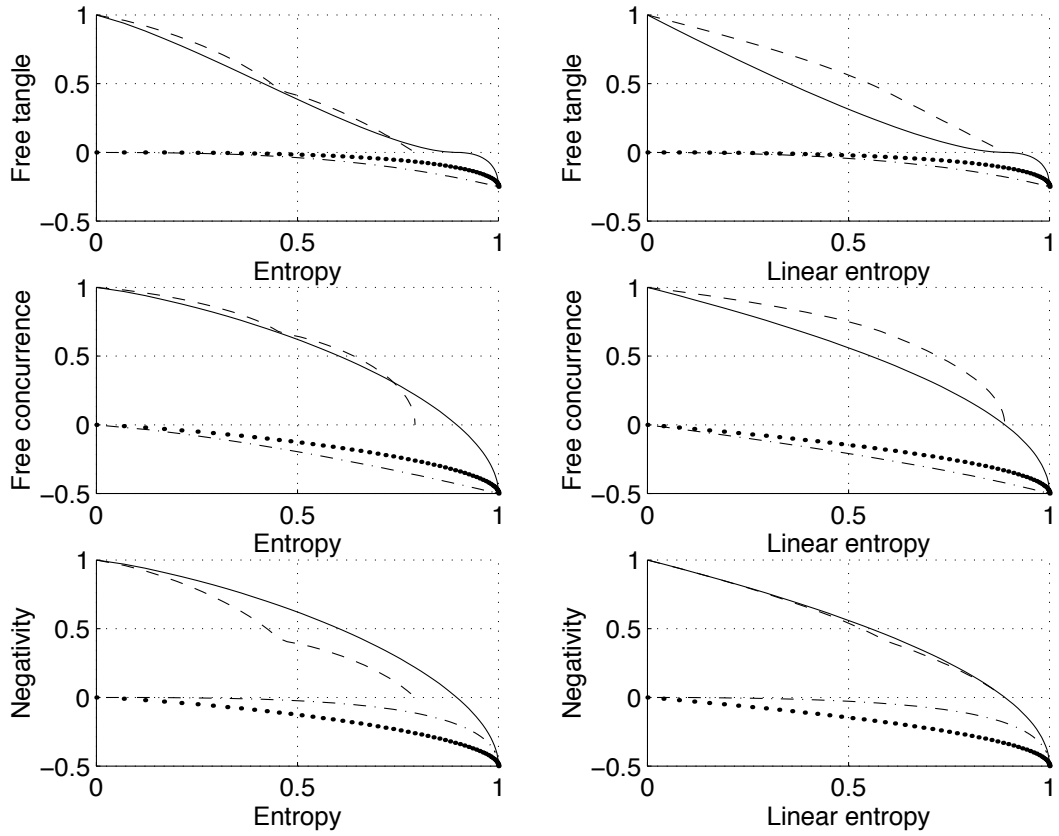

Figure 2.3: The structure of the two-qubit entropy-entanglement plane for different measures. The MEMS states, Werner states and thermal states are plotted using the same symbols as in Figure 2.2. Points on the dotted line are mixtures of the ground state $|00\rangle$ and the totally mixed state $\frac{1}{4}(\mathbf{1}_2 \otimes \mathbf{1}_2)$.

We may make some observations from these graphs. The MEMS states (plotted with a dashed line) are the maximally entangled states only when the free tangle or free concurrence is plotted against linear entropy. It is interesting that the thermal states are not the states with the least possible negativity. We also see that the free concurrence is, in some sense, a more suitable measure to plot than the free tangle, because it scales in a more appropriate manner, thus making the Werner line a "smoother" curve. Recall that the free tangle is a quadratic function of the free concurrence (2.22). In later Chapters we will choose to plot linear entropy against either free concurrence or free tangle.

2.5.4 Ishizaka states

Ishizaka and Hiroshima have recently characterized the two-qubit states whose entanglement of formation (and negativity) cannot be increased by any unitary transformation [61]. These unusual states are given by any local unitary transformation of

$$\rho_{ISH} = p_1 \left|\psi^-\right\rangle \left\langle\psi^-\right| + p_2 \left|00\right\rangle \left\langle 00\right| + p_3 \left|\psi^+\right\rangle \left\langle\psi^+\right| + p_4 \left|11\right\rangle \left\langle 11\right|, \quad (2.26a)$$

where p_i are the eigenvalues of ρ_{ISH} in decreasing order so that

$$p_1 \geq p_2 \geq p_3 \geq p_4, \quad (2.26b)$$

and

$$p_1 + p_2 + p_3 + p_4 = 1. \quad (2.26c)$$

These states include the Werner states. We have randomly generated 2000 of these states and plotted them in Figure 2.4. The Ishizaka states must include the states of maximum entanglement for any given entropy, as measured by any of the 6 combinations of measures plotted in this Figure. Thus we see that the MEMS states (2.23) are not the states of maximum tangle (or concurrence) when plotted against the entropy (as opposed to the linear entropy), as noted in [59].

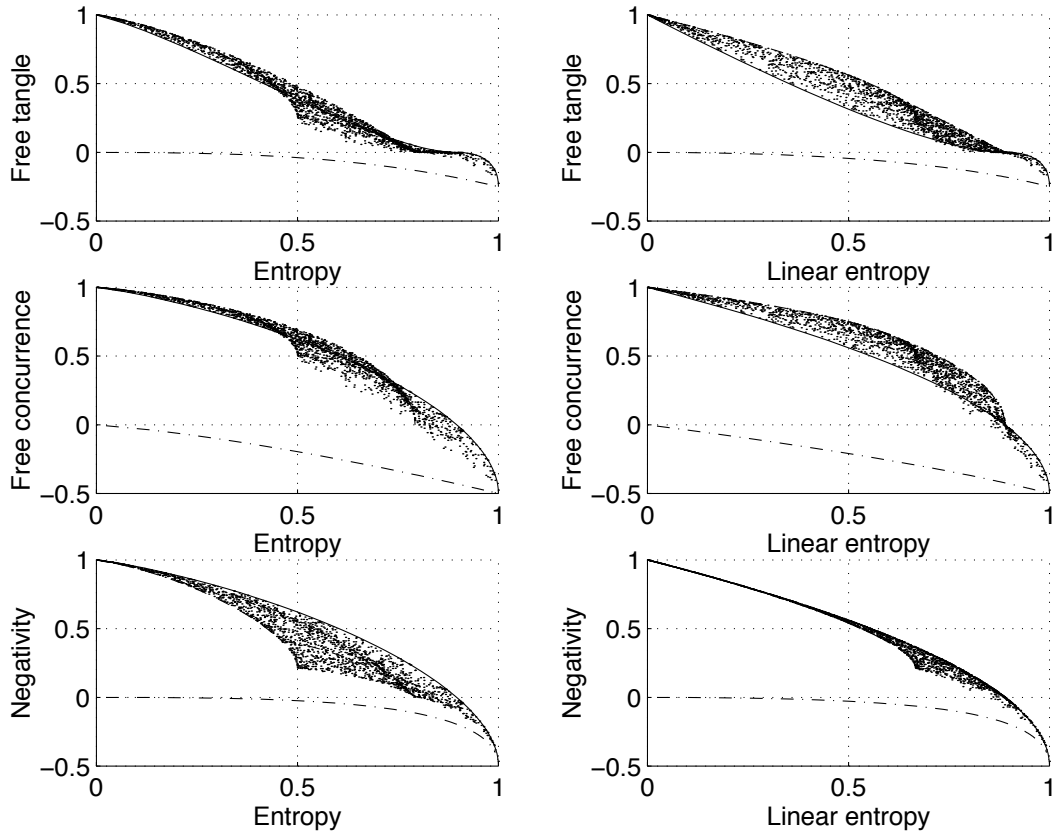

Figure 2.4: 2000 random Ishizaka states, plotted using a variety of entropy and entanglement measures.

Chapter 3

Quantum Optics

This Chapter provides a short background on selected topics in quantum optics that are of relevance to this Thesis.

Contents

3.1 Quantization of the electromagnetic field

In this Thesis we will investigate systems in which single atoms are trapped in optical cavities. In such environments we must use quantum electrodynamics to describe the quantum-mechanical properties of the light field in the

cavity. The quantization of the electromagnetic field is the starting point for quantum optics and there are many text books covering this topic [62, 63, 64].

3.1.1 Maxwell's equations

The canonical quantization of the electromagnetic field starts from Maxwell's equations in free space:

$$\nabla \cdot \mathbf{B} = 0, \tag{3.1a}$$

$$\nabla \times \mathbf{E} = -\frac{\partial \mathbf{B}}{\partial t}, \tag{3.1b}$$

$$\nabla \cdot \mathbf{E} = 0, \tag{3.1c}$$

$$\nabla \times \mathbf{H} = \frac{\partial \mathbf{D}}{\partial t}. \tag{3.1d}$$

where also

$$\mathbf{B} = \mu_0 \mathbf{H}, \tag{3.1e}$$

$$\mathbf{D} = \epsilon_0 \mathbf{E}, \tag{3.1f}$$

and μ_0 and ϵ_0 are the permeability and permittivity of free space, obeying

$$\mu_0 \epsilon_0 c^2 = 1. \tag{3.1g}$$

The vector valued fields $\mathbf{B}$, $\mathbf{H}$, $\mathbf{E}$ and $\mathbf{D}$ are all functions of position $\mathbf{r}$ and time t.

In the Coulomb gauge,

$$\nabla \cdot \mathbf{A} = 0, \tag{3.2}$$

the magnetic and electric fields may be expressed in terms of the vector potential as

$$\mathbf{B} = \nabla \times \mathbf{A}, \tag{3.3a}$$

$$\mathbf{E} = -\frac{\partial \mathbf{A}}{\partial t}. \tag{3.3b}$$

From (3.3) and (3.1d) we obtain the wave equation for the vector potential

$$\nabla^2 \mathbf{A} = \frac{1}{c^2} \frac{\partial^2 \mathbf{A}}{\partial t^2}. \tag{3.4}$$

Using separation of variables, and for any particular bounded volume, we may solve Equation (3.4) and express $\mathbf{A}$ as a Fourier decomposition over a complete set of orthonormal complex-valued vector mode functions $\mathbf{u}_m(\mathbf{r})$,

$$\mathbf{A} = \sum_m \left(\frac{\hbar}{2\omega_m \epsilon_0} \right)^{\frac{1}{2}} \left\{ a_m \mathbf{u}_m(\mathbf{r}) e^{-i\omega_m t} + a_m^\dagger \mathbf{u}_m^*(\mathbf{r}) e^{i\omega_m t} \right\}, \tag{3.5}$$

where the summation is over a discrete set of modes (including polarization states) and the normalization constant is chosen to make a_m and $a_m^\dagger$ dimensionless. From Equation (3.3b), we find for the electric field,

$$\mathbf{E} = i \sum_m \left(\frac{\hbar \omega_m}{2\epsilon_0} \right)^{\frac{1}{2}} \left\{ a_m \mathbf{u}_m(\mathbf{r}) e^{-i\omega_m t} - a_m^\dagger \mathbf{u}_m^*(\mathbf{r}) e^{i\omega_m t} \right\}. \tag{3.6}$$

3.1.2 Canonical quantization

The canonical quantization proceeds by taking the complex amplitudes a and $a^\dagger$ in (3.5) to be mutually adjoint operators, $\hat{a}$ and $\hat{a}^\dagger$, obeying the bosonic commutation relations

$$[\hat{a}_m, \hat{a}_{m'}] = 0, \tag{3.7a}$$

$$\left[\hat{a}_m^\dagger, \hat{a}_{m'}^\dagger\right] = 0, \tag{3.7b}$$

$$\left[\hat{a}_m, \hat{a}_{m'}^\dagger\right] = \delta_{m,m'}. \tag{3.7c}$$

The Hamiltonian for the free electromagnetic field can then be calculated to be

$$\hat{H} = \sum_m \hbar \omega_m \left(\hat{a}_m^\dagger \hat{a}_m + \frac{1}{2} \right). \tag{3.8}$$

This leads naturally to the interpretation of the electromagnetic field as an ensemble of independent quantized harmonic oscillators with annihilation (creation) operators $\hat{a}_m$ ($\hat{a}_m^\dagger$).

3.2 States of the electromagnetic field

In this Section we state some of the properties of the quantized harmonic oscillator. We deal here with a single harmonic oscillator (or mode of the electromagnetic field) with annihilation (creation) operator a ($a^\dagger$). The use of operators is now assumed and we omit the "hat" notation (e.g., we denote $\hat{a}$ by a, etc.). The Hamiltonian for a single mode is then

$$H = \hbar \omega \left(a^\dagger a + \frac{1}{2} \right), \tag{3.9}$$

and the commutation relations for the annihilation and creation operators are

$$\begin{aligned} [a, a] &= 0, && (3.10a) \\ \left[a^\dagger, a^\dagger\right] &= 0, && (3.10b) \\ \left[a, a^\dagger\right] &= 1. && (3.10c) \end{aligned}$$

3.2.1 Fock states

The *Fock states* (or *number states*) are eigenstates of the *number operator* for the harmonic oscillator, $\hat{n} = a^\dagger a$, and may be defined by

$$|n\rangle = \frac{{a^\dagger}^n}{\sqrt{n!}} |0\rangle , \qquad n = 0, 1, 2, \dots , \tag{3.11}$$

where $|0\rangle$ is the ground (vacuum) state such that $a|0\rangle = 0$. The number states are orthogonal,

$$\langle m|n\rangle = \delta_{mn}, \tag{3.12}$$

and form a complete set

$$\sum_n |n\rangle \langle n| = \mathbf{1}. \tag{3.13}$$

The annihilation and creation operators act on the number states as

$$\begin{aligned} a|n\rangle &= \sqrt{n}\,|n-1\rangle , && (3.14a) \\ a^\dagger|n\rangle &= \sqrt{n+1}\,|n+1\rangle , && (3.14b) \end{aligned}$$

and have commutation relations with the number operator

$$\begin{aligned} [a, n] &= a, && (3.15a) \\ \left[a^\dagger, n\right] &= -a^\dagger. && (3.15b) \end{aligned}$$

The number states are useful from a theoretical point of view, but difficult to produce in practice for the electromagnetic field.

3.2.2 Coherent states

The coherent states are an alternative basis for representing states of the harmonic oscillator. They allow an accurate description of the phase at the expense of precise knowledge of the photon number. They provide a

particularly suitable description for the electromagnetic field because they are the quantum-mechanical field that is the closest analog to a classical electromagnetic field of known complex amplitude. The name "coherent state" is due to Glauber [65].

The coherent states are eigenstates of the annihilation operator, and are defined, for any complex α, by

$$a\,|\alpha\rangle = \alpha\,|\alpha\rangle\,. \tag{3.16}$$

They may be generated from the vacuum state, $|0\rangle$, by a unitary displacement

$$\begin{aligned} D(\alpha) &= \exp\left\{\alpha a^\dagger - \alpha^* a\right\}, && \text{(3.17a)}\\ |\alpha\rangle &= D(\alpha)\,|0\rangle\,. && \text{(3.17b)} \end{aligned}$$

The coherent states are an example of a class of states known as the *minimum uncertainty states* (MUS), for which the product of the uncertainties in canonically conjugate variables takes the minimum value allowed by the Heisenberg uncertainty relation.

3.2.3 Squeezed states

The *squeezed states* are another general class of minimum uncertainty states. The *squeeze operator* is defined as

$$S(\epsilon) = \exp\left\{\frac{1}{2}\epsilon^* aa - \frac{1}{2}\epsilon a^\dagger a^\dagger\right\}. \tag{3.18}$$

The squeezed states are obtained by squeezing the vacuum and then displacing it

$$|\alpha,\epsilon\rangle = D(\alpha)S(\epsilon)\,|0\rangle\,. \tag{3.19}$$

We may define quadrature phase operators by

$$\begin{aligned} X_1 &= a + a^\dagger, && \text{(3.20a)}\\ X_2 &= -i\left(a - a^\dagger\right), && \text{(3.20b)} \end{aligned}$$

so that

$$\begin{aligned} a &= \frac{1}{2}\left(X_1 + iX_2\right), && \text{(3.21a)}\\ a^\dagger &= \frac{1}{2}\left(X_1 - iX_2\right). && \text{(3.21b)} \end{aligned}$$

The commutation relation for the quadrature phase operators is then

$$[X_1, X_2] = 2i, \tag{3.22}$$

so we find that the Heisenberg uncertainty principle specifies a minimum allowed product

$$\sqrt{\left\langle (\Delta X_1)^2 \right\rangle}\sqrt{\left\langle (\Delta X_2)^2 \right\rangle} \geq 1, \tag{3.23a}$$

where the variance is given by

$$\left\langle (\Delta X_i)^2 \right\rangle = \left\langle X_i^2 \right\rangle - \left\langle X_i \right\rangle^2 . \tag{3.23b}$$

A state is said to be *squeezed* if either of the variances is less than 1 and said to be *ideally squeezed* if, in addition, the product of the variances is 1. The coherent states are states where the variances satisfy

$$\left\langle (\Delta X_1)^2 \right\rangle = \left\langle (\Delta X_2)^2 \right\rangle = 1. \tag{3.24}$$

3.2.4 Multi-mode squeezed states

For some of the systems investigated in this Thesis we employ a source of multi-mode squeezed light, in which the correlations occur between two distinct modes that differ in frequency or polarization. To model light of this nature we may use the *two-mode squeezed state*, which is the appropriate generalization of (3.19),

$$\begin{aligned} |\alpha_1, \alpha_2, G\rangle &= D(\alpha_1)D(\alpha_2)S(G)\,|0_1, 0_2\rangle\,, && (3.25)\\ S(G) &= \exp\left\{G^* a_1 a_2 - G a_1^\dagger a_2^\dagger\right\}, && (3.26)\\ G &= re^{i\phi}. && (3.27) \end{aligned}$$

Here we perform a two-mode squeezing operation $S(G)$ between modes 1 and 2, and then make a coherent displacement of each system in turn.

In the general case, the modes a_1 and a_2 have different frequencies ω_1 and ω_2. The squeezing occurs with respect to generalized quadrature phase amplitudes

$$\begin{aligned} X_\theta(t) &= \frac{1}{\sqrt{2}}\left\{a_1(t)e^{i(\theta+\epsilon t)} + a_2^\dagger(t)e^{-i(\theta-\epsilon t)} + \text{H.c.}\right\}, && (3.28a)\\ X_{\theta+\pi/2}(t) &= \frac{-i}{\sqrt{2}}\left\{a_1(t)e^{i(\theta+\epsilon t)} + a_2^\dagger(t)e^{-i(\theta-\epsilon t)} - \text{H.c.}\right\}, && (3.28b) \end{aligned}$$

where

$$\epsilon = \frac{\omega_1 - \omega_2}{2}, \tag{3.29}$$

and θ is an arbitrary phase [62]. The electric field may be expressed in terms of the two phase quadratures as

$$E(t) = X_\theta(t)\cos(\omega t + \theta) + X_{\theta+\pi/2}(t)\sin(\omega t + \theta), \tag{3.30}$$

where

$$\omega = \frac{\omega_1 + \omega_2}{2} \tag{3.31}$$

is the average frequency of the modes. Mutli-mode squeezing occurs when the variance of either of these quadratures is reduced below unity.

It should be stressed that, in multi-mode squeezed light, the squeezing arises from the correlations between the two modes and that neither mode is individually squeezed.

3.3 The parametric amplifier

In Chapters 4 and 6, we will employ non-classical squeezed light sources to entangle atoms. The parametric amplifier is the usual source for such squeezed light. A parametric amplifier consists of a non-linear crystal in a cavity which is pumped by a strong coherent laser field. The laser field may be assumed not to be depleted by its interaction in the crystal and may be modelled classically.

The degenerate parametric amplifier (DPA) has only one intracavity mode, denoted by the annihilation operator a. The interaction picture Hamiltonian for the DPA is

$$H = \frac{i\hbar}{2}\left(E{a^\dagger}^2 - E^* a^2\right), \tag{3.32}$$

where E is a parameter describing the pump strength and interaction in the parametric amplifier. Broad bandwidth ideal squeezed light centred on the cavity frequency is produced in the output from the cavity [66].

The non-degenerate parametric amplifier (NDPA) has two intracavity modes, denoted by the annihilation operators a and b. It generates multi-mode squeezed light as described in Section 3.2.4. For the NDPA, the interaction picture Hamiltonian is

$$H = i\hbar\left(Ea^\dagger b^\dagger - E^* ab\right). \tag{3.33}$$

The two output fields from these modes are quantum correlated as described in Section 3.2.4.

Detailed input-output models of both these parametric systems are given in Appendix A, where they are used as sources of quantum-correlated light to drive and entangle pairs of atoms.

3.4 Interaction of radiation and atoms

In this Thesis we will be concerned with the interaction of single atoms with the electromagnetic field. It is appropriate therefore to make some explanatory comments about the interaction of radiation and atoms.

In our model for an atom we may assume that only two atomic energy levels play a part in any transition. We denote the excited level by $|e\rangle$ and the ground level by $|g\rangle$. When employing a two-level description of the atom, we have occasion to use the *Pauli matrices* which are, in the basis $\{|e\rangle, |g\rangle\}$,

$$\sigma_x = \begin{pmatrix} 0 & 1 \\ 1 & 0 \end{pmatrix}, \ \sigma_y = \begin{pmatrix} 0 & -i \\ i & 0 \end{pmatrix}, \ \sigma_z = \begin{pmatrix} 1 & 0 \\ 0 & -1 \end{pmatrix}, \tag{3.34a}$$

$$\sigma^+ = \begin{pmatrix} 0 & 1 \\ 0 & 0 \end{pmatrix}, \ \sigma^- = \begin{pmatrix} 0 & 0 \\ 1 & 0 \end{pmatrix}. \tag{3.34b}$$

The Hamiltonian describing the systematic motion of the atomic levels, relative to the average energy of the levels, may then be written

$$H_{atom} = \frac{1}{2}\hbar\omega\sigma_z, \tag{3.35}$$

where ω is the frequency difference of the two levels.

The electromagnetic field may interact with atoms via the *electric dipole interaction*

$$H_{atom/field} = -e\,\hat{\mathbf{r}} \cdot \hat{\mathbf{E}}, \tag{3.36a}$$

where e is the electronic charge and $\hat{\mathbf{r}}$ is the position operator for the electron. Here we have made the *dipole approximation* - that the electric field does not vary significantly over the extent of the atom. The *electric dipole moment* operator of the atoms is given by

$$\begin{aligned} e\,\hat{\mathbf{r}} &= e \sum_{n\in\{e,g\}} \sum_{m\in\{e,g\}} |n\rangle \langle n| \,\hat{\mathbf{r}}\, |m\rangle \langle m| \\ &= \mathbf{d}_{ee}\sigma^+\sigma^- + \mathbf{d}_{ge}\sigma^- + \mathbf{d}^*_{ge}\sigma^+ + \mathbf{d}_{gg}\sigma^-\sigma^+, \end{aligned} \tag{3.36b}$$

where we have introduced *atomic dipole matrix elements*

$$\mathbf{d}_{nm} = e\,\langle n|\hat{\mathbf{r}}|m\rangle = e\int d^3r\,\phi_m^*(\mathbf{r})\hat{\mathbf{r}}\phi_n(\mathbf{r}). \tag{3.36c}$$

Here $\phi_n(\mathbf{r})$ is the electron wave function, for an electron in state n, assuming that the wavefunction is unperturbed by the electric field. We may assume that the ground and excited states of the atoms are symmetric and have no permanent dipole moment, so that

$$\mathbf{d}_{gg} = \mathbf{d}_{ee} = 0. \tag{3.36d}$$

Then, the dipole moment of the atoms may be written as

$$e\hat{\mathbf{r}} = \mathbf{d}_{ge}\sigma^- + \mathbf{d}_{ge}^*\sigma^+. \tag{3.36e}$$

With $\mathbf{E}$ as given in (3.6), and making the rotating-wave approximation whereby energy non-conserving terms of the form $a_m^\dagger\sigma^+$ and $a_m\sigma_-$ are neglected, we obtain for our total Hamiltonian,

$$\begin{aligned} H &= H_{atom} + H_{field} + H_{atom/field}, && \text{(3.37a)}\\ H_{atom} &= \frac{1}{2}\hbar\omega\sigma_z, && \text{(3.37b)}\\ H_{field} &= \hbar\sum_m \omega_m a_m^\dagger a_m, && \text{(3.37c)}\\ H_{atom/field} &= \hbar\sum_m \left(\kappa_m^* a_m^\dagger\sigma^- + \kappa_m a_m\sigma^+\right), && \text{(3.37d)} \end{aligned}$$

with

$$\kappa_m = -i\left(\frac{\omega_m}{2\hbar\epsilon_0}\right)^{\frac{1}{2}}\mathbf{u}(\mathbf{r})\cdot\mathbf{d}_{ge}. \tag{3.37e}$$

We have dropped the zero point energy of the electromagnetic field in (3.37c).

3.4.1 Cavity quantum electro-dynamics

Experiments are now possible where single atoms are trapped in high-finesse optical cavities in the *strong coupling regime* [14, 15, 16], where the coupling strength g of an atomic transition to a single cavity mode a dominates both the decay rate κ of the cavity and the spontaneous emission rate γ of the atom, i.e.,

$$g \gg \kappa, \gamma. \tag{3.38}$$

In such a situation the interaction between the two-level atom and the electromagnetic field may be modelled by its interaction with just a single mode. This is the *Jaynes-Cummings model*. From (3.37) we obtain the Hamiltonian for the combined cavity/atom system

$$H = \hbar a^\dagger a + \frac{1}{2}\hbar\omega\sigma_z + g\left(a^\dagger\sigma^- + a\sigma^+\right). \tag{3.39}$$

We will use this Hamiltonian for the coupling between trapped atoms and single field modes that we require in later Chapters.

A good review of cavity quantum electro-dynamics, as used for possible implementations of quantum computers, may be found in [67].

Chapter 4

Entangling atoms with squeezed light

This Chapter investigates the effect of squeezed light on two separated two-level atoms, under a number of simplifying assumptions. We consider two methods of generating spatially entangled light beams. The steady state of the atoms is solved, and their degree of entanglement is quantified. The relevance of these systems for investigating violations of Bell inequalities is examined. Finally, the dynamics of their evolution are investigated using the entropy-entanglement plane.

Contents

4.1 Introduction

Palma and Knight showed in 1989 [2] (see also [68]) that two closely spaced atoms bathed in a broadband squeezed vacuum exhibit population decay that is sensitive to the squeezing. They noted that, in a two-atom system, the populations can change through a two-photon absorption or emission, in a manner that is not possible for a single atom. They also showed that the atoms relax to a pure equilibrium state in which the two atoms are either both excited or both in their ground states. This state is far from thermal equilibrium because phase-sensitive correlations are transferred from the reservoir to the atomic system.

In their paper they calculated the steady state interatomic dipole correlation function, for two atoms interacting with squeezed vacuum characterized by the degree and purity of squeezing N and M, to be

$$S(\infty) = \frac{2M}{2N+1}, \tag{4.1a}$$

where

$$S(t) = \left\langle \sigma_1^+(t)\sigma_2^+(t) + \sigma_1^-(t)\sigma_2^-(t) \right\rangle. \tag{4.1b}$$

This shows that the final atomic state contains internal correlations for non-zero M. They found the steady state to be pure, and of the form

$$|\psi_{ss}\rangle = \cos\theta\,|00\rangle + \sin\theta\,|11\rangle, \tag{4.2a}$$

where

$$\cos\theta = \sqrt{\frac{N+1}{2N+1}}, \tag{4.2b}$$

$$\sin\theta = \sqrt{\frac{N}{2N+1}}. \tag{4.2c}$$

Here $|0\rangle$ and $|1\rangle$ refer to the ground and excited states, respectively, of each atom.

This effect was explored further by Ekert *et al.* [69] who showed that dissipative relaxation into a squeezed reservoir by more general systems such as atoms or harmonic oscillators leads to a pure final state. Also, a system of N identical two-level atoms interacting with broadband squeezed radiation was investigated by Agarwal and Puri [70]. They found that, when N is even, the atoms relax into a pure, highly correlated state.

In this Chapter, we investigate the generation of such atomic spin-squeezed states in a pair of separated atoms. We consider two different methods to generate light fields that exhibit quantum correlations between the two spatially distinct modes that are incident on the atoms. The first method is to produce multi-mode squeezed light using a non-degenerate parametric amplifier (NDPA), where the spatially distinct output modes already contain correlated photon pairs. Alternatively, we may take the output field from a degenerate parametric amplifier (DPA) and pass it through a beam-splitter. This will produce two spatially distinct fields with the correlations between them weakened by the introduction of vacuum noise.

In both models we assume a resonant coupling between two relevant atomic states and the squeezed light field incident on each atom. Two major assumptions are made:

1. The squeezing bandwidth of the incident light fields is large compared to the linewidth of the excited states of the atoms.

2. The atoms couple only to their specified input fields.

A practical method of satisfying these conditions will be considered in Chapter 5.

4.2 Model for atoms driven by the NDPA

In this Section we consider the effect on the atoms of squeezed light as produced by the NDPA. The related system, where we pass the output of the DPA through a beamsplitter to drive the atoms, is considered in Section 4.3.

The cascaded quantum systems are defined such that system 1 is the DPA or NDPA and systems 2 and 3 are the two two-level atoms. The subscripts 1, 2 and 3 are used to refer to operators in the spaces of the above systems. The identifiers f and g are used to refer to input and output fields and h is used for vacuum fields introduced by a beam splitter.

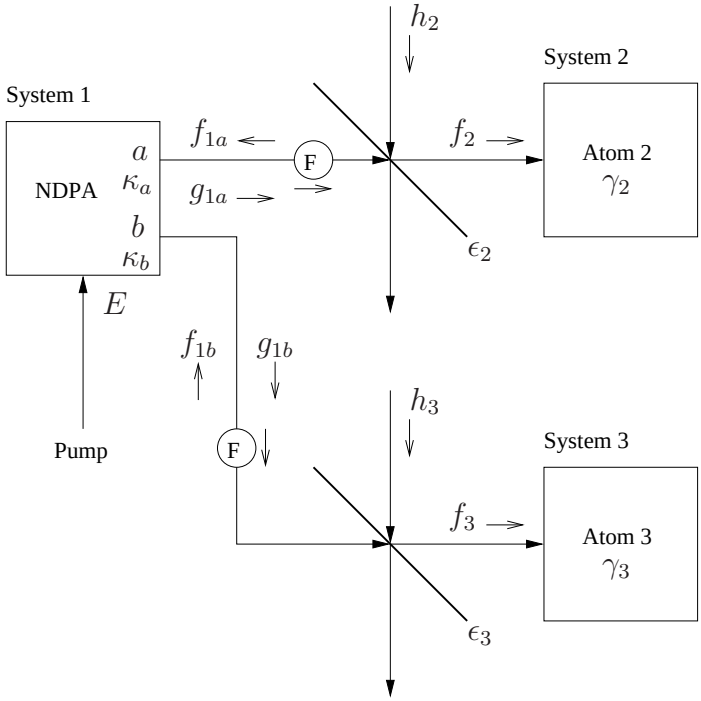

Figure 4.1: Driving two atoms with the NDPA. See the text for the definitions of the identifiers.

4.2.1 Schematic

A schematic of the setup for the NDPA is shown in Figure 4.1. The squeezed output modes from an NDPA are distributed to two spatially separated atoms. Faraday isolators are used to create a uni-directional coupling to the atoms, so that we have a cascaded quantum system. Imperfect coupling between the squeezed modes and the atoms is modelled by two beam splitters. The effect of the imperfect coupling is to introduce a vacuum component into the squeezing seen by the atoms.

The definitions used in Figure 4.1 are:

1. E is a parameter describing the pump strength and interaction in the parametric amplifier.

2. h_2 and h_3 are vacuum input fields introduced by inefficient coupling to the atoms.

3. γ_2 and γ_3 are the linewidths of the atomic transitions for atoms 2 and 3.

4. ω_2 and ω_3 are the frequencies of the atomic transitions for atoms 2 and 3.

5. f_2 and f_3 are the input fields that interact with atoms 2 and 3.

6. ϵ_2 and ϵ_3 are the efficiencies of the couplings of the input fields to atoms 2 and 3.

7. a and b are the signal and idler modes of the NDPA.

8. f_{1a} and g_{1a} are the input and output fields that interact with mode a.

9. f_{1b} and g_{1b} are the input and output fields that interact with mode b.

10. κ_a and κ_b are the decay rates of the NDPA signal and idler modes.

4.2.2 Reduced master equation

The steps required to derive a master equation for the atomic systems alone are:

1. Write quantum Langevin equations for the 3 systems (QLEs).

2. Combine them into one QLE for the combined system.

3. Convert the QLE to a quantum Ito equation.

4. Convert the quantum Ito equation to a master equation for the combined system comprising the parametric amplifier and the atoms.

5. By using a generalized positive-P representation for the modes of the parametric amplifier, reduce the master equation to the atomic systems alone, but with stochastic noise terms.

6. Use a cumulant expansion to second order to average over the noise terms.

The derivation of the master equation is detailed in Appendix A.

The reduced master equation for the atomic systems alone is

$$\begin{aligned}
\frac{d\rho}{dt} &= \frac{1}{2}\gamma_2\left(2\sigma_2^-\rho\sigma_2^+ - \sigma_2^+\sigma_2^-\rho - \rho\sigma_2^+\sigma_2^-\right) \\
&+\frac{1}{2}\gamma_3\left(2\sigma_3^-\rho\sigma_3^+ - \sigma_3^+\sigma_3^-\rho - \rho\sigma_3^+\sigma_3^-\right) \\
&+\frac{1}{2}\gamma_2\epsilon_2 N\left(2\sigma_2^-\rho\sigma_2^+ - \sigma_2^+\sigma_2^-\rho - \rho\sigma_2^+\sigma_2^-\right) \\
&+\frac{1}{2}\gamma_2\epsilon_2 N\left(2\sigma_2^+\rho\sigma_2^- - \sigma_2^-\sigma_2^+\rho - \rho\sigma_2^-\sigma_2^+\right) \\
&+\frac{1}{2}\gamma_3\epsilon_3 N\left(2\sigma_3^-\rho\sigma_3^+ - \sigma_3^+\sigma_3^-\rho - \rho\sigma_3^+\sigma_3^-\right) \\
&+\frac{1}{2}\gamma_3\epsilon_3 N\left(2\sigma_3^+\rho\sigma_3^- - \sigma_3^-\sigma_3^+\rho - \rho\sigma_3^-\sigma_3^+\right) \\
&-\frac{1}{2}\sqrt{\gamma_2\gamma_3\epsilon_2\epsilon_3}M\left(2\sigma_2^+\rho\sigma_3^+ - \sigma_3^+\sigma_2^+\rho - \rho\sigma_3^+\sigma_2^+\right) \\
&-\frac{1}{2}\sqrt{\gamma_2\gamma_3\epsilon_2\epsilon_3}M\left(2\sigma_3^+\rho\sigma_2^+ - \sigma_2^+\sigma_3^+\rho - \rho\sigma_2^+\sigma_3^+\right) \\
&-\frac{1}{2}\sqrt{\gamma_2\gamma_3\epsilon_2\epsilon_3}M\left(2\sigma_2^-\rho\sigma_3^- - \sigma_3^-\sigma_2^-\rho - \rho\sigma_3^-\sigma_2^-\right) \\
&-\frac{1}{2}\sqrt{\gamma_2\gamma_3\epsilon_2\epsilon_3}M\left(2\sigma_3^-\rho\sigma_2^- - \sigma_2^-\sigma_3^-\rho - \rho\sigma_2^-\sigma_3^-\right), \qquad (4.3a)
\end{aligned}$$

where

$$N = \left(\frac{E^2\kappa_a\kappa_b}{{\lambda_1}^2{\lambda_2}^2}\right), \qquad (4.3b)$$

$$M = \sqrt{\kappa_a\kappa_b}\,E\left(\frac{E^2+\frac{\kappa_a\kappa_b}{4}}{{\lambda_1}^2{\lambda_2}^2}\right), \qquad (4.3c)$$

$$\lambda_{1,2} = \frac{1}{2}\left\{-\frac{1}{2}(\kappa_a+\kappa_b) \pm \sqrt{\frac{1}{4}(\kappa_a-\kappa_b)^2+4E^2}\right\}. \qquad (4.3d)$$

We have taken E and M to be real.

4.2.3 Symmetric case

For all subsequent work based on Equation (4.3a) we will consider the symmetrical situation where

$$\gamma \equiv \gamma_2 = \gamma_3, \qquad (4.4a)$$

$$\epsilon \equiv \epsilon_2 = \epsilon_3. \qquad (4.4b)$$

These simplifications allow us to write the master equation more compactly as

$$\begin{aligned}\frac{d\rho}{dt} &= +\frac{\gamma}{2}\left(N'+1\right)\left(2\sigma_2^-\rho\sigma_2^+ - \sigma_2^+\sigma_2^-\rho - \rho\sigma_2^+\sigma_2^-\right)\\ &\quad +\frac{\gamma}{2}N'\left(2\sigma_2^+\rho\sigma_2^- - \sigma_2^-\sigma_2^+\rho - \rho\sigma_2^-\sigma_2^+\right)\\ &\quad +\frac{\gamma}{2}\left(N'+1\right)\left(2\sigma_3^-\rho\sigma_3^+ - \sigma_3^+\sigma_3^-\rho - \rho\sigma_3^+\sigma_3^-\right)\\ &\quad +\frac{\gamma}{2}N'\left(2\sigma_3^+\rho\sigma_3^- - \sigma_3^-\sigma_3^+\rho - \rho\sigma_3^-\sigma_3^+\right)\\ &\quad -\frac{\gamma}{2}M'\left(2\sigma_2^+\rho\sigma_3^+ - \sigma_3^+\sigma_2^+\rho - \rho\sigma_3^+\sigma_2^+\right)\\ &\quad -\frac{\gamma}{2}M'\left(2\sigma_3^+\rho\sigma_2^+ - \sigma_2^+\sigma_3^+\rho - \rho\sigma_2^+\sigma_3^+\right)\\ &\quad -\frac{\gamma}{2}M'\left(2\sigma_2^-\rho\sigma_3^- - \sigma_3^-\sigma_2^-\rho - \rho\sigma_3^-\sigma_2^-\right)\\ &\quad -\frac{\gamma}{2}M'\left(2\sigma_3^-\rho\sigma_2^- - \sigma_2^-\sigma_3^-\rho - \rho\sigma_2^-\sigma_3^-\right). \end{aligned} \tag{4.5a}$$

We have defined rescaled squeezing parameters which include the inefficient coupling:

$$N' = \epsilon N, \tag{4.5b}$$

$$M' = \epsilon M. \tag{4.5c}$$

The first four lines of Equation (4.5a) describe the interaction of each atom individually with a thermal field characterized by a mean photon number N'. The last four lines describe a two-photon interaction with correlated photons from the two output modes of the NDPA.

4.2.4 Steady state solution

We are interested in examining the steady state of the atoms with a view to establishing whether they become entangled, and whether they are suitable for experiments demonstrating violations of Bell inequalities. In this Thesis we find the steady state for a number of two-qubit master equations so the steps in this process have been automated (see Appendix B for details). We find that the steady state solution of Equation (4.5), in the basis $\{|11\rangle, |10\rangle, |01\rangle, |00\rangle\}$, is

$$\rho_{ss} = \begin{pmatrix} a & 0 & 0 & d \\ 0 & b & 0 & 0 \\ 0 & 0 & b & 0 \\ d & 0 & 0 & c \end{pmatrix}, \tag{4.6a}$$

where

$$a = \frac{M'^2(1-2N') + N'^2(1+2N')}{(1+2N')\left((1+2N')^2 - 4M'^2\right)}, \tag{4.6b}$$

$$b = \frac{N'(1+N') - M'^2}{(1+2N')^2 - 4M'^2}, \tag{4.6c}$$

$$c = 1 - a - 2b, \tag{4.6d}$$

$$d = \frac{M'}{(1+2N')\left((1+2N')^2 - 4M'^2\right)}. \tag{4.6e}$$

The single off-diagonal term d is responsible for any entanglement in the steady state. It is significant that it is (approximately) proportional to M', thus the greater the purity of squeezing the more entangled we expect the state to be. The range of steady states produced is graphically examined in Section 4.6.

When we have $\epsilon = 1$ and ideal squeezing, i.e., $M^2 = N(1+N)$, we obtain the pure state

$$a = \frac{N}{1+2N}, \tag{4.7a}$$

$$b = 0, \tag{4.7b}$$

$$c = 1 - a - 2b = \frac{1+N}{1+2N}, \tag{4.7c}$$

$$d = \frac{\sqrt{N(1+N)}}{1+2N}, \tag{4.7d}$$

with corresponding density matrix

$$\rho_{ss} = \frac{1}{1+2N}\begin{pmatrix} N & 0 & 0 & M \\ 0 & 0 & 0 & 0 \\ 0 & 0 & 0 & 0 \\ M & 0 & 0 & 1+N \end{pmatrix}. \tag{4.7e}$$

We may write ρ_{ss} as the pure state $|\psi\rangle\langle\psi|$ where

$$|\psi\rangle = \sqrt{\frac{N}{1+2N}}\,|11\rangle + \sqrt{\frac{N+1}{1+2N}}\,|00\rangle\,. \tag{4.8}$$

This is the identical state to that found by Palma and Knight for two closely spaced atoms (Dicke system) in a broadband squeezed vacuum (4.2). It is significant that a pure state still arises in our model which does not have a collective coupling of the atoms to the squeezed reservoir. The state $|\psi\rangle$ approximates the Bell state $|\phi^+\rangle$ (1.2) as N becomes large.

In the case of $\epsilon = 1$ and no squeezing ($M = 0$) we obtain the mixed diagonal state

$$a = \frac{N^2}{(1+2N)^2}, \tag{4.9a}$$
$$b = \frac{N(1+N)}{(1+2N)^2}, \tag{4.9b}$$
$$c = 1 - a - 2b, \tag{4.9c}$$
$$d = 0, \tag{4.9d}$$

with corresponding density matrix

$$\rho_{ss} = \frac{1}{(1+2N)^2} \begin{pmatrix} N^2 & 0 & 0 & 0 \\ 0 & N(1+N) & 0 & 0 \\ 0 & 0 & N(1+N) & 0 \\ 0 & 0 & 0 & (1+N)^2 \end{pmatrix}. \tag{4.9e}$$

This is the state we would expect to obtain when driving the atoms with thermal light characterized by a mean photon number N.

4.3 Model for atoms driven by the DPA

In this Section we model the effect on two separated atoms of the entangled light that is produced by a DPA after passage through a beam splitter. With this method of generating entangled light beams, the quantum correlations are degraded by mixing with ordinary vacuum, but are still of interest. It is known that a single-mode squeezed state (such as is produced by the DPA) incident on a beam-splitter yields a bipartite entangled state, and that a single-mode squeezed state, distributed among N parties using linear optics, can generate N-partite entanglement [71]. Since the light remains entangled we can hope that it will still remain useful for entangling atoms.

4.3.1 Schematic

A schematic of the setup for the DPA is shown in Figure 4.2. A beam splitter is used to split the output mode of the DPA into two modes with non-classical correlations between them. Faraday isolators are again used to create a unidirectional coupling to the atoms. Inefficient coupling between the squeezed modes and the atoms is modelled by a further two beam splitters.

The definitions used in Figure 4.2 are:

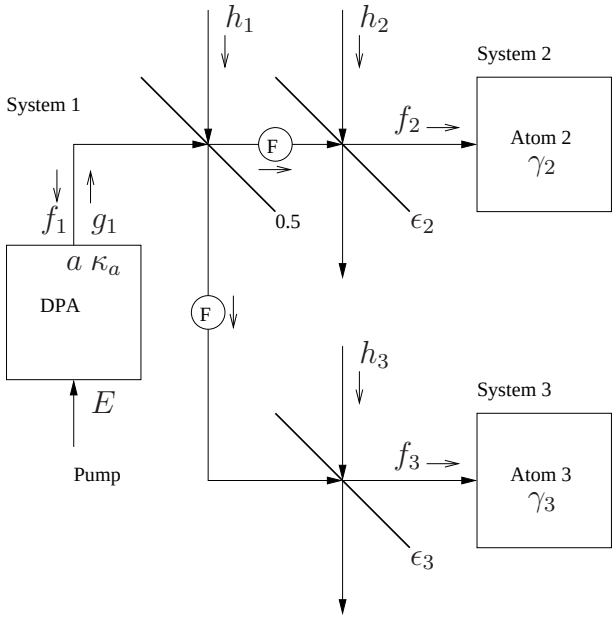

Figure 4.2: Driving two atoms with a DPA. See the text for the definitions of the identifiers.

1. E is a parameter describing the pump strength and interaction in the parametric amplifier.
2. h_2 and h_3 are vacuum input fields introduced by inefficient coupling to the atoms.
3. γ_2 and γ_3 are the linewidths of the atomic transitions for atoms 2 and 3.
4. ω_2 and ω_3 are the frequencies of the atomic transitions for atoms 2 and 3.
5. f_2 and f_3 are the input fields that interact with atoms 2 and 3.
6. ϵ_2 and ϵ_3 are the efficiencies of the couplings of the input fields to atoms 2 and 3.
7. a is the output mode of the DPA.
8. f_1 and g_1 are the input and output fields that interact with mode a.
9. κ_a is the decay rate of the DPA signal mode.
10. h_1 is a vacuum input field introduced by the first beam splitter.

4.3.2 Reduced master equation

We follow the same steps as described in Section 4.2.2 to obtain a master equation for the atomic systems alone. The details of the derivation of this master equation may be found in Appendix A.

The master equation is

$$\begin{aligned}
\frac{d\rho}{dt} &= \frac{1}{2}\gamma_2\left(2\sigma_2^-\rho\sigma_2^+ - \sigma_2^+\sigma_2^-\rho - \rho\sigma_2^+\sigma_2^-\right) \\
&+\frac{1}{2}\gamma_3\left(2\sigma_3^-\rho\sigma_3^+ - \sigma_3^+\sigma_3^-\rho - \rho\sigma_3^+\sigma_3^-\right) \\
&+\frac{1}{4}\gamma_2\epsilon_2 N\left(2\sigma_2^-\rho\sigma_2^+ - \sigma_2^+\sigma_2^-\rho - \rho\sigma_2^+\sigma_2^-\right) \\
&+\frac{1}{4}\gamma_2\epsilon_2 N\left(2\sigma_2^+\rho\sigma_2^- - \sigma_2^-\sigma_2^+\rho - \rho\sigma_2^-\sigma_2^+\right) \\
&+\frac{1}{4}\gamma_3\epsilon_3 N\left(2\sigma_3^-\rho\sigma_3^+ - \sigma_3^+\sigma_3^-\rho - \rho\sigma_3^+\sigma_3^-\right) \\
&+\frac{1}{4}\gamma_3\epsilon_3 N\left(2\sigma_3^+\rho\sigma_3^- - \sigma_3^-\sigma_3^+\rho - \rho\sigma_3^-\sigma_3^+\right) \\
&+\frac{1}{4}\sqrt{\gamma_2\gamma_3\epsilon_2\epsilon_3}N\left(2\sigma_2^-\rho\sigma_3^+ - \sigma_3^+\sigma_2^-\rho - \rho\sigma_3^+\sigma_2^-\right) \\
&+\frac{1}{4}\sqrt{\gamma_2\gamma_3\epsilon_2\epsilon_3}N\left(2\sigma_2^+\rho\sigma_3^- - \sigma_3^-\sigma_2^+\rho - \rho\sigma_3^-\sigma_2^+\right) \\
&+\frac{1}{4}\sqrt{\gamma_2\gamma_3\epsilon_2\epsilon_3}N\left(2\sigma_3^-\rho\sigma_2^+ - \sigma_2^+\sigma_3^-\rho - \rho\sigma_2^+\sigma_3^-\right) \\
&+\frac{1}{4}\sqrt{\gamma_2\gamma_3\epsilon_2\epsilon_3}N\left(2\sigma_3^+\rho\sigma_2^- - \sigma_2^-\sigma_3^+\rho - \rho\sigma_2^-\sigma_3^+\right) \\
&-\frac{1}{4}\gamma_2\epsilon_2 M\left(2\sigma_2^+\rho\sigma_2^+ - \sigma_2^+\sigma_2^+\rho - \rho\sigma_2^+\sigma_2^+\right) \\
&-\frac{1}{4}\gamma_2\epsilon_2 M\left(2\sigma_2^-\rho\sigma_2^- - \sigma_2^-\sigma_2^-\rho - \rho\sigma_2^-\sigma_2^-\right) \\
&-\frac{1}{4}\gamma_3\epsilon_3 M\left(2\sigma_3^+\rho\sigma_3^+ - \sigma_3^+\sigma_3^+\rho - \rho\sigma_3^+\sigma_3^+\right) \\
&-\frac{1}{4}\gamma_3\epsilon_3 M\left(2\sigma_3^-\rho\sigma_3^- - \sigma_3^-\sigma_3^-\rho - \rho\sigma_3^-\sigma_3^-\right) \\
&-\frac{1}{4}\sqrt{\gamma_2\gamma_3\epsilon_2\epsilon_3}M\left(2\sigma_2^+\rho\sigma_3^+ - \sigma_3^+\sigma_2^+\rho - \rho\sigma_3^+\sigma_2^+\right) \\
&-\frac{1}{4}\sqrt{\gamma_2\gamma_3\epsilon_2\epsilon_3}M\left(2\sigma_3^+\rho\sigma_2^+ - \sigma_2^+\sigma_3^+\rho - \rho\sigma_2^+\sigma_3^+\right) \\
&-\frac{1}{4}\sqrt{\gamma_2\gamma_3\epsilon_2\epsilon_3}M\left(2\sigma_2^-\rho\sigma_3^- - \sigma_3^-\sigma_2^-\rho - \rho\sigma_3^-\sigma_2^-\right) \\
&-\frac{1}{4}\sqrt{\gamma_2\gamma_3\epsilon_2\epsilon_3}M\left(2\sigma_3^-\rho\sigma_2^- - \sigma_2^-\sigma_3^-\rho - \rho\sigma_2^-\sigma_3^-\right), \qquad (4.10a)
\end{aligned}$$

where

$$N = \left(\frac{E^2\kappa_a^2}{{\lambda_1}^2{\lambda_2}^2}\right), \tag{4.10b}$$

$$M = \kappa_a E\left(\frac{E^2+\frac{\kappa_a^2}{4}}{{\lambda_1}^2{\lambda_2}^2}\right), \tag{4.10c}$$

$$\lambda_{1,2} = -\frac{\kappa_a}{2} \pm E. \tag{4.10d}$$

In this model, E and M are again taken to be real.

4.3.3 Symmetric case

Consider the symmetrical situation where

$$\gamma \equiv \gamma_2 = \gamma_3, \tag{4.11a}$$

$$\epsilon \equiv \epsilon_2 = \epsilon_3. \tag{4.11b}$$

Then the master equation (4.10) can be written compactly as

$$\begin{aligned}\frac{d\rho}{dt} = &+\frac{\gamma}{2}\left(2\sigma_2^-\rho\sigma_2^+ - \sigma_2^+\sigma_2^-\rho - \rho\sigma_2^+\sigma_2^-\right)\\ &+\frac{\gamma}{2}\left(2\sigma_3^-\rho\sigma_3^+ - \sigma_3^+\sigma_3^-\rho - \rho\sigma_3^+\sigma_3^-\right)\\ &+\frac{\gamma}{2}N'\left(2S\rho S^\dagger - S^\dagger S\rho - \rho S^\dagger S\right)\\ &+\frac{\gamma}{2}N'\left(2S^\dagger\rho S - SS^\dagger\rho - \rho SS^\dagger\right)\\ &-\frac{\gamma}{2}M'\left(2S^\dagger\rho S^\dagger - S^\dagger S^\dagger\rho - \rho S^\dagger S^\dagger\right)\\ &-\frac{\gamma}{2}M'\left(2S\rho S - SS\rho - \rho SS\right).\end{aligned} \tag{4.12a}$$

We have defined rescaled parameters which incorporate the inefficient coupling

$$N' = \epsilon N, \tag{4.12b}$$

$$M' = \epsilon M, \tag{4.12c}$$

and collective operators

$$S = \frac{1}{\sqrt{2}}\left(\sigma_2^- + \sigma_3^-\right), \tag{4.12d}$$

$$S^\dagger = \frac{1}{\sqrt{2}}\left(\sigma_2^+ + \sigma_3^+\right). \tag{4.12e}$$

The first two lines of Equation (4.12) represent non-collective spontaneous emission by each atom into distinct reservoirs. The stimulated emission and absorption terms in N' and M' show a collective interaction with the squeezed light field.

4.3.4 Steady state solution

The steady state solution, in the basis $\{|11\rangle, |10\rangle, |01\rangle, |00\rangle\}$, is

$$\rho_{ss} = \begin{pmatrix} a & 0 & 0 & d \\ 0 & b & e & 0 \\ 0 & e & b & 0 \\ d & 0 & 0 & c \end{pmatrix}, \tag{4.13a}$$

where

$$a = \frac{M'^2(1-2N') + 2N'^2(1+N')}{4\left(1+N'\right)\left(1-2M'^2+3N'+2N'^2\right)}, \tag{4.13b}$$

$$b = \frac{2N'(1+N')^2 - M'^2(1+2N')}{4\left(1+N'\right)\left(1-2M'^2+3N'+2N'^2\right)}, \tag{4.13c}$$

$$c = 1-a-2b, \tag{4.13d}$$

$$d = \frac{2M'}{4\left(1+N'\right)\left(1-2M'^2+3N'+2N'^2\right)}, \tag{4.13e}$$

$$e = \frac{2N'\left(N'+1\right)-2M'^2}{4\left(1+N'\right)\left(1-2M'^2+3N'+2N'^2\right)}. \tag{4.13f}$$

When we have $\epsilon = 1$ and ideal squeezing, i.e., $M^2 = N(1+N)$, we obtain

$$a = b = \frac{N}{4(1+N)}, \tag{4.14a}$$

$$c = \frac{4+N}{4(1+N)}, \tag{4.14b}$$

$$d = \frac{\sqrt{N(1+N)}}{2(1+N)^2}, \tag{4.14c}$$

$$e = 0. \tag{4.14d}$$

As we may expect, this is not a pure state due to the vacuum noise admitted to the system by the initial beamsplitter.

4.4 Entanglement

We now have calculated the steady state solutions for both of our models. In this Section we investigate the degree of entanglement that is present in the atoms.

4.4.1 Regime of separability

It is of interest to calculate the parameter regime in N' and M' for which the steady state density matrix is entangled. The separability criterion of Peres [39] is that the state is separable when the smallest eigenvalue of the partial transpose of the density matrix is non-negative (see Section 2.2). For the NDPA, separability occurs whenever

$$M \leq M_{sep} = \frac{-1 + \sqrt{1 + 4N'\left(1 + N'\right)\left(1 + 2N'\right)^2}}{2\epsilon\left(1 + 2N'\right)}, \tag{4.15}$$

and, for the DPA, separability occurs whenever

$$M \leq M_{sep} = \frac{-1 + \sqrt{1 + 2N'\left(1 + N'\right)^2\left(1 + 2N'\right)}}{\epsilon\left(1 + 2N'\right)}. \tag{4.16}$$

A graph of M_{sep} versus N was plotted for $\epsilon = 1$ (see Figure 4.3). It should be kept in mind when examining this Figure, that values of M greater than

$$M_{ideal} = \sqrt{N\left(N + 1\right)} \tag{4.17}$$

are not physically possible. The area between the M_{sep} and M_{ideal} lines represents that part of the parameter space where the steady state density matrix is non-separable. With the NDPA it is always possible to generate entangled states, for any value of N. For the DPA, however, a maximum value for N exists (≈ 1.6) above which it is not possible to generate entangled states.

4.4.2 Entanglement for ideal squeezing

With the NDPA, and for ideal squeezing ($M^2 = N(N+1)$), the steady state density matrix is

$$\rho_{ss} = \frac{1}{1 + 2N}\begin{pmatrix} N & 0 & 0 & M \\ 0 & 0 & 0 & 0 \\ 0 & 0 & 0 & 0 \\ M & 0 & 0 & 1 + N \end{pmatrix}. \tag{4.18}$$

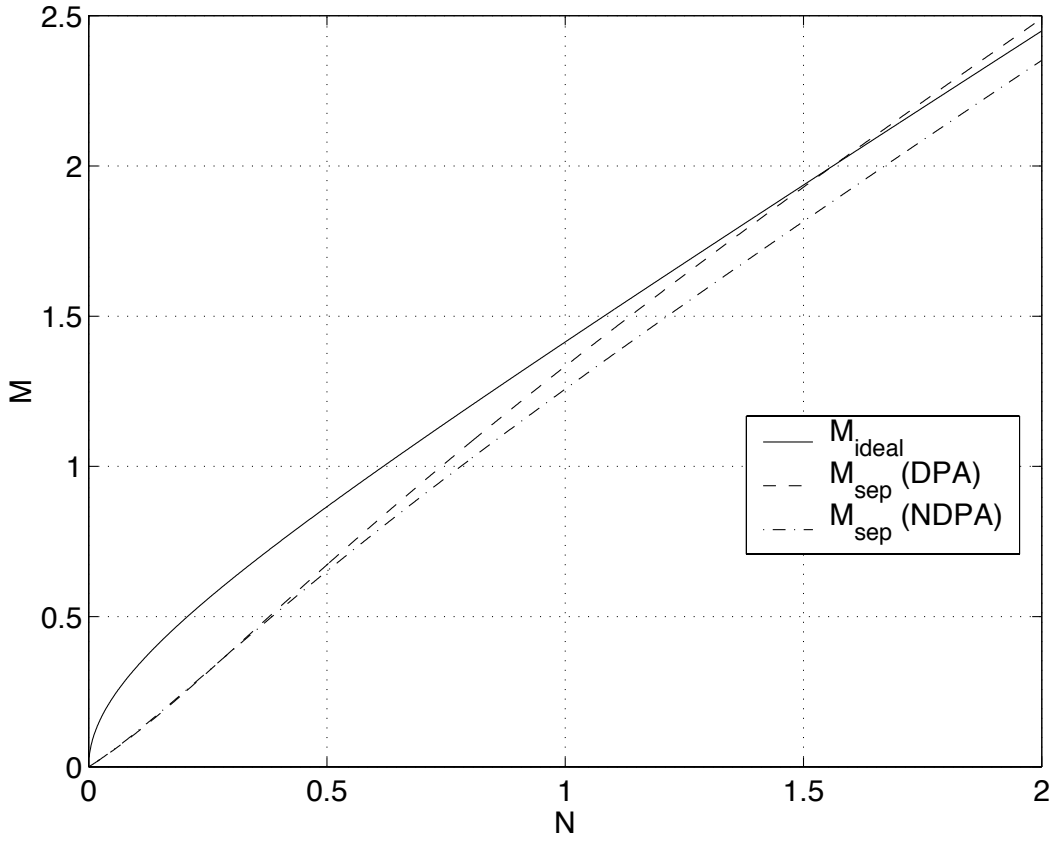

Figure 4.3: M_{sep} as a function of N, for $\epsilon = 1$, plotted for both the NDPA and DPA models. The upper solid line represents the maximum possible value of M for any given N, defined as $M_{ideal} = \sqrt{N\,(N+1)}$.

As we have seen, this corresponds to the pure state

$$|\psi\rangle \;=\; \sqrt{\frac{N}{1+2N}}\,|11\rangle + \sqrt{\frac{N+1}{1+2N}}\,|00\rangle\,. \tag{4.19}$$

As a measure of the entanglement in the system we may calculate the concurrence (see Section 2.3.2). For a pure state this is easily done using the spin-flipped state

$$\left|\tilde{\psi}\right\rangle \;=\; (\sigma_y \otimes \sigma_y)\,|\psi^*\rangle\,. \tag{4.20}$$

The concurrence is then

$$\mathcal{C}(\psi) = \left|\left\langle \psi|\tilde{\psi}\right\rangle\right|. \tag{4.21}$$

For the NDPA, with ideal squeezing, we obtain for the concurrence

$$\mathcal{C}(\psi) = \frac{2M}{1+2N}. \tag{4.22}$$

Note that in the situation of strong ideal squeezing, we have $M \to N + \frac{1}{2}$, and so the concurrence tends to $\mathcal{C}(\psi) = 1$. This is the value which we expect for the resulting Bell state.

4.4.3 Entanglement for general squeezing

For general squeezing, in models using both the DPA and NDPA, we do not have a pure state so the concurrence is calculated from the steady state following the approach of Wootters [30] (see Section 2.3.2). From our solution for the steady state density matrix, which may be written in the same form for both the NDPA and DPA cases,

$$\rho_{ss} = \begin{pmatrix} a & 0 & 0 & d \\ 0 & b & e & 0 \\ 0 & e & b & 0 \\ d & 0 & 0 & c \end{pmatrix}, \tag{4.23}$$

we obtain for the NDPA (for which $e = 0$),

$$\mathcal{C}(\rho_{ss}) = \max\{0, 2d - 2b\}\,, \tag{4.24}$$

and for the DPA,

$$\mathcal{C}(\rho_{ss}) = \begin{cases} \max\{0, 2d-2b\}\,, & d + \sqrt{ac} > b + e \\ 0, & d + \sqrt{ac} \le b + e \end{cases}. \tag{4.25}$$

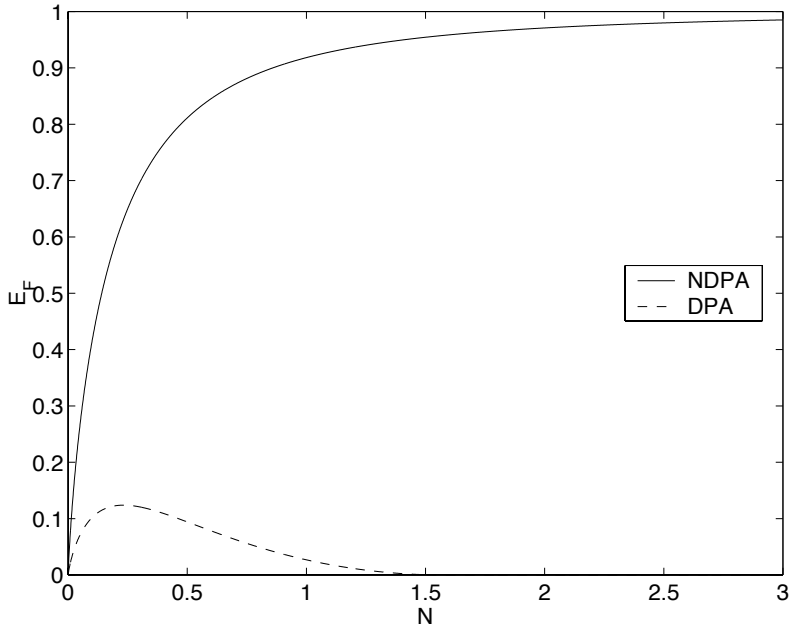

Figure 4.4: The entanglement of formation, E_F, as a function of N for ideal squeezing and $\epsilon = 1$. Results for both the NDPA and DPA are plotted.

The entanglement of formation may be calculated from the concurrence using (2.9)

$$E_F\left(\mathcal{C}\right) = h\left(\frac{1+\sqrt{1-\mathcal{C}^2}}{2}\right). \tag{4.26}$$

A graph of the entanglement of formation versus N was plotted for $\epsilon = 1$ (see Figure 4.4). This graph shows how the NDPA can produce strong entanglement in the atoms, tending asymptotically to 1 in the limit of large N, whereas the DPA produces only weak entanglement, and only for a limited range of N.

4.5 Bell's inequality

We have found conditions for the two atoms to be entangled. We may also consider the (different) regime in which they violate the standard Bell's inequality. An alternative description of the CHSH inequality to that given in Section 2.4 is

$$-2 \leq B \leq 2, \tag{4.27a}$$

with the definitions

$$\begin{aligned} S_i(\phi_i) &= \cos(\phi_i)\left\{|0\rangle\langle 0|_i - |1\rangle\langle 1|_i\right\} \\ &\quad + \sin(\phi_i)\left\{|0\rangle\langle 1|_i + |1\rangle\langle 0|_i\right\}, \qquad (4.27b) \\ E(\phi_1,\phi_2) &= \langle S_1(\phi_1)\otimes S_2(\phi_2)\rangle, \qquad (4.27c) \end{aligned}$$

and

$$\begin{aligned} B(\phi_1,\phi_2,\theta_1,\theta_2) &= E(\phi_1,\phi_2) - E(\phi_1,\theta_2) \\ &\quad + E(\theta_1,\phi_2) + E(\theta_1,\theta_2). \qquad (4.27d) \end{aligned}$$

The angles ϕ_1, ϕ_2, θ_1 and θ_2 are the analyzer angles of the detection apparatus.

Again using our notation for the steady state density matrix, which applies for both the NDPA and DPA cases,

$$\rho_{ss} = \begin{pmatrix} a & 0 & 0 & d \\ 0 & b & e & 0 \\ 0 & e & b & 0 \\ d & 0 & 0 & c \end{pmatrix}, \qquad (4.28)$$

we obtain the expression

$$\begin{aligned} \langle S_1(\phi_1)\otimes S_2(\phi_2)\rangle &= (1-4b)\cos(\phi_1)\cos(\phi_2) \\ &\quad + 2(d+e)\sin(\phi_1)\sin(\phi_2). \qquad (4.29) \end{aligned}$$

Stationary points of B are found when the following are satisfied,

$$\begin{aligned} \tan(\theta_1)\tan(\phi_1) &= \frac{4(d+e)^2}{(1-4b)^2}, \qquad (4.30a) \\ \tan(\phi_2) &= \frac{2(d+e)}{1-4b}\tan\left(\frac{\phi_1+\theta_1}{2}\right), \qquad (4.30b) \\ \tan(\theta_2)\tan(\phi_2) &= -\frac{4(d+e)^2}{(1-4b)^2}, \qquad (4.30c) \\ \tan(\phi_1) &= \frac{2(d+e)}{1-4b}\cot\left(\frac{\phi_2+\theta_2}{2}\right), \qquad (4.30d) \end{aligned}$$

and a stationary point B_{max} (maximum taken over all analyzer angles) occurs when

$$\begin{aligned} \phi_1 &= -\pi/2, \qquad (4.31a) \\ \phi_2 &= \tan^{-1}\left(\frac{-2(d+e)}{1-4b}\right), \qquad (4.31b) \\ \theta_1 &= 0, \qquad (4.31c) \\ \theta_2 &= -\phi_2. \qquad (4.31d) \end{aligned}$$

We obtain the general solution for the maximum violation of the CHSH inequality

$$B_{max}(\rho_{ss}) = 2\left[(1-4b)^2 + 4(d+e)^2\right]^{1/2}. \tag{4.32}$$

We see immediately that large values of b (it has a maximum possible value of $1/4$) reduce B_{max} as expected for a highly mixed state. Also, with b small and $d+e$ large (i.e., significant off-diagonal terms) we obtain $|B_{max}| > 2$ and a violation of the CHSH inequality.

In an alternative derivation, we have calculated $B_{max}(\rho)$ using the technique described in Section 2.4. We can express our general steady state density matrix (4.28) as the simple form

$$\begin{aligned} 4\rho_{ss} &= \mathbf{1}_2 \otimes \mathbf{1}_2 \\ &\quad +(2a+2b-1)\ \sigma_z \otimes \mathbf{1}_2 \\ &\quad +(2a+2b-1)\ \mathbf{1}_2 \otimes \sigma_z \\ &\quad +2(d+e)\ \sigma_x \otimes \sigma_x \\ &\quad -2(d+e)\ \sigma_y \otimes \sigma_y \\ &\quad +(1-4b)\ \sigma_z \otimes \sigma_z. \end{aligned} \tag{4.33}$$

This alternative approach leads immediately to the result (4.32).

From Equation (4.32) we may calculate explicit expressions for the value of B_{max} in terms of the squeezing parameters N' and M'. For the NDPA we have

$$B_{max}(N', M') = \frac{2\left[(1+2N')^2 + 4M'^2\right]^{1/2}}{(1+2N')\left[(1+2N')^2 - 4M'^2\right]}, \tag{4.34}$$

and for the DPA

$$B_{max}(N', M') = \frac{2(1+N'-M')\left[(1+N'+M')^2 + (N'+M')^2\right]^{1/2}}{(1+N')\left[(1+N')(1+2N') - 2M'^2\right]}. \tag{4.35}$$

With these expressions we can identify the behaviour in selected regimes. For the NDPA, in the case of $\epsilon = 1$ and ideal squeezing, we have

$$B_{max}(N) = \frac{2(1+8N+8N^2)^{1/2}}{1+2N} \geq 2. \tag{4.36}$$

For $N > 0$ we find B_{max} is always greater than 2 so the CHSH inequality is always violated. As $N \to \infty$ we find $B_{max} \to 2\sqrt{2}$ - the maximal violation possible.

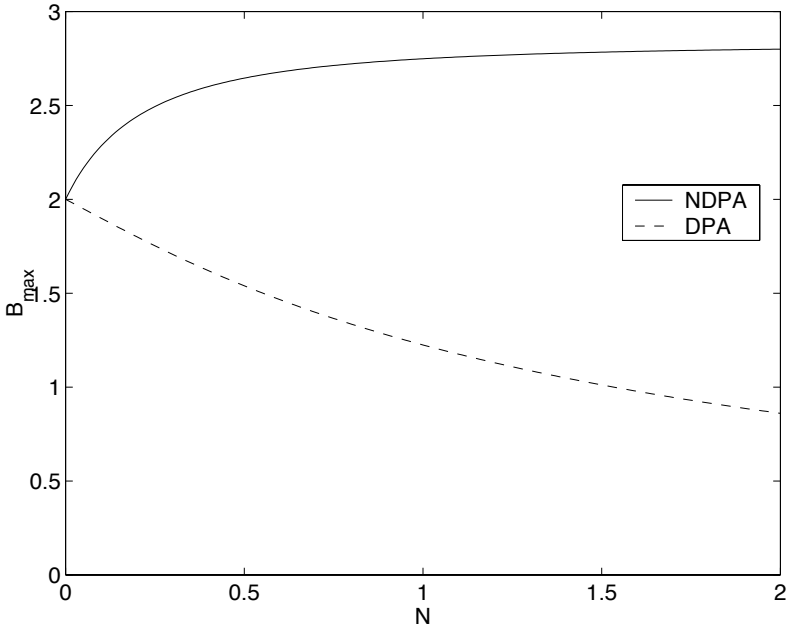

Figure 4.5: B_{max} as a function of N for $\epsilon = 1$ and ideal squeezing. The NDPA always creates states that violate the CHSH inequality, whereas the DPA never does.

For the DPA, in the case of $\epsilon = 1$ and ideal squeezing, we have,

$$B_{max}(N) = 2\left(\frac{1+2N}{(1+N)^3}\right)^{1/2} \leq 2. \tag{4.37}$$

This tends to 2 from below as N tends to 0 from above, showing that the DPA never creates a state that violates the CHSH inequality, even though it is capable of producing entangled states. That this is possible has only recently been realized (see Section 2.4 for a discussion). A graph has been plotted of B_{max} as a function of N for ideal squeezing (see Figure 4.5) that demonstrates the behaviour of Equations (4.36) and (4.37). Another way to visualize the regime in which the CHSH inequality is violated, is to make contour plots of $B_{max}\,(N, M, \epsilon)$, with one of the parameters N, M or ϵ held constant. Two of these plots are shown for the NDPA in Figures 4.6 and 4.7. As N increases, we see that the parameters ϵ and M must have values correspondingly closer to their maxima in order to violate the inequality.

In Figure 4.8, we explore the relationship between the violation of the CHSH inequality and entanglement. For the NDPA, with $\epsilon = 1$, we may define the limiting value M_{CHSH} such that the CHSH inequality is violated

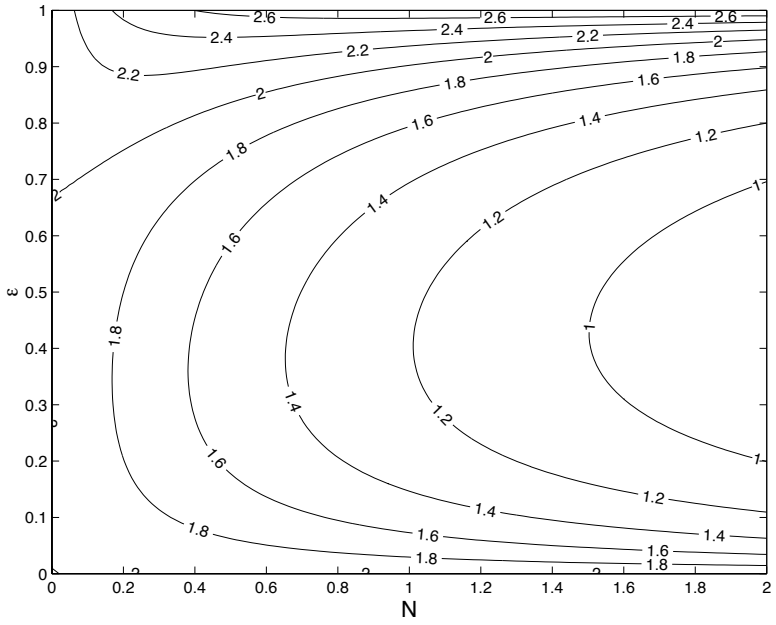

Figure 4.6: Contour plot of B_{max} as a function of N and ϵ, for atoms driven with an NDPA, in the case of ideal squeezing for which $M^2 = N(N+1)$.

when $M > M_{CHSH}$. We plot both M_{sep} and M_{CHSH} against N. This shows again that violation of the CHSH inequality and entanglement are not equivalent for this system.

4.6 Entropy-entanglement plane

In this Section, the relationship between the purity and entanglement is explored for the two models. The steady state for each model (see Equation (4.6) and Equation (4.13)) are plotted in the LEFT plane as defined in Section 2.5 (see Figure 4.9). Each curve represents a particular value of N and the corresponding range of possible M values, $0 \leq M^2 \leq N(N+1)$. We have chosen $\epsilon = 1$.

With the NDPA, by varying N and M, we may generate steady states of the atoms which access all points in the LEFT plane up to and including the line of the Werner states. In general, the greater M, the greater the correlations in the squeezed light, and the greater the purity and entanglement of the steady state of the atoms. It can be shown, in the limit of large N, that

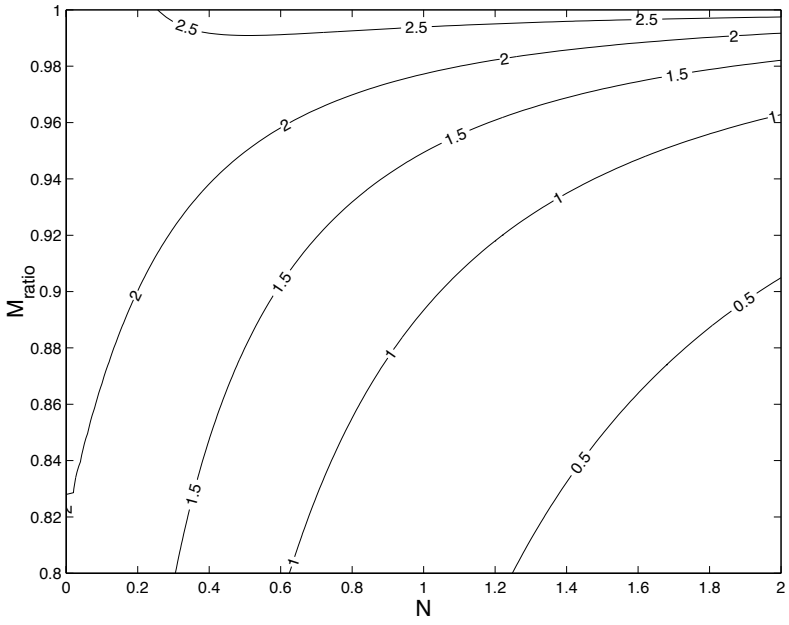

Figure 4.7: Contour plot of B_{max} as a function of N and $M_{ratio} \equiv \frac{M}{\sqrt{N(N+1)}}$, for atoms driven with the NDPA, in the case where $\epsilon = 1$. The value M_{ratio} is plotted, rather than M, to emphasize the region of interest.

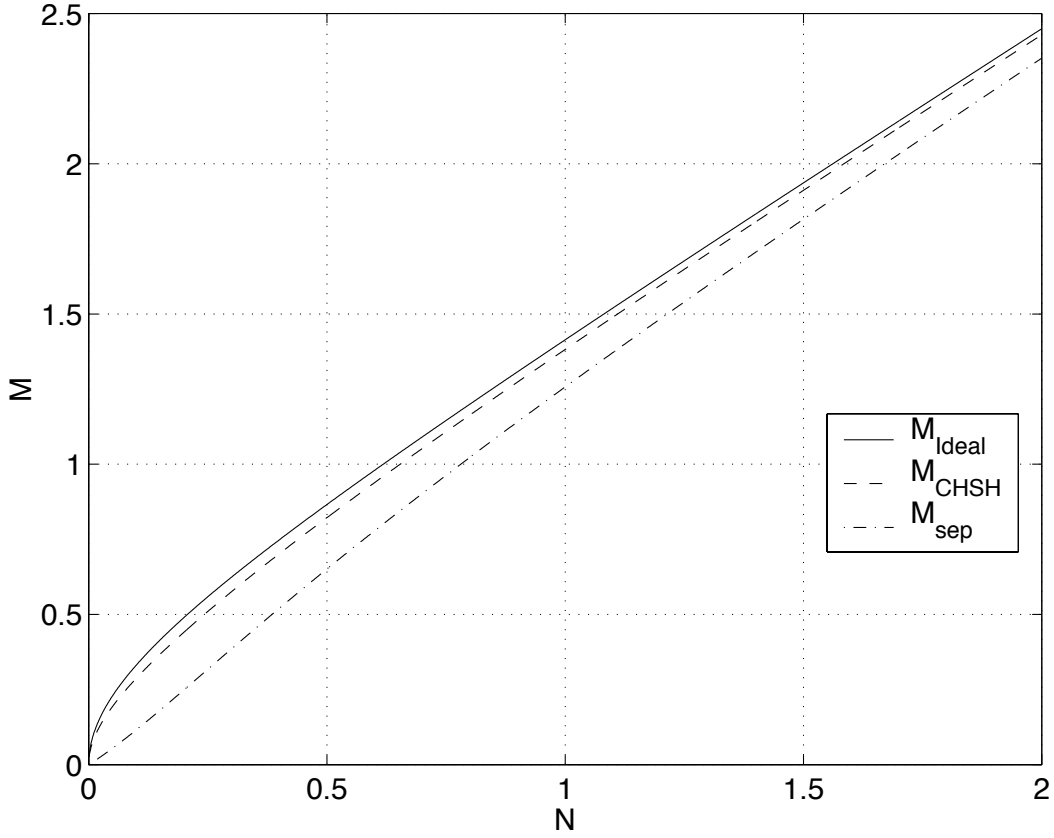

Figure 4.8: M_{idealH}, M_{CHSH} and M_{sep} as a function of N for $\epsilon = 1$ and for atoms driven by the NDPA.

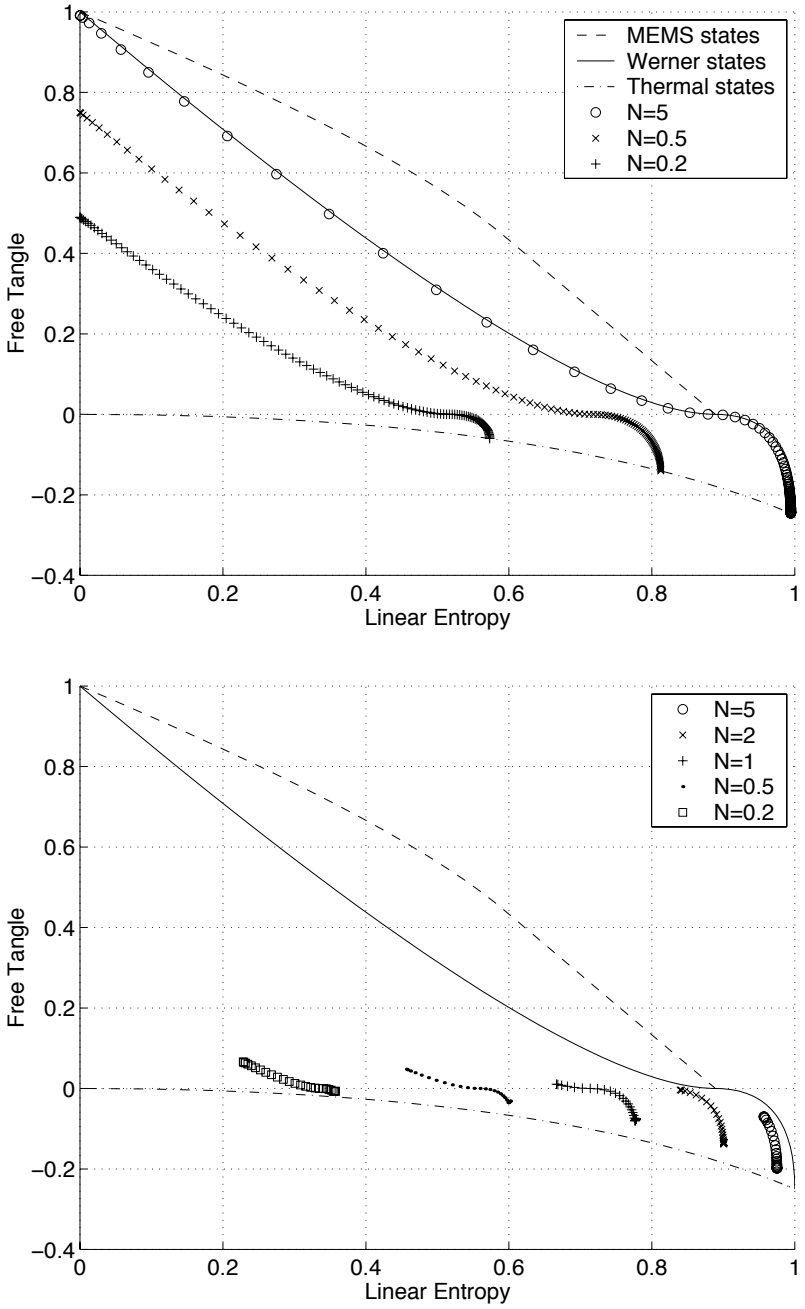

Figure 4.9: Steady states for the NDPA (top) and DPA (bottom), plotted in the LEFT plane, for $\epsilon = 1$, selected values of N, and $0 \leq M \leq \sqrt{N(N+1)}$. Larger values of M generate points on each curve with smaller entropy.

the Werner states are obtained, defined as

$$\begin{aligned} \rho_W(q) &= \frac{q}{4}\left(\mathbf{1}_2 \otimes \mathbf{1}_2\right) + \frac{(1-q)}{2}\left\{|00\rangle + |11\rangle\right\}\left\{\langle 00| + \langle 11|\right\}, \\ & 0 \leq q \leq 1. \end{aligned} \tag{4.38}$$

Using the DPA, however, only a very small proportion of the LEFT plane may be accessed. For comparison, the steady states are also shown in the LEFC plane (see Figure 4.10). The LEFC plane appears a more suitable representation for these states (the entanglement measure scales more naturally against entropy as M changes).

The steady states, for the NDPA, are also shown plotted for the 6 combinations of entropy and entanglement measures that were used in Section 2.5.3 (see Figure 4.11). When the negativity is used as the measure of entanglement, the NDPA is capable of accessing all the entangled region of the entropy-entanglement plane.

Our simple model proves to be unexpectedly powerful in terms of the range of two-qubit states that can be created. In later Chapters we will find methods to generate states that lie above the Werner line.

4.7 Conclusions

We have seen that both schemes considered in this Chapter can lead to entangled atomic steady states. When using the DPA we always have a significant degree of vacuum incident on the atoms. This prevents them from attaining a pure state and from becoming highly entangled. With the NDPA the situation is better - in the case of ideal coupling between the squeezed light and the atoms we obtain pure maximally entangled states.

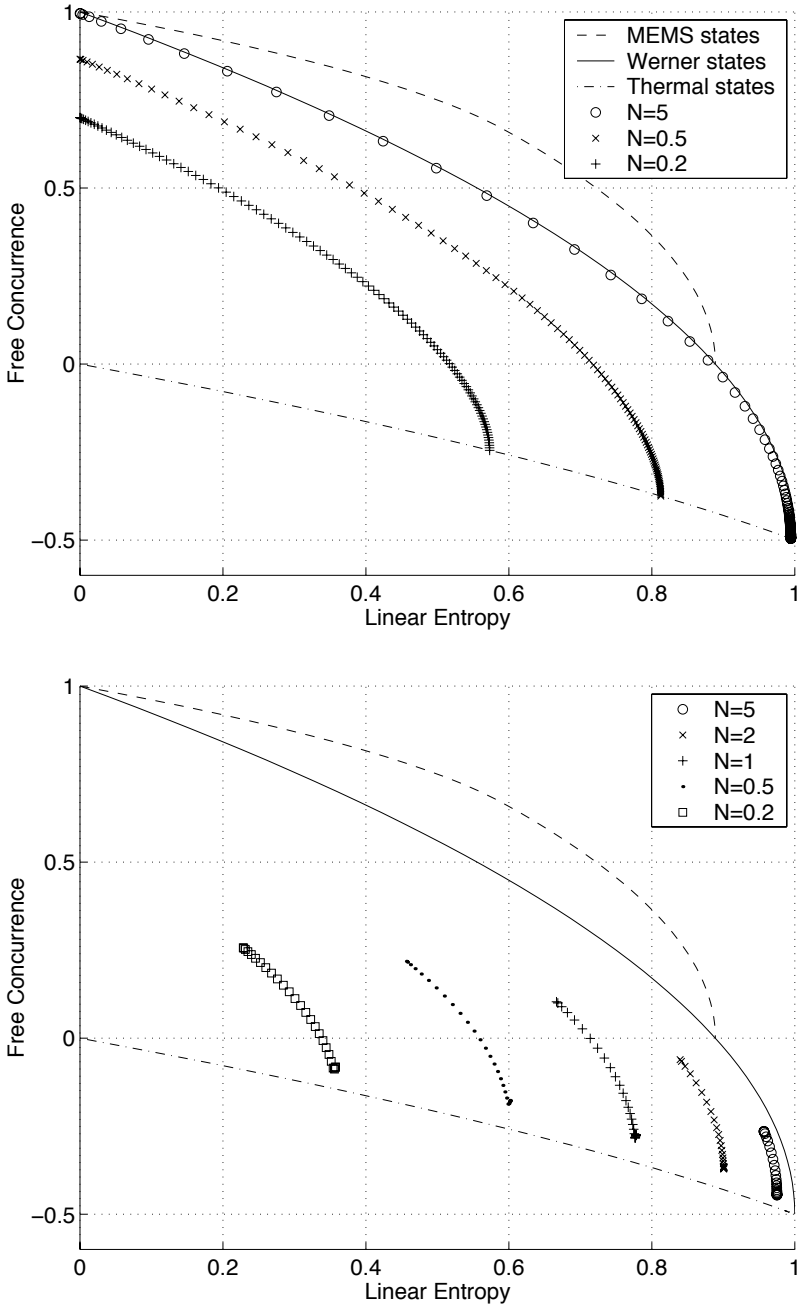

Figure 4.10: Steady states for the NDPA (top) and DPA (bottom), plotted in the LEFC plane, for $\epsilon = 1$, selected values of N, and $0 \leq M \leq \sqrt{N(N+1)}$. Larger values of M generate points on each curve with smaller entropy.

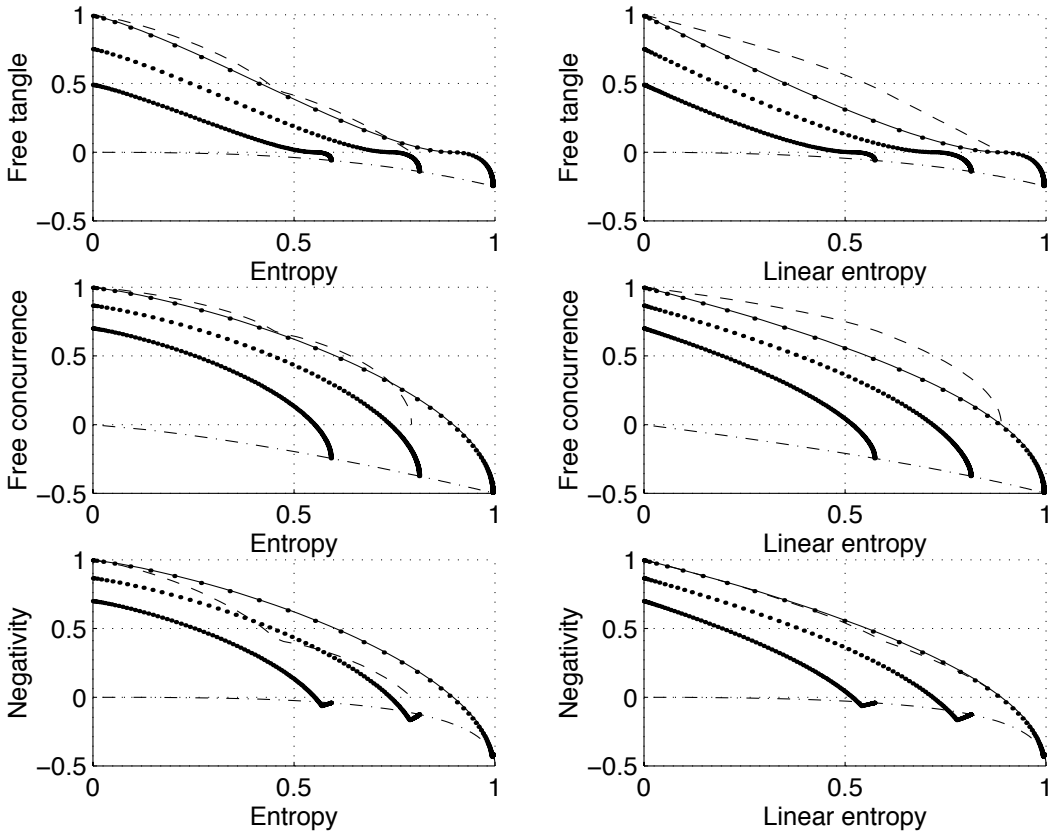

Figure 4.11: Steady states, for the NDPA, in the entropy-entanglement plane for various measures. The MEMS, Werner and thermal lines are plotted with the symbols as in Figure 4.10. In order, from top to bottom, the three dotted curves are for $N = 5$, $N = 0.5$ and $N = 0.2$. For each curve M lies in the range $0 \leq M \leq \sqrt{N(N+1)}$ and $\epsilon = 1$. Larger values of M generate points on each curve with smaller entropy.

Chapter 5

An effective one-dimensional system

A single atom, trapped in a high-finesse optical cavity and with a three-level Λ*-configuration, is known to be a possible implementation of a qubit. It is this system that we investigate in this Chapter. We are interested in determining whether it has the same effective interaction with squeezed light as a free two-level atom. We will see that the 3-level* Λ*-configuration does not have the desired interaction but that a slightly more complicated system employing 4 atomic levels is suitable.*

Contents

5.1 Introduction

The previous Chapter investigated the effects of squeezed light on a pair of two-level atoms. Two major assumptions made in that Chapter were:

1. The squeezing bandwidth is large compared to the linewidths of the excited states of the atoms.

2. The atoms couple only to input channels through which the nonclassical light is incident.

In this Chapter we investigate a technique to validate these assumptions. We consider a single 3-level atom in the Λ-configuration trapped in a high-finesse optical cavity, with a Raman transition between the ground states that is driven by a coupling laser and by the cavity mode. Such a system is a possible implementation of a qubit (see, e.g., [72]).

In this scenario, we require the characteristic correlation time of the squeezed light to be greater than the decay rate of the cavity. Such broadband squeezed light sources are available [73]. The second requirement, that the atoms couple only to squeezed channels, can be satisfied by engineering an effective Jaynes-Cummings interaction (see Section 3.4.1), where the coupling strength of the two-level system to the cavity mode dominates the effective atomic spontaneous emission rate. This ensures that the damped cavity provides the dominant input and output channel to the atom.

5.2 Scheme

In this Section we describe the system we wish to investigate. We consider an atom that is trapped in a high-finesse optical cavity of (field) decay rate κ and frequency ω (see Figure 5.1). The annihilation (creation) operator for the quantized cavity mode is denoted a ($a^\dagger$). The cavity is driven by squeezed light characterized by the parameters N (real) and M (complex). The atom has two meta-stable ground states, $|0\rangle$ and $|1\rangle$, which are degenerate (or nearly so) in energy. A third state $|r\rangle$, at an energy of ω_r, enables a Raman transition between the two ground states. In particular, the transition $|1\rangle \leftrightarrow |r\rangle$ is driven by a highly detuned laser of frequency ω_{L_r} (detuning $\Delta_r = \omega_{L_r} - \omega_r$), phase ϕ and Rabi frequency Ω_r, while the other transition $|0\rangle \leftrightarrow |r\rangle$ is driven by the cavity mode. The total spontaneous emission rate from the excited atomic state $|r\rangle$ is γ_r. The driving laser is detuned from the cavity by an amount $\delta = \omega_{L_r} - \omega$. The squeezed light driving the cavity has a central (or *carrier*) squeezing frequency of ω_{L_r}, i.e., the same as the driving laser.

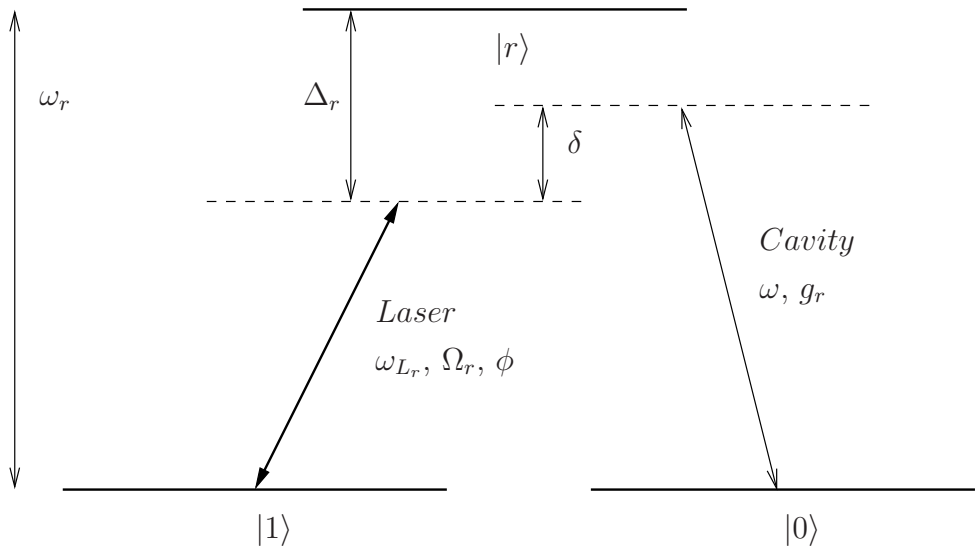

Figure 5.1: Level scheme for a 3-level Λ-atom in a cavity. The non-resonant Raman transition is driven by a coupling laser and the cavity mode. See the text for a description of the variables.

At this point, it is appropriate to describe the naming conventions for the variables which are used here and in the next two Chapters (all of which deal with multi-level atomic schemes undergoing Raman transitions). The excited states of the atoms are named $|r\rangle$, $|s\rangle$ or $|t\rangle$ as required (we shall consider up to 3 excited states), and the ground states are always named $|0\rangle$ and $|1\rangle$ to emphasize their interpretation as qubits. Detunings are denoted by Δ, Ω is used for the Rabi frequency of the coupling lasers and g for the coupling of an atomic transition to the cavity mode. For our laser fields, cavity coupling constants, frequencies and detunings, we use subscripts relating to the excited state of the atoms with which they are involved. Thus, Ω_r refers to the Rabi frequency of a laser field coupling to a particular atomic transition involving the excited state $|r\rangle$.

5.3 Master equation

Setting the zero of energy to be the energy of the (degenerate) ground states $|1\rangle$ and $|0\rangle$, we may write the master equation for this system, in a non-rotating frame, as

$$\dot{\rho} = -i\,[H, \rho] + \mathcal{L}_{cav}\rho + \mathcal{L}_{spon}\rho, \tag{5.1a}$$

where

$$\begin{aligned} H &= H_{cav} + H_{atom} + H_{atom/laser} + H_{atom/cav}, && \text{(5.1b)} \\ H_{cav} &= \omega a^\dagger a, && \text{(5.1c)} \\ H_{atom} &= \omega_r \left|r\right\rangle \left\langle r\right|, && \text{(5.1d)} \\ H_{atom/laser} &= \frac{\Omega_r}{2}\left(e^{-i\phi}e^{-i\omega_{Lr}t}\left|r\right\rangle\left\langle 1\right| + \text{H.c.}\right), && \text{(5.1e)} \\ H_{atom/cav} &= g_r \left|r\right\rangle \left\langle 0\right| a + \text{H.c.}, && \text{(5.1f)} \end{aligned}$$

and

$$\begin{aligned} \mathcal{L}_{cav}\rho &= \kappa(1+N)\left(2a\rho a^\dagger - a^\dagger a\rho - \rho a^\dagger a\right) \\ &\quad +\kappa N\left(2a^\dagger\rho a - aa^\dagger\rho - \rho aa^\dagger\right) \\ &\quad +\kappa M e^{-2i\omega_{Lr}t}\left(2a^\dagger\rho a^\dagger - a^\dagger a^\dagger\rho - \rho a^\dagger a^\dagger\right) \\ &\quad +\kappa M^* e^{2i\omega_{Lr}t}\left(2a\rho a - aa\rho - \rho aa\right). \qquad \text{(5.1g)} \end{aligned}$$

Here we assume that the squeezing bandwidth dominates the decay rate κ of the cavity, enabling us to write the damping of the cavity in the standard form (5.1g). The term $\mathcal{L}_{spon}\rho$ describes atomic spontaneous emission.

5.3.1 Adiabatic elimination of excited states

To isolate the essential dynamics of this system, we assume that the detuning of the light field from the excited atomic state is very large, i.e.,

$$\left|\Delta_r\right| \gg \kappa, \Omega_r, g_r, \gamma_r, \qquad (5.2)$$

so that spontaneous emission from the excited state $\left|r\right\rangle$ during the Raman transition is negligible and the state $\left|r\right\rangle$ may be adiabatically eliminated. We obtain a Hamiltonian (with the cavity in a frame rotating at the laser frequency) of

$$\dot{\rho} = -i\left[H,\rho\right] + \mathcal{L}_{cav}\rho, \qquad (5.3a)$$

where

$$\begin{aligned} H &= H_{atom} + H_{cav} + H_{atom/cav}, && \text{(5.3b)} \\ H_{atom} &= \frac{\Omega_r^2}{4\Delta_r}\sigma^+\sigma^-, && \text{(5.3c)} \\ H_{cav} &= -\delta a^\dagger a, && \text{(5.3d)} \\ H_{atom/cav} &= \frac{g_r^2}{\Delta_r}\sigma^-\sigma^+a^\dagger a + \frac{g_r\Omega_r}{2\Delta_r}\left(e^{i\phi}\sigma^+a + \text{H.c.}\right), && \text{(5.3e)} \end{aligned}$$

and

$$\begin{aligned}\mathcal{L}_{cav}\rho &= \kappa(1+N)\left(2a\rho a^\dagger - a^\dagger a\rho - \rho a^\dagger a\right) \\ &\quad +\kappa N\left(2a^\dagger\rho a - aa^\dagger\rho - \rho aa^\dagger\right) \\ &\quad +\kappa M\left(2a^\dagger\rho a^\dagger - a^\dagger a^\dagger\rho - \rho a^\dagger a^\dagger\right) \\ &\quad +\kappa M^*\left(2a\rho a - aa\rho - \rho aa\right). \end{aligned} \tag{5.3f}$$

We have defined raising and lowering operators between the atomic ground states as

$$\sigma^+ = |1\rangle\langle 0|, \tag{5.4a}$$
$$\sigma^- = |0\rangle\langle 1|. \tag{5.4b}$$

With the excited state eliminated we have an effective two-level system whose interaction with the cavity mode is characterized by the parameters

$$\beta_r = \frac{g_r\Omega_r}{2\Delta_r}, \tag{5.5a}$$
$$\eta_r = \frac{g_r^2}{\Delta_r}. \tag{5.5b}$$

Here β_r is the coupling constant of the effective two-level system to the cavity mode and η_r is the ac-Stark shift induced in $|0\rangle$ per cavity photon.

5.3.2 Adiabatic elimination of cavity

Examining Equation (5.3e) we now see that the interaction between the cavity mode and the atom is nearly in the desired Jaynes-Cummings form, except for the presence of an extra term $\eta_r\sigma^-\sigma^+a^\dagger a$. To understand the effect of this term on the atomic ground states we adiabatically eliminate the cavity mode by assuming that its decay rate κ is larger than its coupling to the atomic system. The method used follows that used by Parkins and Kimble in [74]. The time-scale assumptions we have made are now

$$|\Delta_r| \gg \kappa, \Omega_r, g_r, \gamma_r, \tag{5.6a}$$
$$\kappa \gg \beta_r, \eta_r. \tag{5.6b}$$

Before performing the adiabatic elimination we ensure that all of the cavity operators coupling to the atom have zero mean by defining a new operator

$$\breve{n} = a^\dagger a - N. \tag{5.7}$$

In order to eliminate systematic motion of the cavity mode at frequency δ, and also of the atomic ground states due to their effective level shifts, we make a further transformation to a new interaction picture relative to the Hamiltonian term:

$$H_0 = -\delta a^\dagger a + \frac{\Omega_r^2}{4\Delta_r}\sigma^+\sigma^- + \eta_r N \sigma^-\sigma^+. \tag{5.8}$$

After these minor transformations, the new master equation becomes

$$\dot{\rho} = -i\left[H_{atom/cav}, \rho\right] + \mathcal{L}_{cav}\rho, \tag{5.9a}$$

where

$$H_{atom/cav} = \eta_r \sigma^-\sigma^+ \breve{n} + \beta_r\left(e^{i\phi}e^{i\delta t}e^{i\alpha t}\sigma^+ a + \text{H.c.}\right), \tag{5.9b}$$

and

$$\begin{aligned}\mathcal{L}_{cav}\rho &= \kappa(1+N)\left(2a\rho a^\dagger - a^\dagger a\rho - \rho a^\dagger a\right) \\ &\quad +\kappa N\left(2a^\dagger\rho a - aa^\dagger\rho - \rho aa^\dagger\right) \\ &\quad +\kappa M e^{-2i\delta t}\left(2a^\dagger\rho a^\dagger - a^\dagger a^\dagger\rho - \rho a^\dagger a^\dagger\right) \\ &\quad +\kappa M^* e^{2i\delta t}\left(2a\rho a - aa\rho - \rho aa\right).\end{aligned} \tag{5.9c}$$

After performing the adiabatic elimination of the cavity, we obtain a master equation for the atomic ground states alone:

$$\begin{aligned}\dot{\rho} &= +\beta_r^2\left(\frac{N+1}{\kappa - i\alpha - i\delta}\right)\left\{\sigma^-\rho\sigma^+ - \sigma^+\sigma^-\rho\right\} \\ &\quad +\beta_r^2\left(\frac{N+1}{\kappa + i\alpha + i\delta}\right)\left\{\sigma^-\rho\sigma^+ - \rho\sigma^+\sigma^-\right\} \\ &\quad +\beta_r^2\left(\frac{N}{\kappa + i\alpha + i\delta}\right)\left\{\sigma^+\rho\sigma^- - \sigma^-\sigma^+\rho\right\} \\ &\quad +\beta_r^2\left(\frac{N}{\kappa - i\alpha - i\delta}\right)\left\{\sigma^+\rho\sigma^- - \rho\sigma^-\sigma^+\right\} \\ &\quad +\beta_r^2\left(\frac{-\kappa M}{\kappa - i\delta}\right)\frac{e^{2i\phi}e^{2i\alpha t}}{\kappa + i\alpha - i\delta}\left\{2\sigma^+\rho\sigma^+\right\} \\ &\quad +\beta_r^2\left(\frac{-\kappa M^*}{\kappa + i\delta}\right)\frac{e^{-2i\phi}e^{-2i\alpha t}}{\kappa - i\alpha + i\delta}\left\{2\sigma^-\rho\sigma^-\right\} \\ &\quad +\eta_r^2\left(\frac{1}{2\kappa}\right)\left(N(N+1) + \frac{\kappa^2 M M^*}{\kappa^2+\delta^2}\right) \\ &\qquad \left\{2\sigma^-\sigma^+\rho\sigma^-\sigma^+ - \sigma^-\sigma^+\rho - \rho\sigma^-\sigma^+\right\},\end{aligned} \tag{5.10a}$$

where

$$\alpha = \frac{\Omega_r^2}{4\Delta_r} - \frac{g_r^2 N}{\Delta_r} = \frac{\beta_r^2}{\eta_r} - \eta_r N. \tag{5.10b}$$

5.4 Comparison to two-level atom

We are now in a position to analyze the differences between a two-level atom in a squeezed vacuum and our Λ-system interacting with squeezed light through a cavity. For the purposes of comparison, the master equation for a two-level atom with atomic transition linewidth γ, interacting resonantly with a broadband squeezed vacuum, is [75]

$$\begin{aligned}\dot{\rho} &= \frac{\gamma}{2}(N+1)\left(2\sigma^-\rho\sigma^+ - \sigma^+\sigma^-\rho - \rho\sigma^+\sigma^-\right) \\ &\quad + \frac{\gamma}{2}N\left(2\sigma^+\rho\sigma^- - \sigma^-\sigma^+\rho - \rho\sigma^-\sigma^+\right) \\ &\quad - \gamma M\sigma^+\rho\sigma^+ - \gamma M^*\sigma^-\rho\sigma^-.\end{aligned} \tag{5.11}$$

First of all we note that there is a time dependence in master equation (5.10a), which can only be removed when parameters are chosen such that $\alpha = 0$. This is a prerequisite for keeping the phase of the atomic ground states constant with respect to the phase of the squeezed light. We see that the detuning δ between the cavity and the laser has not provided a degree of freedom to cancel with α as we might have hoped.

Even if we choose parameters such that α and δ are zero we still do not have a master equation of the appropriate form (5.11) due to the term that is proportional to η_r^2. This term may be interpreted as phase damping of the qubit caused by a coherent scattering process between the atom and the intra-cavity photons. The effects of this term will be negated if we can choose parameters such that

$$\beta_r^2 N \gg \eta_r^2 N (N+1). \tag{5.12}$$

Unfortunately, the requirement of $\alpha = 0$ means that $\beta_r^2 = \eta_r^2 N$ and therefore Equation (5.12) cannot be simultaneously satisfied. Therefore we seem to be in a situation where we cannot simulate a two-level atom in a squeezed vacuum by using a three-level Λ-system in a cavity driven by squeezed light.

5.4.1 Bloch equations

To understand further the effect of the term containing η_r^2 in Equation (5.10a) it is informative to compare the Bloch equations for the Λ-system with those

for a two-level atom in a broadband squeezed vacuum. For clarity, we choose $\kappa = 1$, $\alpha = 0$, $\delta = 0$ and M real, so that the reduced master equation for the Λ-system simplifies to

$$\begin{aligned}\dot{\rho} &= \beta_r^2(N+1)\left\{2\sigma^-\rho\sigma^+ - \sigma^+\sigma^-\rho - \rho\sigma^+\sigma^-\right\} \\ &\quad +\beta_r^2 N\left\{2\sigma^+\rho\sigma^- - \sigma^-\sigma^+\rho - \rho\sigma^-\sigma^+\right\} \\ &\quad -\beta_r^2 M\left\{2\sigma^+\rho\sigma^+ + 2\sigma^-\rho\sigma^-\right\} \\ &\quad +\eta_r^2\frac{N(N+1)+M^2}{2}\left\{2\sigma^-\sigma^+\rho\sigma^-\sigma^+ - \sigma^-\sigma^+\rho - \rho\sigma^-\sigma^+\right\}.\end{aligned} \tag{5.13}$$

If we define the constant

$$B = \frac{\eta_r^2}{2\beta_r^2}\left(N(N+1)+M^2\right), \tag{5.14a}$$

the Bloch equations are

$$\langle\dot{\sigma_x}\rangle = -\beta_r^2(2N+1+2M+B)\langle\sigma_x\rangle, \tag{5.14b}$$

$$\langle\dot{\sigma_y}\rangle = -\beta_r^2(2N+1-2M+B)\langle\sigma_y\rangle, \tag{5.14c}$$

$$\left\langle\dot{\sigma^-\sigma^+}\right\rangle = 2\beta_r^2(N+1)\left\langle\sigma^+\sigma^-\right\rangle - 2\beta_r^2 N, \tag{5.14d}$$

$$\left\langle\dot{\sigma^+\sigma^-}\right\rangle = -2\beta_r^2(N+1)\left\langle\sigma^+\sigma^-\right\rangle + 2\beta_r^2 N. \tag{5.14e}$$

These equations may be compared to the Bloch equations for a single two-level atom in squeezed vacuum, calculable from (5.11), which are

$$\langle\dot{\sigma_x}\rangle = -\frac{\gamma}{2}(2N+1+2M)\langle\sigma_x\rangle, \tag{5.15a}$$

$$\langle\dot{\sigma_y}\rangle = -\frac{\gamma}{2}(2N+1-2M)\langle\sigma_y\rangle, \tag{5.15b}$$

$$\left\langle\dot{\sigma^-\sigma^+}\right\rangle = \gamma(N+1)\left\langle\sigma^+\sigma^-\right\rangle - \gamma N, \tag{5.15c}$$

$$\left\langle\dot{\sigma^+\sigma^-}\right\rangle = -\gamma(N+1)\left\langle\sigma^+\sigma^-\right\rangle + \gamma N. \tag{5.15d}$$

We see that the Bloch equations would be of the same form except for the extra term B present in the phase decay equations for the Λ-atom in a cavity. This extra factor causes enhanced phase decay in both quadratures but does not affect the populations or their decay rates.

With the requirement of $\alpha = 0$, we see that $\beta_r^2 = \eta_r^2 N$ and so B cannot be chosen to be significantly less than $2M$. Hence, there is always significant phase decay in each quadrature (i.e. the term $2N + 1 - 2M + B$ cannot be made small). We conclude that it is not possible to choose a parameter regime which permits the Λ-atom in a cavity to have similar phase decay dynamics to the equivalent two-level atom.

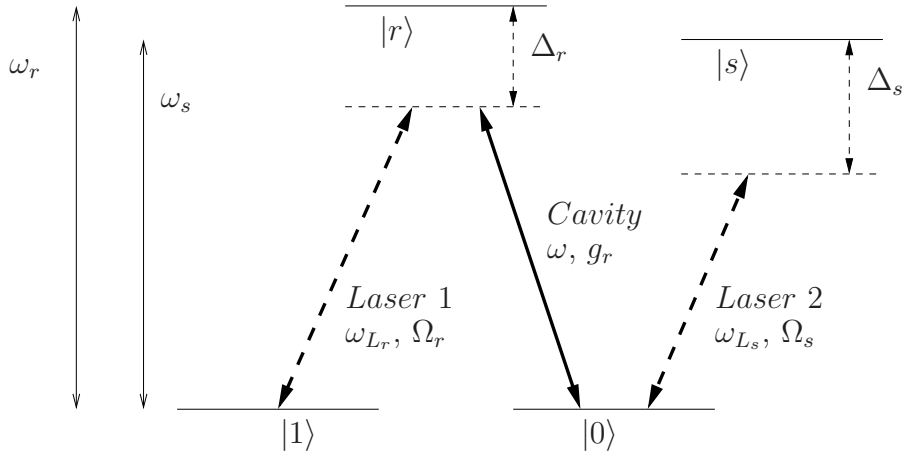

Figure 5.2: The atomic levels and transitions for a four-level atom, showing the resonant Raman transition and the virtual excitation of state $|s\rangle$. The two lasers have frequencies ω_{L_r} and ω_{L_s}, and Rabi frequencies Ω_r and Ω_s, respectively. The excited levels have frequencies ω_r and ω_s and spontaneous emission rates γ_r and γ_s. The lasers are strongly detuned by $\Delta_r = \omega_{L_r} - \omega_r$ and $\Delta_s = \omega_{L_s} - \omega_s$. As drawn, the detunings Δ_r and Δ_s are negative.

5.5 Four-level Λ-system

The time dependence in Equation (5.10a) arises from the differing level shifts experienced by states $|0\rangle$ and $|1\rangle$ in our effective two level system. This suggests that the addition of another level shift into one of these ground states could provide a degree of freedom with which to cancel the time dependence. A technique to achieve this is to virtually excite a fourth atomic level by driving it selectively from one of the ground states via a second laser field.

A new atomic level scheme to achieve this is shown in Figure 5.2. This configuration has the same basic structure as that shown in Figure 5.1 except for the addition of a new excited state $|s\rangle$ and a second laser field coupling it to level $|0\rangle$. We also now choose $\delta = 0$ (i.e. drive the transition $|0\rangle \leftrightarrow |1\rangle$ on Raman resonance). The state $|s\rangle$ is virtually excited from $|0\rangle$ by a second strongly detuned laser with Rabi frequency Ω_s and detuning Δ_s. It has a spontaneous emission rate γ_s. We expect that the state $|s\rangle$ will add an additional ac-Stark shift to the ground state $|0\rangle$ due to the laser field Ω_s.

Following the approach for the three-level Λ-system used earlier in the Chapter we may again adiabatically eliminate the excited states of the atoms and then the cavity mode. The timescale conditions for the adiabatic elimi-

nation become

$$|\Delta_r|, |\Delta_s| \gg \kappa, \Omega_r, \Omega_s, g_r, \gamma_r, \gamma_s, \tag{5.16a}$$

$$\kappa \gg \beta_r, \eta_r. \tag{5.16b}$$

We obtain the master equation

$$\begin{aligned}
\dot{\rho} = & +\beta_r^2 \left(\frac{N+1}{\kappa - i\alpha}\right) \left\{\sigma^- \rho \sigma^+ - \sigma^+ \sigma^- \rho\right\} \\
& +\beta_r^2 \left(\frac{N+1}{\kappa + i\alpha}\right) \left\{\sigma^- \rho \sigma^+ - \rho \sigma^+ \sigma^-\right\} \\
& +\beta_r^2 \left(\frac{N}{\kappa + i\alpha}\right) \left\{\sigma^+ \rho \sigma^- - \sigma^- \sigma^+ \rho\right\} \\
& +\beta_r^2 \left(\frac{N}{\kappa - i\alpha}\right) \left\{\sigma^+ \rho \sigma^- - \rho \sigma^- \sigma^+\right\} \\
& -\beta_r^2 M \frac{e^{2i\phi} e^{2i\alpha t}}{\kappa + i\alpha} \left\{2\sigma^+ \rho \sigma^+\right\} \\
& -\beta_r^2 M^* \frac{e^{-2i\phi} e^{-2i\alpha t}}{\kappa - i\alpha} \left\{2\sigma^- \rho \sigma^-\right\} \\
& +\eta_r^2 \frac{N(N+1) + MM^*}{2\kappa} \left\{2\sigma^- \sigma^+ \rho \sigma^- \sigma^+ - \sigma^- \sigma^+ \rho - \rho \sigma^- \sigma^+\right\},
\end{aligned} \tag{5.17a}$$

where the definition of α becomes

$$\alpha = \frac{\Omega_r^2}{4\Delta_r} - \frac{\Omega_s^2}{4\Delta_s} - \frac{g_r^2 N}{\Delta_r}. \tag{5.17b}$$

It is now possible to satisfy the condition $\alpha = 0$, while simultaneously satisfying conditions (5.16), and also choosing parameters to ensure

$$B \ll 2N + 1 - 2M. \tag{5.18}$$

This means that we can choose a parameter regime to make the behaviour of the ground states of a 4-level Λ-system in a cavity driven by squeezed light identical to the behaviour of a free two-level atom interacting directly with squeezed light.

5.6 Conclusions

We have seen that we can create a system, based on cavity QED, which has the same interaction with squeezed light as a free atom. However, in

the cavity QED system, the atom is effectively one-dimensional; we need only squeeze the modes into which the cavity decays and do not need to squeeze the full 4π of modes with which a free atom can interact. This is a substantially simpler technical challenge. Therefore, the use of a 4-level system offers a solution to the problem of driving an atom from all directions with broadband squeezed light. This was the major assumption made in Chapter 4.

In the next Chapter, we shall consider a cavity QED situation using two of these 4-level atoms. We may expect that all of the results obtained in Chapter 4 should continue to apply if we take the systems considered there and substitute, for an atom in free space with linewidth γ, a subsystem comprising a 4-level Λ-atom trapped in a cavity with effective linewidth $2\frac{\beta_r^2}{\kappa}$.

Chapter 6

Entangling one-dimensional atoms with squeezed light

In this Chapter we investigate two schemes to transfer entanglement from squeezed light to a pair of one-dimensional atoms created by the cavity QED setup described in Chapter 5. In an extension of the work of Palma and Knight [2], we first consider two 4-level atoms that are both trapped in a single high-finesse optical cavity which is driven by quadrature-squeezed light from a degenerate parametric amplifier. In another scenario, based on the idealized models of Chapter 4, we consider two 4-level atoms that are trapped in individual optical cavities each driven by a different output field from a non-degenerate parametric amplifier. In both cases we show how the quantum correlations in the light fields are transferred to the atoms. For the DPA system we show how atomic two-qubit states of arbitrary entanglement and entropy may be generated.

Contents

6.1 Introduction

The system of a pair of atoms in a cavity driven resonantly by broadband squeezed light was considered by Banerjee in 1996 [76], under the assumption that the distance between the two atoms was much smaller than the resonant wavelength (Dicke model). The steady state solution for the atoms was found and the degree of atomic squeezing characterized as a function of the spontaneous emission rate of the atoms and of the squeezing parameters (N and M) of the light driving the cavity.

In this Chapter, the first system we consider bears many similarities to that of [76], except we employ the effective one-dimensional atoms of Chapter 5. We do not consider the effect of spontaneous emission during the Raman transition because we assume that it can be made small using the arguments made in Section 5.3.1. We find that the resulting master equation contains a collective phase decay term that degrades the entanglement, but which can be made negligible in the appropriate parameter regime.

The second system that we investigate is an extension of the system of two separate atoms driven by an NDPA, which was considered in Chapter 4. We use the two output modes from an NDPA to drive two different cavities, each containing a 4-level atom in the cavity QED setup described in Chapter 5.

6.2 Entangling atoms with the DPA

In the first part of this Chapter we will consider the two atoms to be trapped in the same optical cavity. The alternative situation, where the atoms are trapped in individual cavities, is considered in Section 6.7.

The details of the experimental setup are as follows. The squeezed output mode from a degenerate parametric amplifier (DPA) is mode-matched to a resonant high-finesse optical cavity, with field decay rate κ, containing two trapped atoms (see Figure 6.1). The quantized annihilation (creation) operator for the cavity mode is denoted a ($a^\dagger$). The atoms are trapped at sites with sufficient separation so that there is no direct interaction between the atoms and so that they can be individually addressed by probe lasers if necessary. The output from the DPA is characterized by two parameters N (real) and M (complex) for which $0 \leq |M|^2 \leq N(N+1)$. When $M = 0$ we have thermal light, and for $|M|^2 = N(N+1)$ we have ideally squeezed light.

The relevant level scheme of each atom is shown in Figure 6.2. The atoms are considered to be identical in every respect except position, to have the same coupling strengths to the cavity, and to be driven by identical strength laser fields. This level scheme is identical to that described in Figure 5.2;

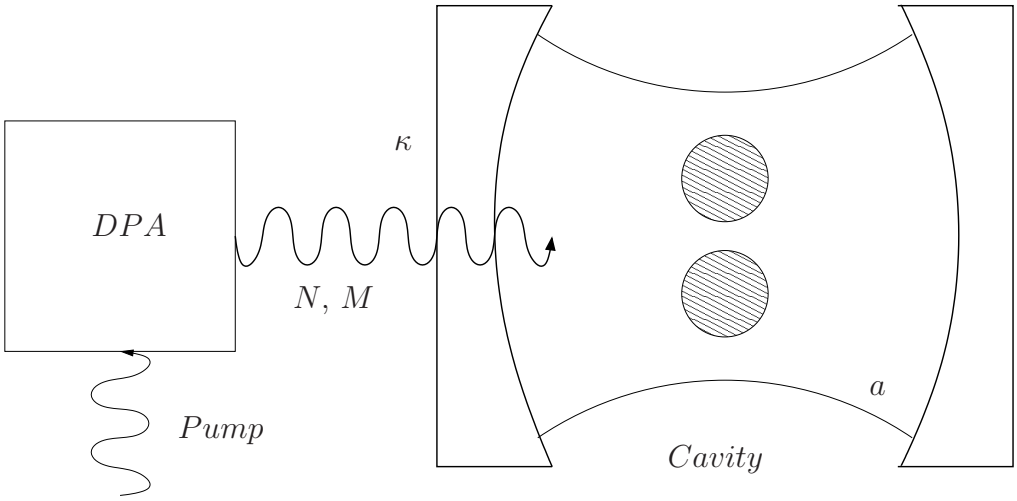

Figure 6.1: Cavity containing two atoms and driven by squeezed light.

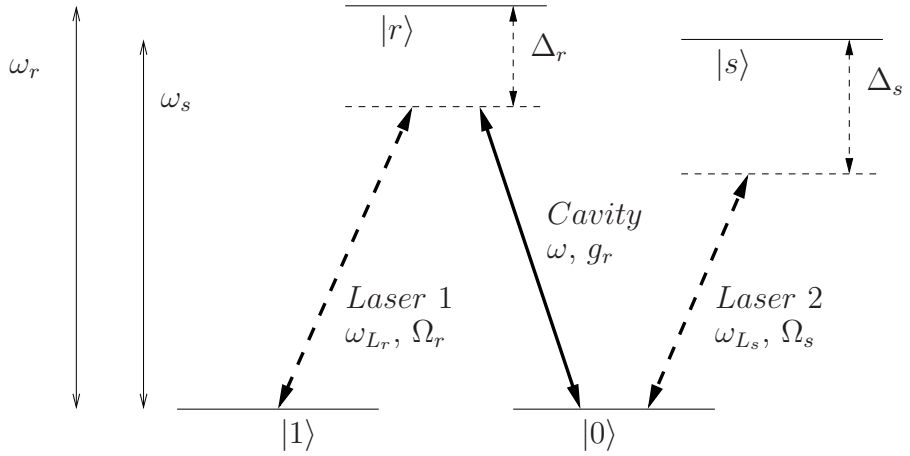

Figure 6.2: The atomic levels and transitions for each atom, showing the Raman transition and the virtual excitation of state $|s\rangle$. The two lasers have frequencies ω_{L_r} and ω_{L_s}, and Rabi frequencies Ω_r and Ω_s respectively. The excited levels have frequencies ω_r and ω_s. The lasers are strongly detuned by $\Delta_r = \omega_{L_r} - \omega_r$ and $\Delta_s = \omega_{L_s} - \omega_s$. As drawn, the detunings Δ_r and Δ_s are negative.

it is briefly described again here. The states $|1\rangle$, $|r\rangle$ and $|0\rangle$ are in the Λ-configuration as employed in [72]. A strongly detuned laser drives the transition $1 \leftrightarrow r$ with a Rabi frequency of Ω_r and detuning Δ_r. The transition $r \leftrightarrow 0$ is coupled with strength g_r and the same detuning Δ_r to the cavity mode. A fourth state $|s\rangle$ is virtually excited from $|0\rangle$ by another strongly detuned laser with Rabi frequency Ω_s and detuning Δ_s. As we have seen in Chapter 5, the state $|s\rangle$ adds an additional ac-Stark shift to the ground state $|0\rangle$ due to the laser field Ω_s and is required to create an interaction with the squeezed light of the desired form.

6.3 Master Equation

The master equation for the entire system, assuming broadband squeezed light with respect to the cavity decay rate, is given by

$$\begin{aligned}
\dot{\rho} &= -i\left[H,\rho\right] + \mathcal{L}_{cav}\rho, && \text{(6.1a)}\\
\mathcal{L}_{cav}\rho &= \kappa(1+N)\left(2a\rho a^\dagger - a^\dagger a\rho - \rho a^\dagger a\right)\\
&\quad +\kappa N\left(2a^\dagger\rho a - aa^\dagger\rho - \rho aa^\dagger\right)\\
&\quad -\kappa M e^{-2i\omega t}\left(2a^\dagger\rho a^\dagger - a^\dagger a^\dagger\rho - \rho a^\dagger a^\dagger\right)\\
&\quad -\kappa M^* e^{2i\omega t}\left(2a\rho a - aa\rho - \rho aa\right), && \text{(6.1b)}\\
H &= H_{cav} + H_{atoms} + H_{atoms/lasers} + H_{atoms/cav}, && \text{(6.1c)}\\
H_{cav} &= \omega a^\dagger a, && \text{(6.1d)}\\
H_{atoms} &= \sum_{i=1,2}\left(\omega_r\left|r\right\rangle\left\langle r\right|_i + \omega_s\left|s\right\rangle\left\langle s\right|_i\right), && \text{(6.1e)}\\
H_{atoms/lasers} &= \frac{\Omega_r}{2}e^{-i[\omega_{Lr}t+\phi_r]}\left|r\right\rangle\left\langle 1\right|_i + \text{H.c.}\\
&\quad +\frac{\Omega_s}{2}e^{-i[\omega_{Ls}t+\phi_s]}\left|s\right\rangle\left\langle 0\right|_i + \text{H.c.}, && \text{(6.1f)}\\
H_{atoms/cav} &= \sum_{i=1,2} g_r\left|r\right\rangle\left\langle 0\right|_i a + \text{H.c.}. && \text{(6.1g)}
\end{aligned}$$

Here H.c. refers to the Hermitian conjugate of the previous term. In this Chapter we assume that spontaneous emission from the excited states of the atoms during their Raman transitions can be neglected. The effects of such spontaneous emission are investigated in depth in Chapter 7 in a closely related system.

6.4 Reduced master equation

To understand the dynamics of this system we wish to find a reduced master equation for a pair of effective two-level systems. We first adiabatically eliminate the excited states of the atoms as in Section 5.3.1. We then operate the cavity in the bad-cavity limit where the decay rate of the cavity dominates its interaction with the atoms. This enables us to adiabatically eliminate the cavity as well and obtain the master equation

$$\begin{aligned}\dot{\rho} &= \frac{2\beta_r^2}{\kappa}(N+1)\left(2S\rho S^\dagger - S^\dagger S\rho - \rho S^\dagger S\right) \\ &+\frac{2\beta_r^2}{\kappa}N\left(2S^\dagger\rho S - SS^\dagger\rho - \rho SS^\dagger\right) \\ &-\frac{2\beta_r^2}{\kappa}Me^{2i\phi_r}\left(2S^\dagger\rho S^\dagger - S^\dagger S^\dagger\rho - \rho S^\dagger S^\dagger\right) \\ &-\frac{2\beta_r^2}{\kappa}M^*e^{-2i\phi_r}\left(2S\rho S - SS\rho - \rho SS\right) \\ &+\frac{\eta_r^2}{2\kappa}\left\{N(N+1)+MM^*\right\}\left(2P\rho P^\dagger - P^\dagger P\rho - \rho P^\dagger P\right), \quad (6.2a)\end{aligned}$$

where we have defined the collective operators

$$S = \frac{1}{\sqrt{2}}\left(\sigma_1^- + \sigma_2^-\right), \quad (6.2b)$$

$$P = \sigma_1^-\sigma_1^+ + \sigma_2^-\sigma_2^+. \quad (6.2c)$$

The reduced system is characterized by the parameters

$$\beta_r = \frac{g_r\Omega_r}{2\Delta_r}, \quad (6.3a)$$

$$\eta_r = \frac{g_r^2}{\Delta_r}, \quad (6.3b)$$

which are respectively the coupling constant of each effective two-level system to the cavity and the ac-Stark shift induced in $|0\rangle$ per cavity photon. With these definitions, the bad-cavity limit can be quantified as

$$\kappa \gg |\beta_r|, |\eta_r|. \quad (6.4)$$

This master equation is in the interaction picture such that the rotation of the effective two-level system is stopped. Its validity depends on the additional assumption that we have chosen parameters such that the effective

two-level system remains at a constant phase relative to the squeezed light field, i.e.,

$$\frac{\Omega_r^2}{4\Delta_r} - \frac{\Omega_s^2}{4\Delta_s} - \frac{g_r^2}{\Delta_r}N = 0. \tag{6.5}$$

As we have seen in Chapter 5, it is for this reason that we employ the additional state $|s\rangle$ and the laser driving the transition $0 \leftrightarrow s$. The extra degree of freedom provided by varying Ω_s and/or Δ_s will permit us the flexibility to make η_r negligible if desired, while still satisfying (6.5).

We now examine Equation (6.2a). This bears much similarity to Equation (4.12), which was for the system of two atoms driven by a DPA (considered in Chapter 4). In (6.2a), stimulated emission into and absorption from the squeezed reservoir, is through collective couplings, as expected for two atoms in the same cavity. In contrast to Equation (4.12) however, even the terms describing (effective) spontaneous emission are collective, since the mechanism for spontaneous emission of the effective two-level systems is through decay of the shared cavity mode. The term proportional to η_r^2 may be interpreted as a collective phase damping of the qubits caused by a coherent scattering process between the atoms and the intra-cavity photons.

The collective coupling of two atoms to a single cavity mode leads to decoherence-free states. Repeating the definition of the Bell states for convenience,

$$\left|\phi^{\pm}\right\rangle = \frac{1}{\sqrt{2}}\left(|00\rangle \pm |11\rangle\right), \tag{6.6a}$$

$$\left|\psi^{\pm}\right\rangle = \frac{1}{\sqrt{2}}\left(|01\rangle \pm |10\rangle\right), \tag{6.6b}$$

we find that $|\psi^-\rangle$ is coherently trapped for all possible combinations of β_r, η_r, N and M and that $|\psi^+\rangle$ is trapped when $\beta_r = 0$. We will interpret the dynamics of the system within the entanglement-entropy plane by considering these trapped states.

A significant feature of the system we propose is that the parameters β_r and η_r are independently adjustable, as long as Equation (6.5) and our timescale assumptions remain satisfied. When $\beta_r = \eta_r = 0$ the dynamics of the system are frozen.

6.5 Steady state solution

Equation (6.2a) has been solved in the steady state under the assumption that the phase decay term η_r is negligible, $\phi_r = 0$ and M is real. The solution

is a function of the initial state, due to the existence of the trapping state $|\psi^-\rangle$, so we only consider steady states that have no projection onto $|\psi^-\rangle$. The resulting density matrix, specified in the basis $\{|11\rangle, |10\rangle, |01\rangle, |00\rangle\}$, is

$$\rho_{ss} = \begin{pmatrix} \rho_{11} & 0 & 0 & \rho_{14} \\ 0 & \rho_{22} & \rho_{23} & 0 \\ 0 & \rho_{32} & \rho_{33} & 0 \\ \rho_{41} & 0 & 0 & \rho_{44} \end{pmatrix}, \tag{6.7a}$$

where

$$\rho_{11} = \frac{M^2(1-2N) + N^2(1+2N)}{(1+2N)L}, \tag{6.7b}$$

$$\rho_{22} = \rho_{23} = \rho_{32} = \rho_{33} = \frac{1}{6} - \frac{1}{6L}, \tag{6.7c}$$

$$\rho_{44} = 1 - \rho_{11} - \rho_{22} - \rho_{33}, \tag{6.7d}$$

$$\rho_{14} = \rho_{41} = \frac{M}{(1+2N)L}, \tag{6.7e}$$

$$L = 1 + 3N(1+N) - 3M^2. \tag{6.7f}$$

A few comments can be made about this solution. When driven from the ground state $|00\rangle\langle 00|$ with strong ($N \to \infty$) ideally squeezed light, we obtain the pure state $|\phi^+\rangle$. Changing the phase of M rotates this state into $|\phi^-\rangle$; in general we can generate correlated Bell states $|\phi^\pm\rangle$ but not anticorrelated Bell states $|\psi^\pm\rangle$ in this manner due to the correlated (as opposed to anticorrelated) nature of the squeezed light. Less strong ideally squeezed light drives the ground state to a state that is still pure and of the form

$$|\psi\rangle = \sqrt{\frac{N}{1+2N}}\,|11\rangle + \sqrt{\frac{N+1}{1+2N}}\,|00\rangle\,. \tag{6.8}$$

It is informative to plot these steady states in the LEFT and LEFC planes (see Figure 6.3). In contrast to the states displayed in Figure 4.9, here we do not access all of the (entangled) LEFC plane below the Werner line.

For nonideal ($M^2 < N(N+1)$) strongly squeezed light ($N \gg 1$) we obtain states (see, for example, the $N = 5$ line of Figure 6.3) that lie just below the Werner line. These steady states are mixtures of $|\phi^+\rangle\langle\phi^+|$ and the state

$$\rho = \begin{pmatrix} 1/3 & 0 & 0 & 0 \\ 0 & 1/6 & 0 & 0 \\ 0 & 0 & 1/6 & 0 \\ 0 & 0 & 0 & 1/3 \end{pmatrix}. \tag{6.9}$$

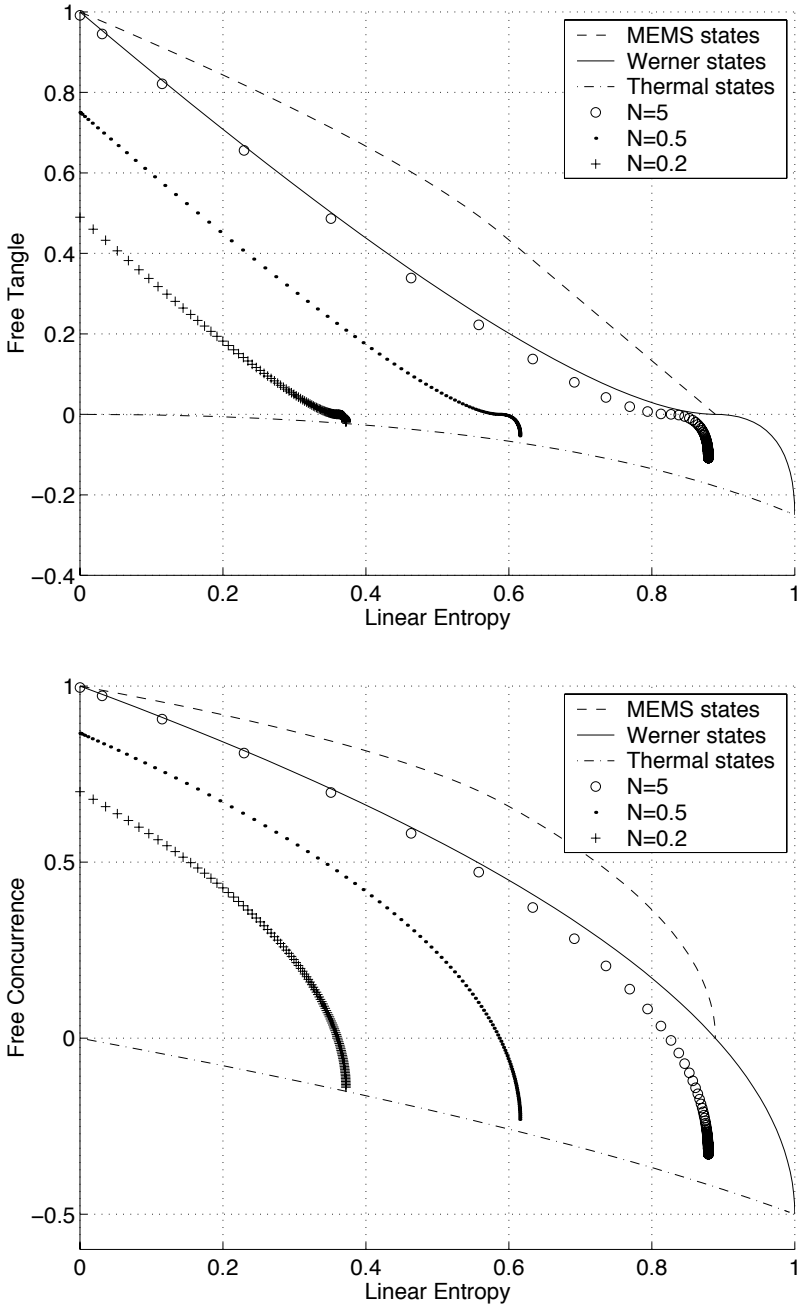

Figure 6.3: Steady states for two four-level atoms trapped in a cavity driven by squeezed light, plotted for a variety of N with $0 \leq M^2 \leq N(N+1)$. The top graph is the LEFT plane; the bottom graph is the LEFC plane.

These states are not true Werner states because $|\psi^-\rangle$ is a trapped state and our choice of initial condition prevents us from having a component of $|\psi^-\rangle$ in our mixture (as exists in true Werner states). In a related scenario considered in Section 6.7, we will consider a system that does not have trapped states and hence true Werner states are created.

Time evolution to the steady state is plotted in Figure 6.4 in both the LEFT and LEFC planes. Evolution from the ground state $|00\rangle$ creates states that are entangled at all times but always below the Werner line. Note that the larger the degree of squeezing N, the greater the maximum entropy achieved and the greater the final entanglement.

6.6 Entanglement and entropy engineering

In this Section we demonstrate that, by appropriate manipulations of the amplitude ($\propto \beta_r^2$) and phase ($\propto \eta_r^2$) couplings into the reservoir, we can access all entangled regions in the linear entropy-free tangle plane.

First we note, that by enabling the amplitude-decay channel at the expense of the phase-decay channel (i.e., selecting parameters such that $\beta_r \gg \eta_r$), we can generate states covering almost all the entangled area under the Werner line.

To generate states above the Werner line we use coherent Raman transitions induced by auxiliary laser fields to prepare the separable pure superposition state

$$|\psi\rangle = R_{DPA}(\theta)\,|00\rangle\,, \tag{6.10a}$$

where

$$R_{DPA}(\theta) = \{\cos(\theta/2)\mathbf{1}_2 + i\sin(\theta/2)\sigma_y\}^{\otimes 2}\,, \tag{6.10b}$$

for arbitrary $0 < \theta \leq \pi/2$. We then drive the atoms with strong ideally squeezed light by selecting $\beta_r \neq 0$, $\eta_r \ll \beta_r$, N large and $M^2 = N\,(N+1)$. The resulting states are shown in Figure 6.5. This technique accesses much of the region between the Werner and MEMS lines. It should be remembered that at any time the evolution of the system can be stopped by turning off all sources of light (setting $N, M, \Omega_r, \Omega_s = 0$).

These dynamics permit us to access most of the plane. To access the rest of the plane we stop the system somewhere on the $\theta = \pi/2$ curve in Figure 6.5 (the path followed during strong squeezing, commencing from the initial state $\frac{1}{2}\{|0\rangle + |1\rangle\}^{\otimes 2}$). A further local unitary transformation,

$$U = \frac{1}{\sqrt{2}}\{\sigma_x + \sigma_z\} \otimes \frac{1}{\sqrt{2}}\{\mathbf{1}_2 - i\sigma_y\}\,, \tag{6.11}$$

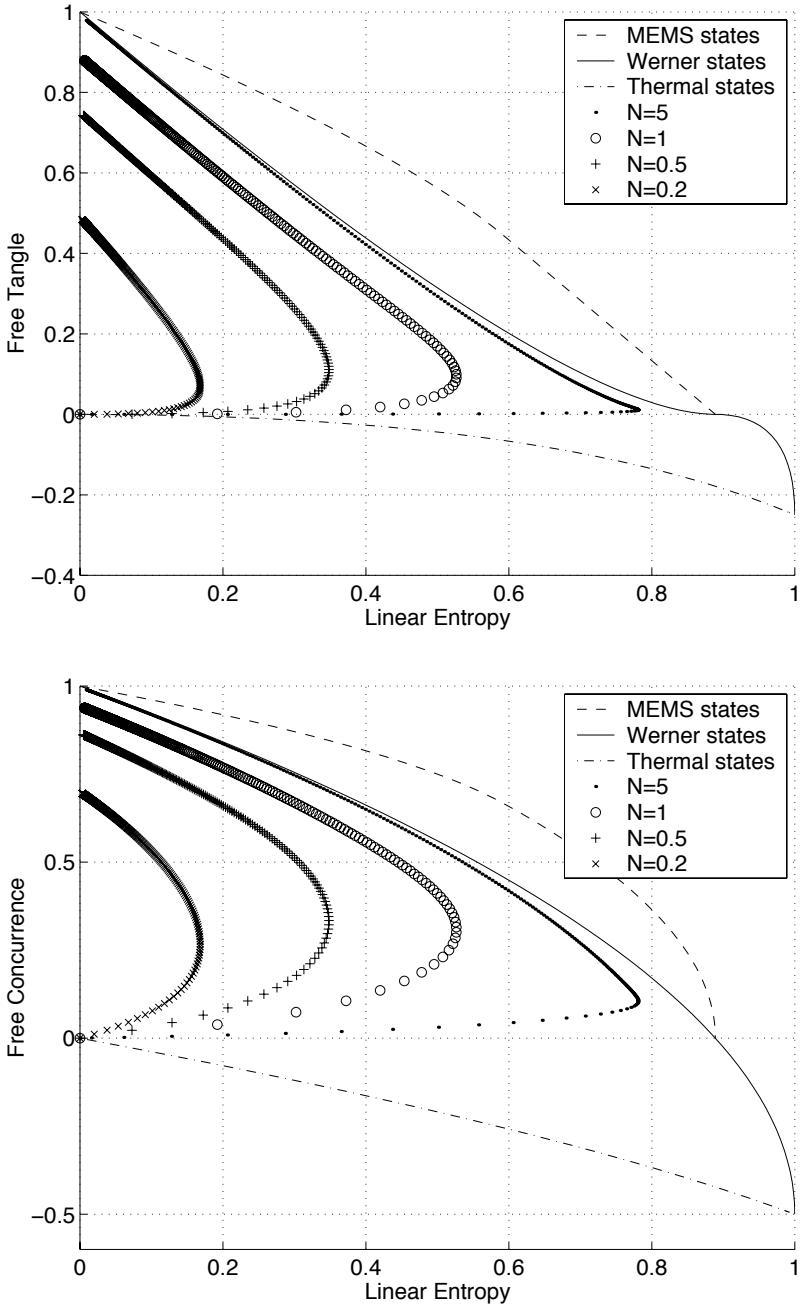

Figure 6.4: Evolution to the steady state in ideally squeezed light, plotted in both the LEFT and LEFC planes. The initial state is $|00\rangle$. Evolution is from bottom-left to top-left.

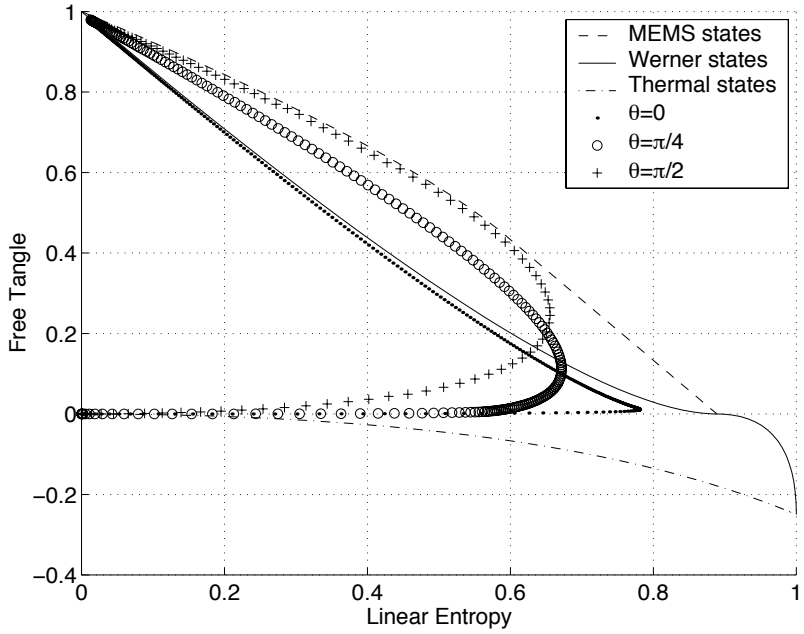

Figure 6.5: Evolution from a rotated ground state in squeezed light. $N = 5$ and $M = -\sqrt{N(N+1)}$.

is performed on the state. This transformation differs from (6.10b) in that it requires single atom addressing. We then disable the amplitude decay channel and enable the phase decay channel by setting $\beta_r = 0$, $\eta_r \neq 0$, $N > 0$ and $M = 0$. The subsequent evolution is shown in Figure 6.6. We can see that the remaining area under the Werner line is accessed in this manner. The phase decay results in a final state that lies on the border between entangled and separable (where $\tau_{free} = 0$).

6.7 Entangling atoms with the NDPA

In this Section we investigate another scenario based on the idealized model of Section 4.2, where two separated atoms each interact with spatially separated output modes from an NDPA. The alteration we make is to replace each atom with an effective one-dimensional atom, as developed in Chapter 5, consisting of an optical cavity containing a trapped 4-level atom (see Figure 6.7). As compared to the system described in Section 6.2, this experimental setup may hold advantages in loading and individually addressing the atoms.

We have seen, in the limit $\beta_r \gg \eta_r$, that the four-level cavity QED

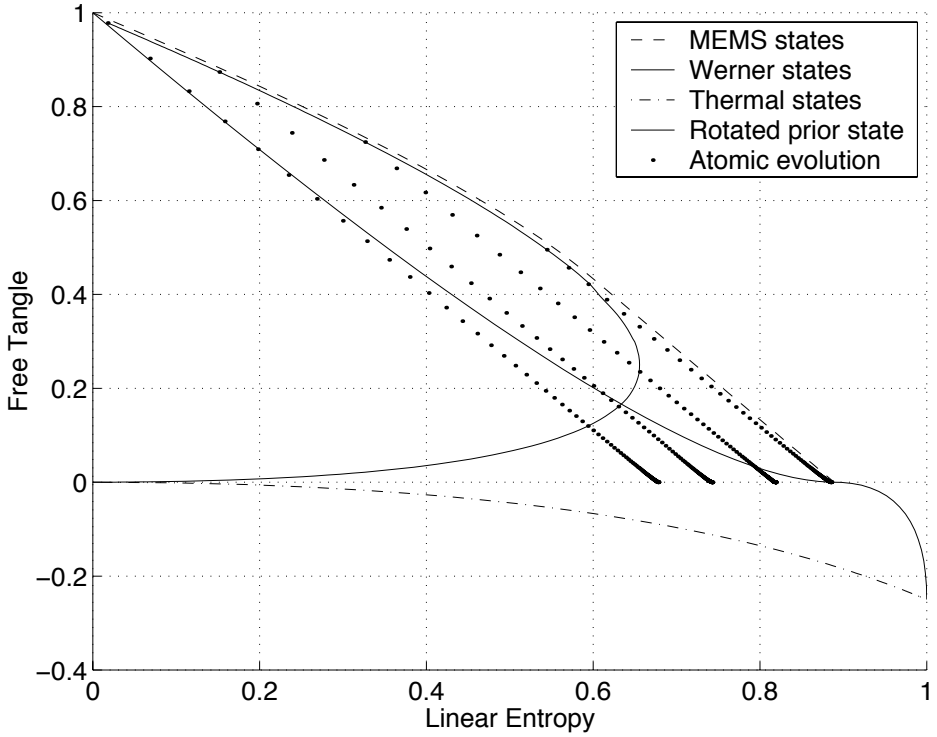

Figure 6.6: Phase decay initiated by thermal light. Evolution is from top-left to bottom-right. Initial states are local unitary transformations (6.11) of selected states from the $\theta = \pi/2$ curve of Figure 6.5 (shown here as the solid line).

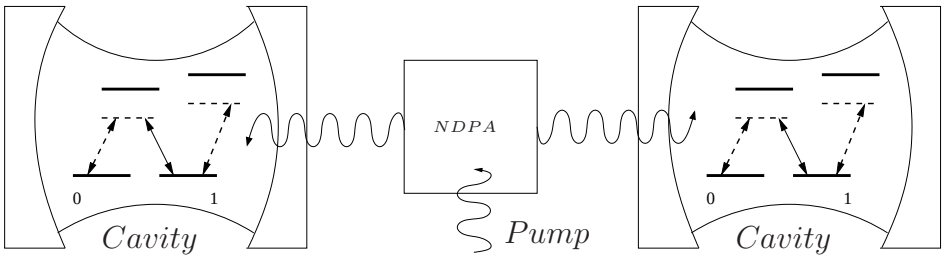

Figure 6.7: Two cavities containing a 4-level atom driven by squeezed light from an NDPA.

system of Chapter 5 interacts with squeezed light in the same manner as a two-level atom (that is not in a cavity); we need only rescale the coupling with the correspondence $\frac{\gamma}{2} \leftrightarrow \frac{\beta_r^2}{\kappa}$. Therefore, from Equation (4.5), we may immediately write the master equation for two one-dimensional atoms driven by an NDPA as

$$\begin{aligned}
\frac{d\rho}{dt} &= +\frac{\beta_r^2}{\kappa}\left(N'+1\right)\left(2\sigma_2^-\rho\sigma_2^+ - \sigma_2^+\sigma_2^-\rho - \rho\sigma_2^+\sigma_2^-\right) \\
&\quad +\frac{\beta_r^2}{\kappa}N'\left(2\sigma_2^+\rho\sigma_2^- - \sigma_2^-\sigma_2^+\rho - \rho\sigma_2^-\sigma_2^+\right) \\
&\quad +\frac{\beta_r^2}{\kappa}\left(N'+1\right)\left(2\sigma_3^-\rho\sigma_3^+ - \sigma_3^+\sigma_3^-\rho - \rho\sigma_3^+\sigma_3^-\right) \\
&\quad +\frac{\beta_r^2}{\kappa}N'\left(2\sigma_3^+\rho\sigma_3^- - \sigma_3^-\sigma_3^+\rho - \rho\sigma_3^-\sigma_3^+\right) \\
&\quad -\frac{\beta_r^2}{\kappa}M'\left(2\sigma_2^+\rho\sigma_3^+ - \sigma_3^+\sigma_2^+\rho - \rho\sigma_3^+\sigma_2^+\right) \\
&\quad -\frac{\beta_r^2}{\kappa}M'\left(2\sigma_3^+\rho\sigma_2^+ - \sigma_2^+\sigma_3^+\rho - \rho\sigma_2^+\sigma_3^+\right) \\
&\quad -\frac{\beta_r^2}{\kappa}M'\left(2\sigma_2^-\rho\sigma_3^- - \sigma_3^-\sigma_2^-\rho - \rho\sigma_3^-\sigma_2^-\right) \\
&\quad -\frac{\beta_r^2}{\kappa}M'\left(2\sigma_3^-\rho\sigma_2^- - \sigma_2^-\sigma_3^-\rho - \rho\sigma_2^-\sigma_3^-\right). \qquad (6.12)
\end{aligned}$$

We now consider how to access various regions of the entropy-entanglement plane. Evolution from the ground state is shown in Figure 6.8. The entire entangled region of the LEFT plane below the Werner line can be sampled. This area should be compared to that in Figure 6.4, which was for the situation with two atoms in the same cavity.

In contrast to the scheme with both atoms in one cavity (described in Section 6.2), for this scheme of two atoms each in their own cavity, we have not yet identified an initial state which can be driven directly to a state that lies above the Werner line. However, it is is still possible to generate states above the Werner line with a short sequence of operations. First we drive the system from the ground state $|00\rangle$ with strong ideally squeezed light to generate the Bell state $|\phi^+\rangle$. Then we make the local unitary transformation

$$R_{NDPA}(\theta)\left|\phi^+\right\rangle, \qquad (6.13a)$$

where

$$R_{NDPA}(\theta) = \mathbf{1}_2 \otimes \{\cos(\theta/2)\mathbf{1}_2 - i\sin(\theta/2)\sigma_x\}. \qquad (6.13b)$$

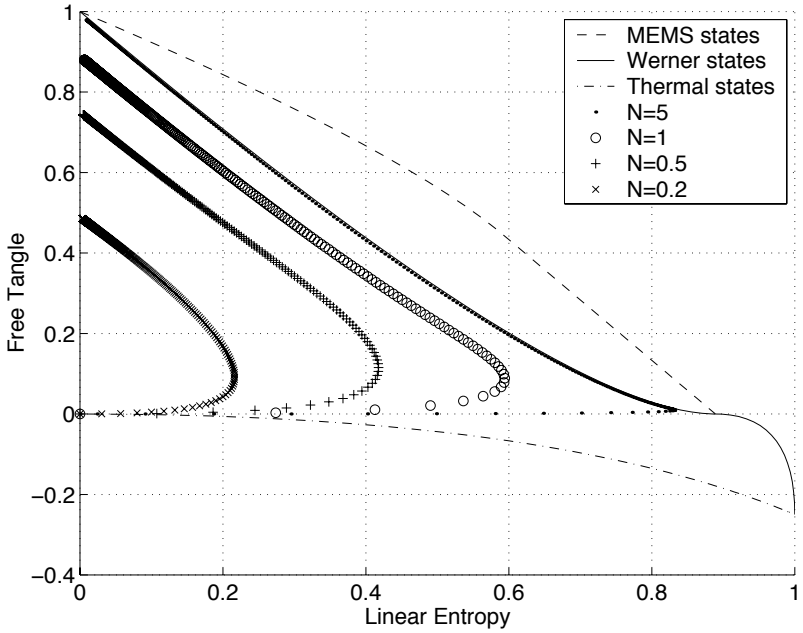

Figure 6.8: Evolution from the ground state $|00\rangle$ in ideally squeezed light.

If we then choose $\beta_r \neq 0$ and $\eta_r \ll \beta_r$, and allow the system to decay into vacuum $(N, M = 0)$, we generate the states swept out in Figure 6.9. In this manner we access a large area above the Werner line.

6.8 Conclusions

In this Chapter we have combined the ideas of Chapters 4 and 5 in creating two systems capable of generating long-lived entanglement in two separated trapped atoms. The technical difficulties involved in squeezing all of the modes with which the atoms might interact are dramatically lessened by coupling the atoms primarily to just one cavity mode. Then only this mode needs to be squeezed.

The decay of the atoms into the squeezed reservoir is through two mechanisms we have described as amplitude decay and phase decay. The strengths of these channels are independently adjustable. This flexibility allows us to engineer states of all physically allowed combinations of entropy and entanglement, as measured by the linear entropy and entanglement of formation, respectively.

We have not yet characterized all the states that can be produced using

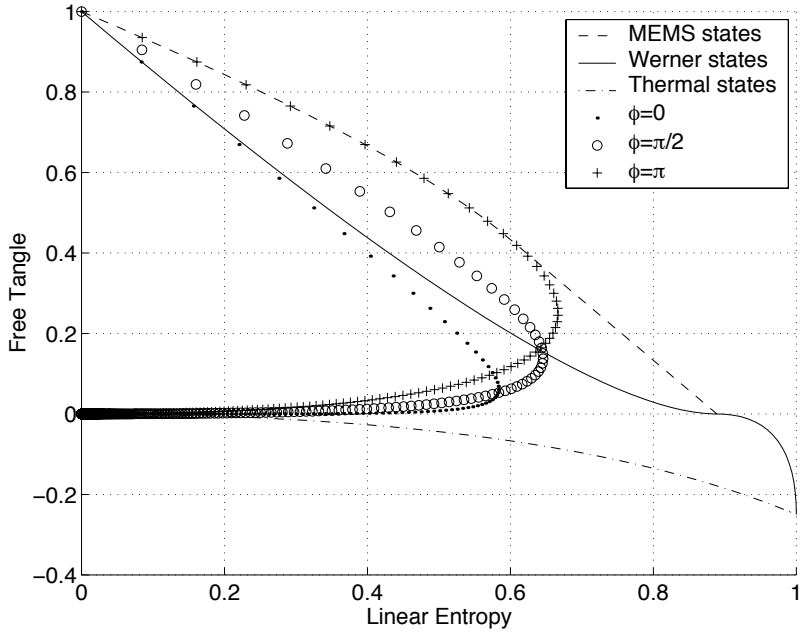

Figure 6.9: Amplitude decay into vacuum from a rotated Bell state.

the adjustable parameters of our systems. It would be interesting to find a physically realizable system that could access every state in the Hilbert space of two qubits and not just those of distinct entanglement and purity.

Chapter 7

Engineering a quantum reservoir

This chapter introduces quantum reservoir engineering and shows how it can be used to entangle atoms in a cavity QED setting without the necessity of using non-classical sources of light. The effects of atomic spontaneous emission during the Raman transitions are also investigated for realistic experimental parameters.

Contents

7.1 Introduction

In the previous chapters we used squeezed light to create a quantum reservoir for the atoms we wish to entangle. However, it is possible to create an effective quantum reservoir by driving a cavity with classical (thermal) light. The technique used to achieve this is known as *quantum reservoir engineering* and is the subject of this Chapter.

The concept of quantum reservoir engineering was first explicitly stated by Poyatos *et al.* [1]. They suggested ways to engineer particular couplings between the motional states of a trapped ion and its environment. The dissipation associated with each coupling drives the system into a particular steady state. They considered couplings capable of generating "Schrödinger Cat states" and squeezed states, among others.

A more general treatment can be found in the paper by Carvalho *et al.* [77]. Consider a reduced master equation for a system interacting with its environment, to which we have added an additional decay channel described by $\mathcal{L}_{eng}$:

$$\dot{\rho} = -i\left[H,\rho\right] + \mathcal{L}_{dec}\rho + \mathcal{L}_{eng}\rho, \tag{7.1a}$$

$$\mathcal{L}_{env}\rho \equiv \sum_i \frac{\gamma_i}{2}\left(2c_i\rho{c_i}^\dagger - {c_i}^\dagger c_i\rho - \rho{c_i}^\dagger c_i\right), \tag{7.1b}$$

$$\mathcal{L}_{eng}\rho \equiv \frac{\Gamma_{eng}}{2}\left(2d\rho d^\dagger - d^\dagger d\rho - \rho d^\dagger d\right). \tag{7.1c}$$

Under the assumption that we can ignore the internal dynamics of the system described by H, we see that the engineered decay channel will dominate the natural decay channel when $\Gamma_{eng} \gg \gamma_i$ and that the steady state of the system will be very close to the pointer states of the operator d.

The scheme for quantum-reservoir engineering that we propose is a variation of that described by Lütkenhaus, Cirac and Zoller in 1998 [78]. In their paper they investigated the dynamics of a driven multi-level atom coupled to a normal vacuum and showed how an effective squeezed reservoir is created for the atoms. Their scheme did not involve cavity QED and relied on spontaneous decay from excited states to produce the effective interaction. The lack of detailed control over the decay mechanisms allowed unwanted cross-decay channels to limit the degree of squeezing they could achieve.

7.2 Scheme

In the scenario considered in this Chapter, two atoms are trapped in a high-finesse optical cavity that has a decay rate of κ and frequency ω (see Fig-

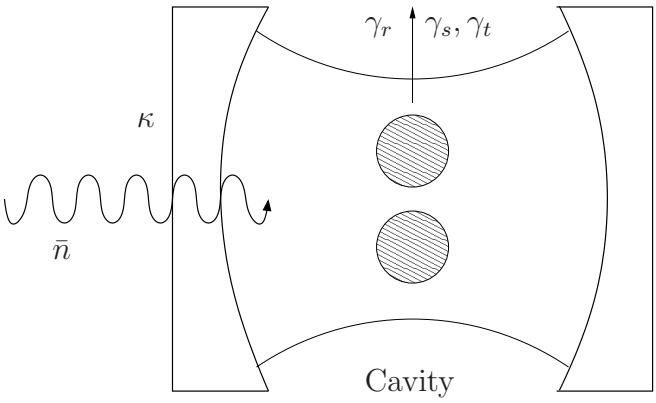

Figure 7.1: The cavity containing two trapped 5-level atoms. The cavity has a field decay rate κ and frequency ω, and the annihilation (creation) operator for the cavity mode is denoted a ($a^\dagger$). The spontaneous emission rates from the three excited levels of the atoms are γ_r, γ_s, and γ_t. The cavity may optionally be resonantly driven by thermal light of mean photon number $\bar{n}$.

ure 7.1). The cavity is resonantly driven with thermal light characterized by a mean photon number $\bar{n}$. It is necessary to trap the atoms at sites with a separation much greater than one optical wavelength, so that they can be individually addressed by probe lasers and so that there is no direct dipole-dipole interaction between them.

Two stable ground states of the atoms consititute the qubit states (see Figure 7.2). The cavity field and two auxiliary laser fields drive two different Raman transitions between these states. Transitions $|1\rangle \leftrightarrow |r\rangle$ and $|0\rangle \leftrightarrow |s\rangle$ are driven independently by strongly detuned lasers of Rabi frequency Ω_r and Ω_s respectively. The transitions $|0\rangle \leftrightarrow |r\rangle$ and $|1\rangle \leftrightarrow |s\rangle$, of frequencies ω_r and ω_s, are strongly coupled to the cavity mode, with coupling strengths g_r and g_s, and detunings Δ_r and Δ_s, respectively. The phase difference between the two lasers driving the Raman transitions is taken to be ϕ. A detuning Δ_{01} has been added between the ground states of the atoms, but it proves to have no significant effect (other than to the interaction picture we consider the system in) as long as both Raman transitions are Raman-resonant.

In the scheme of Lütkenhaus *et al.* [78], the laser fields Ω_r and Ω_s are chosen to be of opposite circular polarization so that they couple selectively to their respective atomic transitions, chosen to have $\Delta m_j = \pm 1$. In this Chapter we shall take this selectivity for granted and not concern ourselves with the exact mechanism used to achieve it.

A fifth state $|t\rangle$ is virtually excited from $|1\rangle$ by another strongly detuned

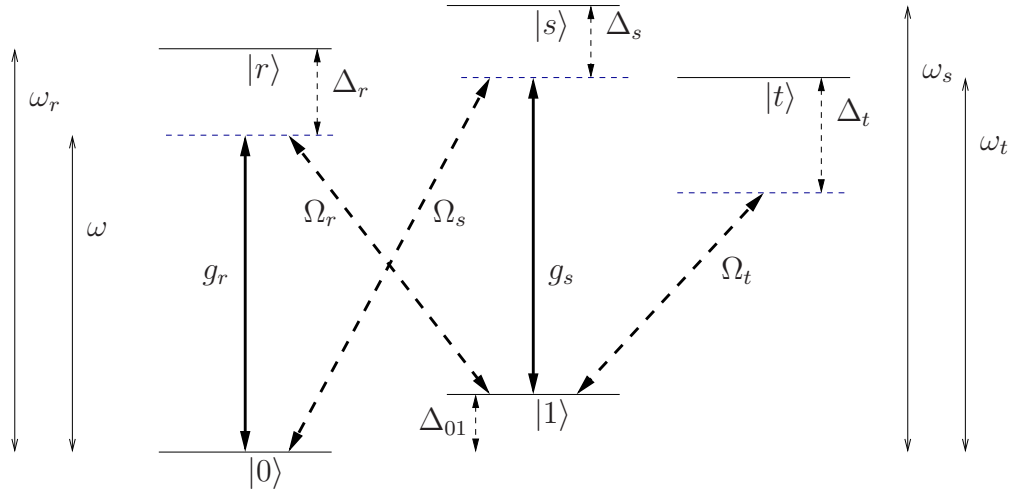

Figure 7.2: The atomic levels and transitions for each atom, showing the two Raman transitions and the virtual excitation of state $|t\rangle$. The three lasers have frequencies ω_{L_r}, ω_{L_s} and ω_{L_t}, and Rabi frequencies Ω_r, Ω_s and Ω_t respectively. The excited levels have frequencies ω_r, ω_s and ω_t. The lasers are strongly detuned by $\Delta_r = \omega_{L_r} - \omega_r + \Delta_{01}$, $\Delta_s = \omega_{L_s} - \omega_s$ and $\Delta_t = \omega_{L_t} - \omega_t + \Delta_{01}$. The ground states $|0\rangle$ and $|1\rangle$ are detuned by an amount Δ_{01}. As drawn, the detunings Δ_r, Δ_s and Δ_t are negative and Δ_{01} is positive.

laser field of Rabi frequency Ω_t. This driving adds an additional ac-Stark shift to the ground state $|1\rangle$, which may be used to cancel the other level shifts in the atomic ground states (in the manner which we have already employed in Chapter 5). The phase of the laser Ω_t is not significant and is set to zero.

7.3 Master equation

The master equation for the system comprising the cavity and the two 5-level atoms, in a frame rotating at the frequency of state $|0\rangle$, is

$$\dot{\rho} = \mathcal{L}\rho, \tag{7.2a}$$

where

$$\begin{aligned}
\mathcal{L}\rho &= -i\left[H,\rho\right] + \mathcal{L}_{cav}\rho + \mathcal{L}_{spon}\rho, && \text{(7.2b)}\\
\mathcal{L}_{cav}\rho &= \kappa(1+\bar{n})\left(2a\rho a^\dagger - a^\dagger a\rho - \rho a^\dagger a\right) \\
&\quad +\kappa\bar{n}\left(2a^\dagger\rho a - aa^\dagger\rho - \rho aa^\dagger\right), && \text{(7.2c)}
\end{aligned}$$

and

$$\begin{aligned}
H &= H_{cav} + H_{atoms} + H_{atoms/lasers} + H_{atoms/cav}, && \text{(7.2d)}\\
H_{cav} &= \omega a^\dagger a, && \text{(7.2e)}\\
H_{atoms} &= \sum_{i=1,2}\Big(\omega_r\left|r\right\rangle\left\langle r\right|_i + \omega_s\left|s\right\rangle\left\langle s\right|_i + \omega_t\left|t\right\rangle\left\langle t\right|_i \\
&\quad +\Delta_{01}\left|1\right\rangle\left\langle 1\right|_i\Big), && \text{(7.2f)}\\
H_{atoms/lasers} &= \sum_{i=1,2}\Big(\frac{\Omega_r}{2}e^{-i\omega_{L_r}t}\left|r\right\rangle\left\langle 1\right|_i + \text{H.c.} \\
&\quad +\frac{\Omega_s}{2}e^{-i[\omega_{L_s}t+\phi]}\left|s\right\rangle\left\langle 0\right|_i + \text{H.c.} \\
&\quad +\frac{\Omega_t}{2}e^{-i\omega_{L_t}t}\left|t\right\rangle\left\langle 1\right|_i + \text{H.c.}\Big), && \text{(7.2g)}\\
H_{atoms/cav} &= \sum_{i=1,2}\left(g_r\left|r\right\rangle\left\langle 0\right|_i a + g_s\left|s\right\rangle\left\langle 1\right|_i a + \text{H.c.}\right). && \text{(7.2h)}
\end{aligned}$$

The details of the spontaneous emission channels depend on the particular atomic levels chosen. In the level scheme used in [78] the linearly polarized photons produced in the decays $|r\rangle \rightarrow |0\rangle$ and $|s\rangle \rightarrow |1\rangle$ interfere (in that scheme there was no detuning Δ_{01}). However, for generality, we will assume

that all spontaneous emission channels are distinct, from each excited state to each ground state, and for each atom. Thus we obtain a spontaneous emission term as follows:

$$\mathcal{L}_{spon}\rho = \sum_{i\in\{1,2\}}\sum_{j\in\{r,s,t\}}\sum_{k\in\{0,1\}} \frac{\gamma_j}{2}\Big(2Y_{ijk}\rho {Y_{ijk}}^\dagger - \rho {Y_{ijk}}^\dagger Y_{ijk} - {Y_{ijk}}^\dagger Y_{ijk}\rho\Big), \tag{7.3a}$$

where

$$Y_{ijk} = g_{jk}\left|k\right\rangle\left\langle j\right|_i, \tag{7.3b}$$

and γ_r, γ_s and γ_t are the total spontaneous emission rates from each excited state. The summations, in turn, are over each atom, each excited state, and each ground state. Here, g_{jk} are coupling strengths (e.g., Clebsch-Gordon coefficients) that specify the branching ratios for the decays. We assume a closed system so that the branching ratios obey

$$g_{j0}^2 + g_{j1}^2 = 1. \tag{7.4}$$

Since we are not specifying a particular atomic level configuration we will choose, for simplicity, all values of g_{jk} to be $\frac{1}{\sqrt{2}}$.

We do have occasion later to distinguish two types of spontaneous emission, depending on whether decay from an excited atomic state causes an effective transition between the ground states or not (assuming we were driven to the excited state via a laser, not the cavity). Therefore we define

$$g_l = g_{r0}, g_{s1}, g_{t0}, \tag{7.5a}$$

$$g_c = g_{r1}, g_{s0}, g_{t1}, \tag{7.5b}$$

where g_l represents decay channels that induce a Raman transition. In general this type of decay proves to be more detrimental to our state preparation schemes.

7.4 Reduced master equation

In this Section we will adiabatically eliminate first the excited states of the atoms and then the cavity mode from Equation (7.2) to find a reduced master equation for the atomic ground states alone. This adiabatic elimination will be performed assuming no atomic spontaneous emission during the Raman transitions. In the reduced master equation that arises the effective squeezing interaction will be apparent. We shall consider the effects of atomic spontaneous emission in Section 7.6.

7.4.1 Adiabatic elimination of excited states

We proceed by assuming that the the light fields are highly detuned from the the excited atomic states, i.e. that

$$|\Delta_j| \gg \Omega_j, g_r, g_s, \kappa, \gamma_j, \qquad (j = r, s, t). \tag{7.6}$$

We may then adiabatically eliminate the excited states $|r\rangle_i$, $|s\rangle_i$ and $|t\rangle_i$ to obtain a reduced master equation for a pair of effective two-level atoms (consisting of the states $|0\rangle_i$ and $|1\rangle_i$) coupled to the shared cavity mode. The details of the adiabatic elimination may be found in Appendix C.

In this way, for the case where spontaneous emission may be entirely neglected (i.e., $\gamma_r, \gamma_s, \gamma_t = 0$), we obtain a master equation for the cavity and for the ground states of the atoms

$$\dot{\rho} = -i\left[H_{reduced}, \rho\right] + \mathcal{L}_{cav}\rho, \tag{7.7a}$$

where

$$\begin{aligned} H_{reduced} &= \sum_{i=1,2} a^\dagger a \left(\eta_r \sigma_i^- \sigma_i^+ + \eta_s \sigma_i^+ \sigma_i^-\right) \\ &\quad + \sum_{i=1,2} \left[\beta_r \left(a\sigma_i^+ + a^\dagger \sigma_i^-\right) + \beta_s \left(e^{i\phi} a \sigma_i^- + e^{-i\phi} a^\dagger \sigma_i^+\right)\right] \\ &\quad + \sum_{i=1,2} \left(\frac{\Omega_r^2}{4\Delta_r}\sigma_i^+\sigma_i^- + \frac{\Omega_s^2}{4\Delta_s}\sigma_i^-\sigma_i^+ + \frac{\Omega_t^2}{4\Delta_t}\sigma_i^+\sigma_i^-\right), \end{aligned} \tag{7.7b}$$

and

$$\begin{aligned} \mathcal{L}_{cav}\rho &= \kappa(1+\bar{n})\left(2a\rho a^\dagger - a^\dagger a\rho - \rho a^\dagger a\right) \\ &\quad + \kappa\bar{n}\left(2a^\dagger \rho a - aa^\dagger\rho - \rho aa^\dagger\right). \end{aligned} \tag{7.7c}$$

Here $\sigma_i^- = |0\rangle\langle 1|_i$ is the lowering operator for atom i.

This (partially) reduced system is characterized by the parameters

$$\beta_r = \frac{g_r\Omega_r}{2\Delta_r},\ \beta_s = \frac{g_s\Omega_s}{2\Delta_s},\ \eta_r = \frac{g_r^2}{\Delta_r},\ \eta_s = \frac{g_s^2}{\Delta_s}, \tag{7.8}$$

where β_r and β_s are two (Raman) coupling strengths to the cavity mode for each effective two-level atom and the cavity mode and η_r and η_s are the ac-Stark shifts per cavity photon induced in $|0\rangle$ and $|1\rangle$, respectively.

7.4.2 Adiabatic elimination of cavity

We further reduce the model by assuming the "bad-cavity limit" with respect to the two-level systems, i.e.

$$\kappa \gg |\beta_r|, |\beta_s|, |\eta_r|, |\eta_s|. \tag{7.9}$$

This enables us to adiabatically eliminate the cavity mode to obtain the master equation in a form in which the effective squeezing interaction is easily recognized, i.e.,

$$\begin{aligned}
\dot{\rho} &= \frac{2\beta^2}{\kappa}(N+1)\left(2S\rho S^\dagger - S^\dagger S\rho - \rho S^\dagger S\right) \\
&\quad + \frac{2\beta^2}{\kappa}N\left(2S^\dagger\rho S - SS^\dagger\rho - \rho SS^\dagger\right) \\
&\quad - \frac{2\beta^2}{\kappa}M\left(2S^\dagger\rho S^\dagger - S^\dagger S^\dagger\rho - \rho S^\dagger S^\dagger\right) \\
&\quad - \frac{2\beta^2}{\kappa}M^*\left(2S\rho S - SS\rho - \rho SS\right) \\
&\quad + \frac{\eta^2}{2\kappa}\bar{n}(\bar{n}+1)\left(2P\rho P^\dagger - P^\dagger P\rho - \rho P^\dagger P\right).
\end{aligned} \tag{7.10a}$$

Here, we have defined parameters describing the effective degree and purity of squeezing:

$$N = \frac{(\bar{n}+1)\beta_s^2 + \bar{n}\beta_r^2}{\beta^2}, \tag{7.10b}$$

$$M = \frac{-(2\bar{n}+1)\beta_r\beta_s}{\beta^2}\mathrm{e}^{i\phi}, \tag{7.10c}$$

effective amplitude and phase coupling constants:

$$\beta^2 = \beta_r^2 - \beta_s^2, \tag{7.10d}$$

$$\eta^2 = (\eta_r - \eta_s)^2, \tag{7.10e}$$

and collective atomic operators:

$$S = \frac{1}{\sqrt{2}}\left(\sigma_1^- + \sigma_2^-\right), \tag{7.10f}$$

$$P = \sigma_1^-\sigma_1^+ + \sigma_2^-\sigma_2^+. \tag{7.10g}$$

It should be noted that we absorb the phase angle between the driving lasers into our definition of M (7.10c), hence we will not restrict ourselves to M real.

The derivation of this master equation (7.10) also requires that the light shifts induced in the atoms, by the driving lasers and by photons in the cavity, are the same for each ground state. Then, the phase of the effective two-level system will remain constant with respect to the phase difference ϕ between the two lasers driving the Raman transitions. In other words, the atomic system and effective squeezed reservoir must be "resonant" with each other, requiring

$$\frac{\Omega_s^2}{4\Delta_s} - \frac{\Omega_r^2}{4\Delta_r} - \frac{\Omega_t^2}{4\Delta_t} + \frac{g_r^2}{\Delta_r}\bar{n} - \frac{g_s^2}{\Delta_s}\bar{n} = 0. \tag{7.11}$$

It is to satisfy this condition, while maximizing flexibility in our choices of $\Omega_{r,s}$ and $\Delta_{r,s}$, that we employ the additional transition $|1\rangle \leftrightarrow |t\rangle$. The level shift $\Omega_t^2/(4\Delta_t)$ provides an extra degree of freedom with which to satisfy Equation (7.11).

We now examine Equation (7.10). It bears a striking resemblance to Equation (6.2), which was for a pair of 4-level atoms in a cavity driven by squeezed light, despite the fact that in the current system there are no sources of non-classical light. The terms in (7.10) that are proportional to β^2 describe the collective coupling, with strength β^2/κ, of our pair of effective two-level atoms to an effective squeezed reservoir, with the degree of purity of squeezing characterized by the parameters N and M [2, 70]. Ideal squeezing corresponds to the case where $|M|^2 = N(N+1)$, which requires $\bar{n} = 0$ (i.e., no thermal driving of the cavity). The last line of Equation (7.10a) may again be interpreted as phase damping of the atomic qubits caused by a coherent scattering process between the atoms and the (thermal) intra-cavity photons. There is no phase damping when there is no thermal driving (i.e., $\bar{n} = 0$) or when the level shifts caused by intra-cavity photons are the same for each ground state (i.e., $\eta_r = \eta_s$).

The phase damping in this system differs from that occurring in Equation (6.2), where two 4-level atoms are driven by squeezed light in a cavity. In that system, the phase damping is induced by the squeezed light itself and can only be made negligible by reducing the level shift η_r. Here, the degree of phase damping depends on both $\bar{n}$ and η^2 and may be eliminated by setting either of these to zero. It is easy to choose parameters such that $\eta = 0$ (just take $\eta_r = \eta_s$). Also, $\bar{n}$ is zero when generating ideal squeezing. Thus the effects of phase damping are more controllable than in the system of Section 6.3.

The relative strengths of the amplitude decay terms (proportional to β^2) and the phase damping term (proportional to η^2) are independently adjustable, so long as Equation (7.11) is satisfied and our timescale assumptions (7.6) and (7.9) remain justified. Again, it is worth remembering that,

when we choose $\beta, \bar{n} = 0$ or $\beta, \eta_r - \eta_s = 0$, the state of the system is frozen.

7.5 Entanglement and entropy engineering

In this Section we demonstrate that, by adjusting the amplitude ($\propto \beta^2$) and phase ($\propto \eta^2$) couplings into the reservoir, we can access states in the entirety of the entangled part of the linear entropy-free concurrence plane.

In the absence of phase damping terms, our master equation (7.10) has a form identical to Equation (6.2) for two 4-level atoms in a cavity driven by squeezed light (the system considered in Section 6.3). Therefore, the results described in this section largely duplicate those obtained in Section 6.6. The differences relate to the way in which the phase damping channel is manipulated.

7.5.1 Steady state solutions

We first examine the states in the entropy-entanglement plane that can be generated in the steady state.

The collective coupling of two atoms to the reservoir leads as usual to certain decoherence-free states, which decouple completely from the dynamics. Restating the Bell states again for convenience,

$$\left|\phi^{\pm}\right\rangle = \frac{1}{\sqrt{2}}\left(|00\rangle \pm |11\rangle\right), \tag{7.12a}$$

$$\left|\psi^{\pm}\right\rangle = \frac{1}{\sqrt{2}}\left(|01\rangle \pm |10\rangle\right), \tag{7.12b}$$

we find that $|\psi^-\rangle$ is decouples in all parameter regimes and that $|\psi^+\rangle$ is also decoupled when $N, M = 0$.

We restrict ourselves to initial states (such as the ground state $|00\rangle$) which have no projection onto $|\psi^-\rangle$. With such initial states, we may solve Equation (7.10) to obtain the steady state in the case where the phase decay term can be neglected in comparison to the other terms (i.e., through choices of parameters such that $\eta^2 \ll \beta^2$). The steady state density matrix ρ_{ss}, specified in the basis $\{|11\rangle, |10\rangle, |01\rangle, |00\rangle\}$, is then

$$\rho_{ss} = \begin{pmatrix} \rho_{11} & 0 & 0 & \rho_{14} \\ 0 & \rho_{22} & \rho_{23} & 0 \\ 0 & \rho_{32} & \rho_{33} & 0 \\ \rho_{41} & 0 & 0 & \rho_{44} \end{pmatrix}, \tag{7.13a}$$

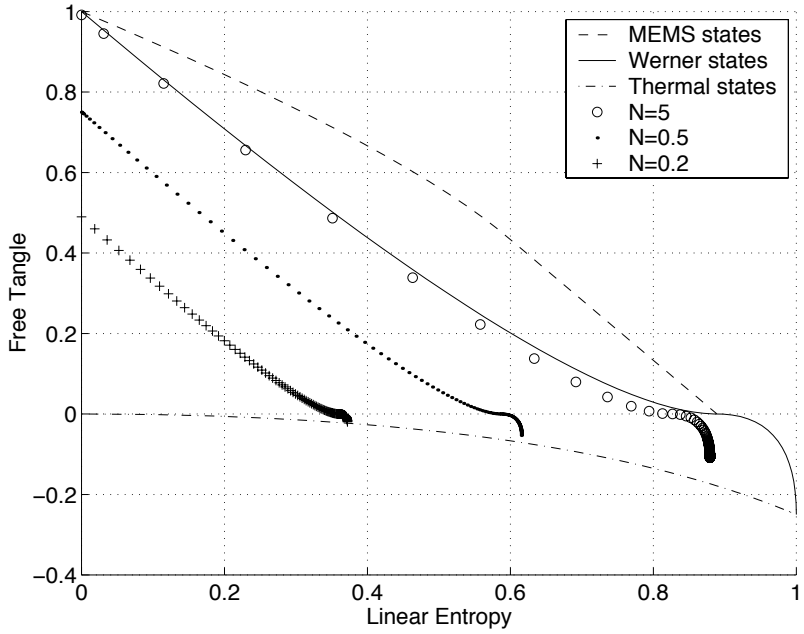

Figure 7.3: The steady state, plotted in the LEFT plane, for selected values of N and $0 \leq M \leq \sqrt{N(N+1)}$ and for an initial state of $|00\rangle$. It is not possible to generate states up to the Werner line as $N \to \infty$.

where

$$\rho_{11} = \frac{|M|^2(1-2N) + N^2(1+2N)}{(1+2N)L}, \tag{7.13b}$$

$$\rho_{22} = \rho_{23} = \rho_{32} = \rho_{33} = \frac{1}{6} - \frac{1}{6L}, \tag{7.13c}$$

$$\rho_{44} = 1 - \rho_{11} - \rho_{22} - \rho_{33}, \tag{7.13d}$$

$$\rho_{14} = {\rho_{41}}^* = \frac{M}{(1+2N)L}, \tag{7.13e}$$

$$L = 1 + 3N(1+N) - 3|M|^2. \tag{7.13f}$$

The steady state (see Equation (7.13)) and time evolution to the steady state are shown in Figure 7.3 and Figure 7.4 respectively, plotted in the LEFT plane as defined in Section 2.5.

With ideal squeezing ($\bar{n} = 0$, $|M|^2 = N(N+1)$), the steady state (7.13) is a pure state, $\rho_{ss} = |\Psi\rangle\langle\Psi|$, with [2]

$$|\Psi\rangle = \sqrt{\frac{N+1}{1+2N}}\,|00\rangle - e^{i\phi}\sqrt{\frac{N}{1+2N}}\,|11\rangle\,. \tag{7.14}$$

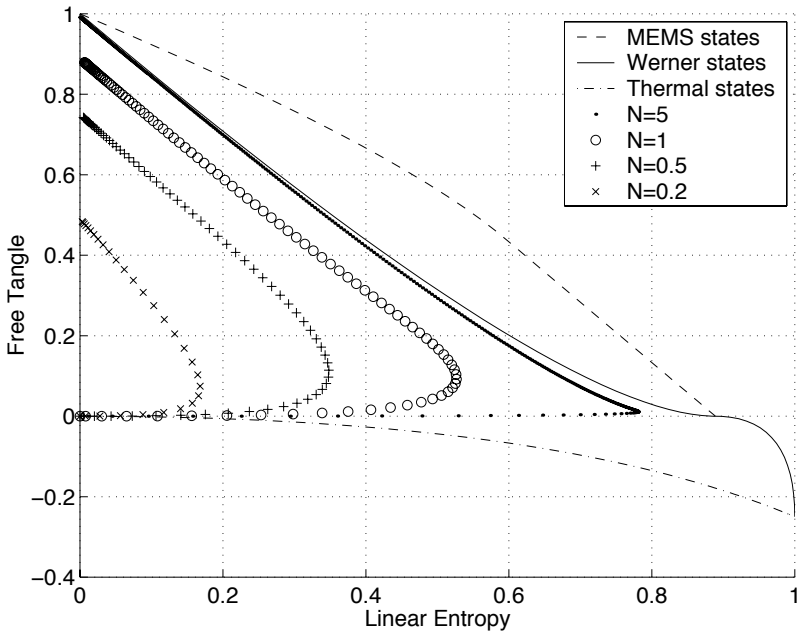

Figure 7.4: Evolution in the LEFT plane, from $|00\rangle$ to the steady state with ideal squeezing, plotted for various values of N. The data points are not equally spaced in time. Pure states always result. Evolution is from bottom-left to top-left.

These states lie on the y-axis of Figure 7.3. In the limit of strong ideal squeezing ($N \to \infty$, $\bar{n} = 0$, $|M|^2 = N(N+1)$), the phase values $\phi = 0$ and $\phi = \pi$ generate the Bell states $|\phi^-\rangle$ and $|\phi^+\rangle$, respectively.

Strong nonideal squeezing ($N \to \infty$, $|M|^2 = N(N+1)$, $\eta = 0$) generates states that lie just below the Werner line (see $N = 5$ line of Figure 7.3). These states are mixtures of $|\phi^-\rangle\langle\phi^-|$ and the state $\rho' = \mathrm{diag}\{1/3, 1/6, 1/6, 1/3\}$.

7.5.2 States above the Werner line

States above the Werner line (see Figure 7.5) can be generated by initially preparing the separable pure superposition state

$$|\psi\rangle = R_{QRE}(\theta)\,|00\rangle\,, \tag{7.15a}$$
$$R_{QRE}(\theta) = \{\cos(\theta/2)\mathbf{1}_2 + i\sin(\theta/2)\sigma_y\}^{\otimes 2}\,, \tag{7.15b}$$

for arbitrary $0 < \theta \leq \pi/2$, and then allowing it to decay into a strongly squeezed quantum reservoir. From Figure 7.3 and Figure 7.5 we see that we can produce states covering most of the Linear Entropy-Tangle plane. The remaining area in the plane may be accessed by performing the local unitary transformation

$$U = \frac{1}{\sqrt{2}}\{\sigma_x + \sigma_z\} \otimes \frac{1}{\sqrt{2}}\{\mathbf{1}_2 - i\sigma_y\} \tag{7.16}$$

on states from the $\theta = \pi/2$ curve of Figure 7.5, and then enabling the phase decay channel at the expense of amplitude decay as shown in Figure 7.6. To do this we must drive the cavity with thermal light ($\bar{n} \neq 0$), while choosing parameters such that $\beta = 0$ and $\eta \neq 0$.

It is also straightforward to generate the interesting states on the boundary between separable and entangled, where $\tau_{free} = 0$. These are swept out when the initial state $|01\rangle$ decays into a reservoir with strong ideal squeezing. Included in this range is the maximally mixed entangled state on the intersection of the Werner line and the MEMS line.

7.6 Spontaneous emission

It is possible to find the reduced master equation for the cavity and the atomic ground states in the presence of spontaneous emission (details are given in Appendix C). In that derivation we make the assumptions that the detunings are all the same (i.e., $\Delta_r = \Delta_s = \Delta_t = \Delta$) and that the

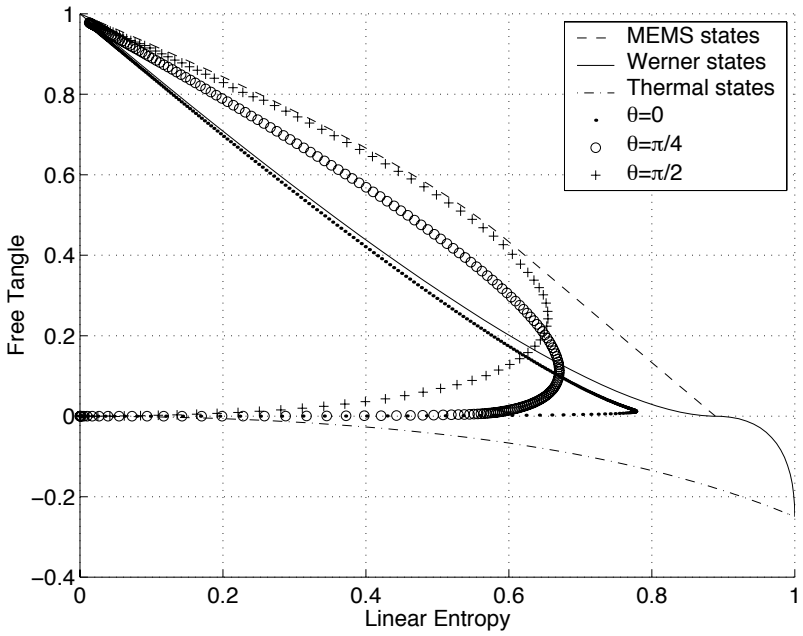

Figure 7.5: Evolution from various rotated initial ground states $R_{QRE}(\theta)\,|00\rangle$, as defined in (7.15b), plotted in the LEFT plane. Parameters are $\kappa = 1$, $\beta_r = 0.11$, $\beta_s = 0.1$, $\bar{n} = 0$, so that $N = 4.8$. The data points are not equally spaced in time. Evolution is from bottom-left to top-left.

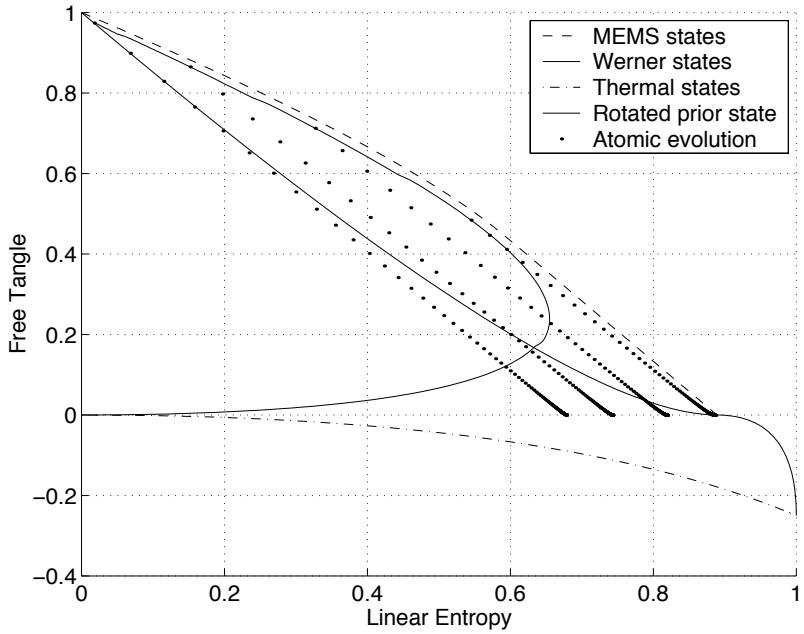

Figure 7.6: Phase decay commencing after application of the unitary transformation (7.16) to a selection of states from the $\theta = \pi/2$ curve of Figure 7.5. Phase decay is enabled, and amplitude decay is disabled. The parameters are $\kappa = 1$, $\beta_r = 0$, $\beta_s = 0$, $\bar{n} = 1$, $\eta_r = 0.1$, $\eta_s = 0.08$. Evolution is from top-left to bottom-right.

spontaneous emission rates from the excited states are all the same (i.e., $\gamma_r = \gamma_s = \gamma_t = \gamma$). We obtain the master equation

$$\begin{aligned}\dot{\rho} &= -i\left(H_{eff}\rho - \rho H_{eff}^{\dagger}\right) \\ &+ \sum_{j\in\{r,s,t\}}\sum_{k\in\{0,1\}} \frac{\gamma}{\Delta^2 + \frac{\gamma^2}{4}} \left(Y_{1jk}Q_1^{\dagger}\otimes\mathbf{1}\right)\rho\left(Q_1 Y_{1jk}^{\dagger}\otimes\mathbf{1}\right) \\ &+ \sum_{j\in\{r,s,t\}}\sum_{k\in\{0,1\}} \frac{\gamma}{\Delta^2 + \frac{\gamma^2}{4}} \left(\mathbf{1}\otimes Y_{2jk}Q_2^{\dagger}\right)\rho\left(\mathbf{1}\otimes Q_2 Y_{2jk}^{\dagger}\right),\end{aligned} \tag{7.17a}$$

where

$$H_{eff} = \frac{1}{\Delta + i\frac{\gamma}{2}}\left(Q_1 Q_1^{\dagger}\otimes\mathbf{1} + \mathbf{1}\otimes Q_2 Q_2^{\dagger}\right), \tag{7.17b}$$

and

$$\begin{aligned}Q_1^{\dagger} &= g_r a\left|r\right\rangle\left\langle 0\right|_1 + g_s a\left|s\right\rangle\left\langle 1\right|_1 \\ &\quad + \frac{\Omega_r}{2}\left|r\right\rangle\left\langle 1\right|_1 + \frac{\Omega_s}{2}e^{-i\phi}\left|s\right\rangle\left\langle 0\right|_1 + \frac{\Omega_t}{2}\left|t\right\rangle\left\langle 1\right|_1, \qquad (7.17c) \\ Q_2^{\dagger} &= g_r a\left|r\right\rangle\left\langle 0\right|_2 + g_s a\left|s\right\rangle\left\langle 1\right|_2 \\ &\quad + \frac{\Omega_r}{2}\left|r\right\rangle\left\langle 1\right|_2 + \frac{\Omega_s}{2}e^{-i\phi}\left|s\right\rangle\left\langle 0\right|_2 + \frac{\Omega_t}{2}\left|t\right\rangle\left\langle 1\right|_2. \qquad (7.17d)\end{aligned}$$

The definitions of the spontaneous emission terms Y_{ijk} can be found in Equation (7.3a).

We may now estimate the effect of spontaneous emission. First we consider the slowest rate associated with the dynamics of the reduced master equation (7.10). Taking M to be real and positive, and $\bar{n} = 0$ (i.e., no phase decay), we find the slowest rate to be

$$\tau_{slow} = \frac{4\beta^2}{\kappa}\left(2N - 2M + 1\right), \tag{7.18}$$

whose form is typical of the inhibited phase decay associated with atomic damping by a squeezed reservoir [79]. Analysis of Equation (7.17) reveals characteristic rates

$$\tau_{emiss} = \gamma_i \frac{\Omega_i^2}{2\Delta_i^2},\ (i = r, s, t), \tag{7.19}$$

for spontaneous emission from the finite populations of the excited atomic states. We then expect that spontaneous emission can be neglected when $\tau_{slow} \gg$

τ_{emiss}. So, taking the rate for $i = r$ to be the maximum value for τ_{emiss}, the condition that atomic spontaneous emission be negligible during the state preparation period can be expressed (after some manipulation) as

$$\frac{2g_r^2}{\gamma_r \kappa} \gg \left(1 - \sqrt{\frac{N}{N+1}}\right)^{-2}. \tag{7.20}$$

This amounts to the condition of strong coupling in cavity QED, made somewhat more stringent due to the inhibited atomic decay rate associated with the effective squeezed reservoir interaction.

We will now investigate the dynamics of Equation (7.17) in the LEFT plane, tracing over the cavity (which is negligibly populated) to calculate the free tangle. The numerical simulation is not sensitive to the detailed state of the cavity, and we can use a truncated number basis containing only 2 states. We use parameters, as achieved recently in a cavity QED experiment [15], of $(g_r, \kappa, \gamma_r)/2\pi = (110, 14.2, 5.2)\,\mathrm{MHz}$. With the degree of squeezing $N = 2$, the condition for neglecting spontaneous emission (7.20) reduces to the inequality $332 \gg 30$, indicating that a sufficiently strong coupling is experimentally realistic with significant levels of effective squeezing.

Another requirement is that the state we are trying to prepare is established on a timescale much less than typical trap confinement times for single atoms. Taking $\Omega_r/\Delta_r = 0.02$ (for example), and using the above parameters for g_r, κ and γ_r, the characteristic state preparation time is computed to be less than 50μs, which is orders of magnitude less than single-atom trapping times in tightly-confining optical dipole traps (see, e.g., [14, 12, 80]).

Starting from the rotated ground state $R_{QRE}(\pi/2)\,|00\rangle$ (7.15b), and disabling the phase decay channel with $\bar{n} = 0$, we obtain a curve in the LEFT plane as in Figure 7.7. Examining this graph we see that, rather unexpectedly, spontaneous emission induces a slow late-time decay in the entanglement. The explanation for this effect can be found in Figure 7.8, which shows the projection of ρ onto the four Bell states. The Bell state $|\psi^-\rangle$ decouples from Equation (7.10), but no longer does so when spontaneous emission is included into the model. Therefore, the evolving state of the system acquires a projection onto $|\psi^-\rangle$ which significantly degrades the maximum entanglement generated. The slowest rate found in condition (7.18) is more precisely the slowest non-zero rate, since the trapped state does not evolve.

We see that, despite the negative effects of spontaneous emission, we can still generate states above the Werner line. Although the maximum value of the tangle becomes limited to ≈ 0.5, we nevertheless still achieve a high peak overlap (≈ 0.85) with the Bell state $|\phi^-\rangle$, as seen in Figure 7.8.

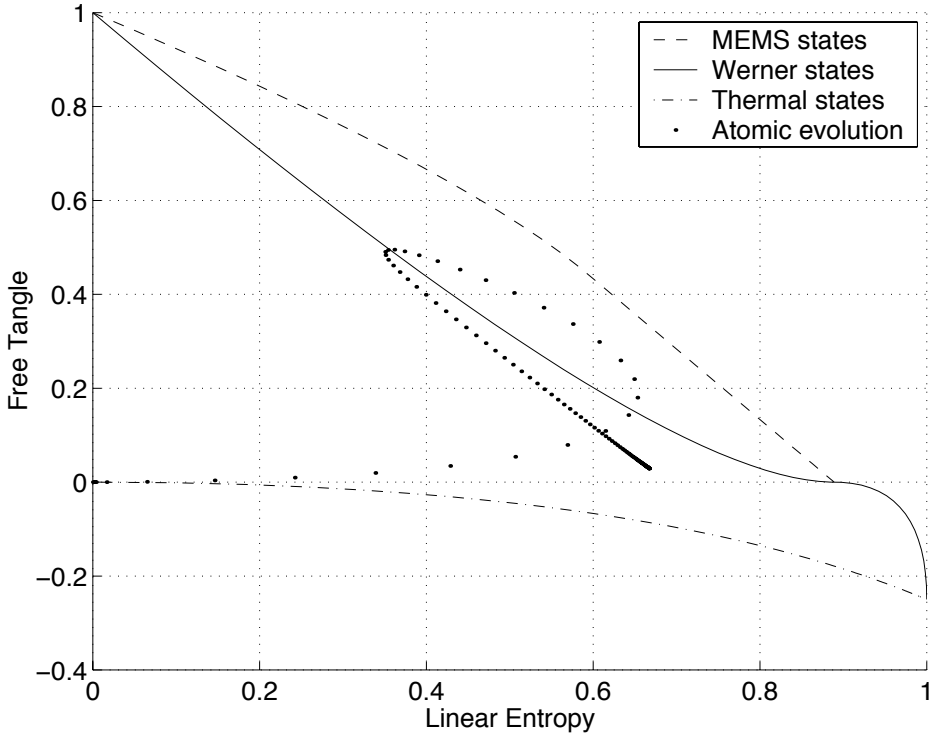

Figure 7.7: Evolution with spontaneous emission included, plotted in the LEFT plane. The points plotted are not equally spaced in time. The free tangle is calculated after tracing over the cavity. The initial atomic state is $|00\rangle$. Parameters are $(g_r, g_s, \kappa, \gamma, \Omega_r, \Omega_s, \Omega_t, \Delta_r, \Delta_s, \Delta_t)/2\pi = (110, 132, 14.2, 5.2, 100, 100, 66.3, 8000, 8000, 8000)$ MHz and $\bar{n} = 0$, $g_c = g_l = \frac{1}{\sqrt{2}}$. The effective degree and purity of squeezing are $N = 2.27$ and $M = -2.72$. Late-time decay of the entanglement occurs, nevertheless states above the Werner line are still generated during the evolution.

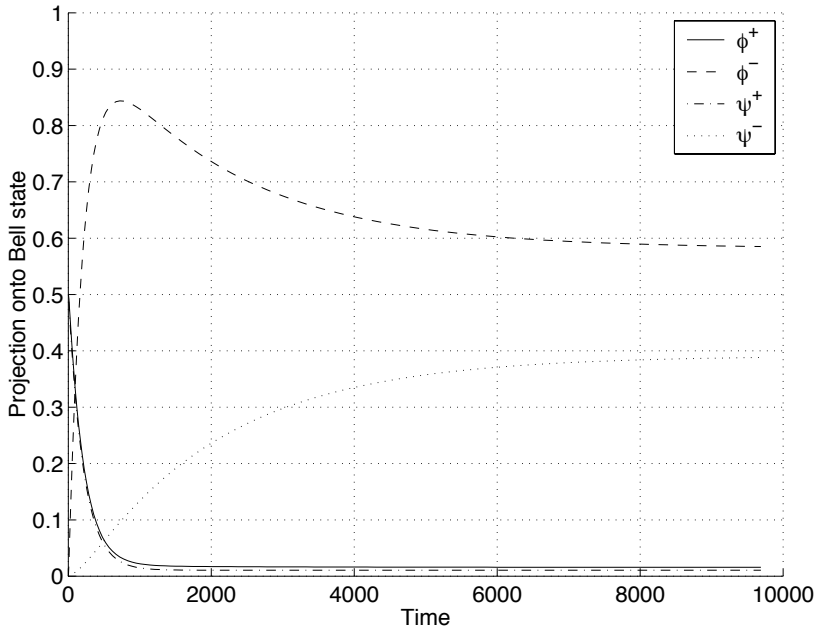

Figure 7.8: Projections of the states obtained in Figure 7.7 onto the Bell states as functions of time. Spontaneous emission is included. The late-time decay of the entanglement seen in Figure 7.7 is caused by the gradual increase of the unwanted component of $|\psi^-\rangle$. All parameters are as in Figure 7.7.

7.7 Collective spin operators

The effective squeezed reservoir can be expected to induce squeezing in the collective atomic spin operators of the trapped atoms. These squeezed atomic states were introduced by Barnett and Dupertuis in 1987 [81]. The relevant Heisenberg uncertainty relation for the collective spin operators S_x, S_y and S_z is

$$\Delta S_x \Delta S_y \geq \frac{1}{2} \left| \langle S_z \rangle \right| . \tag{7.21}$$

It is convenient to normalize these with the definitions

$$\Delta X = \sqrt{2} \frac{\Delta S_x}{|\langle S_z \rangle|^{\frac{1}{2}}}, \tag{7.22a}$$

$$\Delta Y = \sqrt{2} \frac{\Delta S_y}{|\langle S_z \rangle|^{\frac{1}{2}}}. \tag{7.22b}$$

so that

$$\Delta X \Delta Y \geq 1. \tag{7.23}$$

The evolution of the spin quadrature variables is shown in Figure 7.9. The atomic system evolves into a spin-squeezed state ($\Delta X < 1$) even in the presence of spontaneous emission. Interestingly, the squeezing does not seem to undergo late-time decay (in contrast to the entanglement).

7.8 Conclusions

In this Chapter we have proposed a system for entangling two atoms in a cavity, based on the principle of quantum-reservoir engineering. By designing an appropriate coupling between the atoms and their environment (through the cavity mode), an effective squeezing interaction arises without requiring non-classical light sources. As we have seen, the effective squeezing interaction generates entangled atomic-squeezed states. It is thought that this system will prove to be more experimentally accessible than those in Chapter 6, which are based on the use of squeezed light.

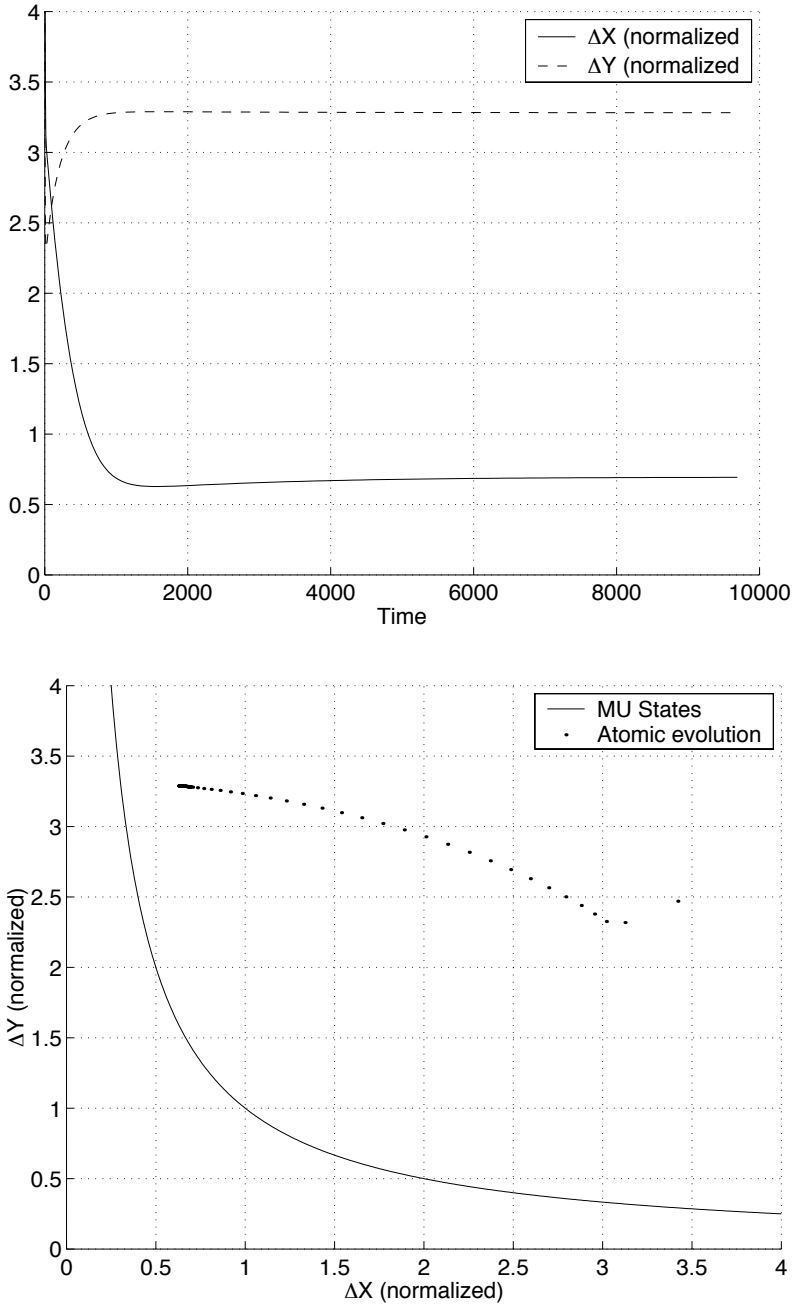

Figure 7.9: Evolution of the spin quadratures plotted against time (top) and as a parametric plot (bottom). Parameters are as in Figure 7.7. The solid line of the bottom Figure defines the minimum uncertainty states (MUS) where $\Delta X \Delta Y = 1$. Evolution is from right to left. The atomic system evolves into a spin-squeezed state ($\Delta X < 1$) even in the presence of spontaneous emission. The squeezing does not seem to undergo the same degree of late-time decay as the entanglement.

Chapter 8

Conclusions

This final Chapter summarizes the results obtained in this Thesis and suggests some avenues of future research.

Contents

8.1 Results

In this Thesis, our original aim was to investigate the possibility of using squeezed light to entangle atoms in a realistic cavity QED situation. This investigation has been successful and forms the content of Chapters 4, 5 and 6. The realization that the technique of quantum-reservoir engineering could be used to achieve similar results came as an unexpected bonus, and this idea was developed in Chapter 7.

In Chapter 4 the two schemes investigated are both very idealized, but set the goals for later, more realistic models. It was shown, in an extension of the work of Palma and Knight [2], that separated atoms interacting with spatially separated entangled light modes can be entangled themselves. In the limit of ideal two-mode squeezing from an NDPA, it was found that pure states arise. The parameter regimes where the atoms are entangled and where their correlations violate the CHSH inequality were also calculated.

The scheme in which the squeezed light from a DPA is passed through a beam splitter before interacting with the atoms was also investigated as an

alternative method of producing entangled light beams. In this case, only limited entanglement can be produced. Nevertheless, entanglement purification procedures could conceivably be used to concentrate the entanglement in the atoms, so this scheme is still of interest.

Realistic schemes to entangle atoms with squeezed light require that they interact predominantly with squeezed modes. In Chapter 5, a method was described for creating an effective one-dimensional atom where the predominant coupling to the outside world is via a single cavity mode. In particular, the use of a 4-level atom and Raman transitions in a cavity QED situation offers a practical alternative to the problem of driving an atom from all directions with broadband squeezed light.

Such effective one-dimensional atoms were then used in Chapter 6, in conjunction with the ideas of Chapter 4, to design realistic schemes which may be used to generate long-lived entanglement in two separated trapped atoms. The technical difficulties involved in squeezing all of the modes with which the atoms might interact are dramatically lessened through the primary coupling of the atoms to just one cavity mode. Only this single mode needs to be squeezed.

The decay of the atoms into the squeezed reservoir is through either amplitude coupling or phase coupling. The strengths of these channels are independently adjustable and it was shown how the flexibility provided by these channels allows one to engineer states of all physically allowed combinations of entropy and entanglement, as measured by the linear entropy and entanglement of formation, respectively.

In Chapter 7 a system was proposed, based on the idea of quantum-reservoir engineering, for entangling two atoms in a cavity. It employs the one-dimensional atoms developed in Chapter 5, albeit in a slightly more complicated 5-level atomic scheme. It was found that, by designing an appropriate coupling between the atoms and the cavity mode, an effective squeezing interaction arises without requiring non-classical light sources. This system should be more experimentally accessible than that of Chapter 6 and it should provide a simpler method of achieving strong squeezing interactions.

8.2 Future research

There are a number of areas of future research that suggest themselves and they are listed as follows:

1. Finding a two-atom cavity QED system capable of generating states above the Werner line in the steady state.

2. Characterizing more comprehensively all the states that can be produced using the adjustable parameters of our systems. Also, it would be interesting to find a physically realizable system that could access every state of two qubits and not just those of distinct entanglement and purity.

3. Finding general solutions to the master equations considered with both phase damping and spontaneous emission included.

4. Isolating actual atomic level configurations that would be suitable for realizing the cavity QED schemes of Chapters 5, 6 and 7.

5. Finding ways to minimize the deleterious effects that the trapping states (i.e., Bell state $|\psi^-\rangle$) have on the entanglement in the presence of spontaneous emission.

6. Considering the spin-squeezing of a large number of atoms trapped in a single cavity using quantum-reservoir engineering.

In conclusion, it is hoped that the ideas proposed in this Thesis might lead to the experimental production of atomic states of controllable purity and entanglement. These atomic states would allow a thorough experimental exploration of quantum information protocols such as quantum teleportation, entanglement purification and entanglement distillation.

Appendix A

Derivation of the two-qubit master equations

In this Appendix we provide details of the derivation of the reduced master equations (4.3a) and (4.10) for a pair of two-level atoms interacting with broadband squeezed light from a parametric amplifier, as investigated in Chapter 4. The cascaded quantum systems technique is used as in [82].

Contents

Chapter 4 considers two systems in which either an NDPA or a DPA is used to provide squeezed light for the atoms. In the main text of this Appendix we provide details of the derivation of the master equation (4.3a)

for atoms driven by the NDPA. The equations applicable to the atoms being driven by the DPA are placed in rectangular boxes.

A.1 Quantum Langevin equations

We assume resonant interaction between the output mode(s) of the parametric amplifier and the atoms. The operators governing the interactions of the systems with their input fields are a, b, σ_2^- and σ_3^-. Therefore, we can write the quantum Langevin equations for the individual systems, in the interaction picture, as

$$\begin{aligned}
\dot{x_1} &= -i\left[x_1, H_1\right] \\
&\quad - \left[x_1, a^\dagger\right]\left\{\frac{\kappa_a}{2}a + \sqrt{\kappa_a}f_{1a}\right\} + \left\{\frac{\kappa_a}{2}a^\dagger + \sqrt{\kappa_a}f_{1a}^\dagger\right\}\left[x_1, a\right] \\
&\quad - \left[x_1, b^\dagger\right]\left\{\frac{\kappa_b}{2}b + \sqrt{\kappa_b}f_{1b}\right\} + \left\{\frac{\kappa_b}{2}b^\dagger + \sqrt{\kappa_b}f_{1b}^\dagger\right\}\left[x_1, b\right], \qquad \text{(A.1a)} \\
\dot{x_2} &= -\left[x_2, \sigma_2^+\right]\left\{\frac{\gamma_2}{2}\sigma_2^- + \sqrt{\gamma_2}f_2\right\} + \left\{\frac{\gamma_2}{2}\sigma_2^+ + \sqrt{\gamma_2}f_2^\dagger\right\}\left[x_2, \sigma_2^-\right], \qquad \text{(A.1b)} \\
\dot{x_3} &= -\left[x_3, \sigma_3^+\right]\left\{\frac{\gamma_3}{2}\sigma_3^- + \sqrt{\gamma_3}f_3\right\} + \left\{\frac{\gamma_3}{2}\sigma_3^+ + \sqrt{\gamma_3}f_3^\dagger\right\}\left[x_3, \sigma_3^-\right]. \qquad \text{(A.1c)}
\end{aligned}$$

where

$$H_1 = i\left(Ea^\dagger b^\dagger - E^* ab\right). \qquad \text{(A.1d)}$$

$$\begin{aligned}
\dot{x_1} &= -i\left[x_1, H_1\right] \\
&\quad - \left[x_1, a^\dagger\right]\left\{\frac{\kappa_a}{2}a + \sqrt{\kappa_a}f_1\right\} + \left\{\frac{\kappa_a}{2}a^\dagger + \sqrt{\kappa_a}f_1^\dagger\right\}\left[x_1, a\right], \qquad \text{(A.2a)} \\
\dot{x_2} &= -\left[x_2, \sigma_2^+\right]\left\{\frac{\gamma_2}{2}\sigma_2^- + \sqrt{\gamma_2}f_2\right\} + \left\{\frac{\gamma_2}{2}\sigma_2^+ + \sqrt{\gamma_2}f_2^\dagger\right\}\left[x_2, \sigma_2^-\right], \qquad \text{(A.2b)} \\
\dot{x_3} &= -\left[x_3, \sigma_3^+\right]\left\{\frac{\gamma_3}{2}\sigma_3^- + \sqrt{\gamma_3}f_3\right\} + \left\{\frac{\gamma_3}{2}\sigma_3^+ + \sqrt{\gamma_3}f_3^\dagger\right\}\left[x_3, \sigma_3^-\right], \qquad \text{(A.2c)} \\
H_1 &= \frac{i}{2}\left(Ea^{\dagger 2} - E^* a^2\right). \qquad \text{(A.2d)}
\end{aligned}$$

Here x_i is an arbitrary operator in system i.

A.1.1 Boundary conditions

The relationships of the output fields to the input fields for each system are given by

$$g_{1a} = f_{1a} + \sqrt{\kappa_a}a, \tag{A.3a}$$
$$g_{1b} = f_{1b} + \sqrt{\kappa_b}b, \tag{A.3b}$$
$$g_2 = f_2 + \sqrt{\gamma_2}\sigma_2^-, \tag{A.3c}$$
$$g_3 = f_3 + \sqrt{\gamma_3}\sigma_3^-. \tag{A.3d}$$

$$g_1 = f_1 + \sqrt{\kappa_a}a, \tag{A.4a}$$
$$g_2 = f_2 + \sqrt{\gamma_2}\sigma_2^-, \tag{A.4b}$$
$$g_3 = f_3 + \sqrt{\gamma_3}\sigma_3^-. \tag{A.4c}$$

The fields at the beam splitters are related by

$$f_2 = \sqrt{\epsilon_2}g_{1a} + \sqrt{1-\epsilon_2}h_2, \tag{A.5a}$$
$$f_3 = \sqrt{\epsilon_3}g_{1b} + \sqrt{1-\epsilon_3}h_3. \tag{A.5b}$$

$$f_2 = \sqrt{\epsilon}_2\left(\sqrt{\frac{1}{2}}g_1 + \sqrt{\frac{1}{2}}h_1\right) + \sqrt{1-\epsilon_2}h_2, \tag{A.6a}$$
$$f_3 = \sqrt{\epsilon}_3\left(\sqrt{\frac{1}{2}}g_1 + \sqrt{\frac{1}{2}}h_1\right) + \sqrt{1-\epsilon_3}h_3. \tag{A.6b}$$

After substituting for g_{1a} and g_{1b} we obtain

$$f_2 = \sqrt{\epsilon_2}\left(f_{1a} + \sqrt{\kappa_a}a\right) + \sqrt{1-\epsilon_2}h_2, \tag{A.7a}$$
$$f_3 = \sqrt{\epsilon_3}\left(f_{1b} + \sqrt{\kappa_b}b\right) + \sqrt{1-\epsilon_3}h_3, \tag{A.7b}$$

$$f_2 = \sqrt{\epsilon}_2\left(\sqrt{\frac{1}{2}}f_1 + \sqrt{\kappa_a}a + \sqrt{\frac{1}{2}}h_1\right) + \sqrt{1-\epsilon}h_2, \tag{A.8a}$$
$$f_3 = \sqrt{\epsilon}_3\left(\sqrt{\frac{1}{2}}f_1 + \sqrt{\kappa_a}a + \sqrt{\frac{1}{2}}h_1\right) + \sqrt{1-\epsilon}h_3, \tag{A.8b}$$

and rearranging further we obtain

$$f_2 = \sqrt{\kappa_a\epsilon_2}a + \sqrt{\epsilon_2}f_{1a} + \sqrt{1-\epsilon_2}h_2, \tag{A.9a}$$
$$f_3 = \sqrt{\kappa_b\epsilon_3}b + \sqrt{\epsilon_3}f_{1b} + \sqrt{1-\epsilon_3}h_3. \tag{A.9b}$$

$$f_2 = \sqrt{\kappa_a \epsilon_2}\, a + \sqrt{\frac{\epsilon_2}{2}} f_1 + \sqrt{\frac{\epsilon_2}{2}} h_1 + \sqrt{1-\epsilon_2}\, h_2, \qquad \text{(A.10a)}$$

$$f_3 = \sqrt{\kappa_a \epsilon_3}\, a + \sqrt{\frac{\epsilon_3}{2}} f_1 + \sqrt{\frac{\epsilon_3}{2}} h_1 + \sqrt{1-\epsilon_3}\, h_3. \qquad \text{(A.10b)}$$

A.1.2 Combined quantum Langevin equation

With x defined to be any operator in the space of the three systems, and writing *conj* to indicate the Hermitian conjugate of everything except x, the combined quantum Langevin equation is

$$\begin{aligned} \dot{x} = & -i\,[x, H_1] \\ & - \left[x, a^\dagger\right] \left\{ \frac{\kappa_a}{2} a + \sqrt{\kappa_a} f_{1a} \right\} - conj \\ & - \left[x, b^\dagger\right] \left\{ \frac{\kappa_b}{2} b + \sqrt{\kappa_b} f_{1b} \right\} - conj \\ & - \left[x, \sigma_2^+\right] \left\{ \frac{\gamma_2}{2} \sigma_2^- + \sqrt{\gamma_2} f_2 \right\} - conj \\ & - \left[x, \sigma_3^+\right] \left\{ \frac{\gamma_3}{2} \sigma_3^- + \sqrt{\gamma_3} f_3 \right\} - conj. \end{aligned} \qquad \text{(A.11)}$$

$$\begin{aligned} \dot{x} = & -i\,[x, H_1] \\ & - \left[x, a^\dagger\right] \left\{ \frac{\kappa_a}{2} a + \sqrt{\kappa_a} f_1 \right\} - conj \\ & - \left[x, \sigma_2^+\right] \left\{ \frac{\gamma_2}{2} \sigma_2^- + \sqrt{\gamma_2} f_2 \right\} - conj \\ & - \left[x, \sigma_3^+\right] \left\{ \frac{\gamma_3}{2} \sigma_3^- + \sqrt{\gamma_3} f_3 \right\} - conj. \end{aligned} \qquad \text{(A.12)}$$

Then expanding for f_2 and f_3, we have

$$\begin{aligned}
\dot{x} &= -i\,[x, H_1] \\
&\quad - \left[x, a^\dagger\right] \left\{ \frac{\kappa_a}{2} a + \sqrt{\kappa_a} f_{1a} \right\} - conj \\
&\quad - \left[x, b^\dagger\right] \left\{ \frac{\kappa_b}{2} b + \sqrt{\kappa_b} f_{1b} \right\} - conj \\
&\quad - \left[x, \sigma_2^+\right] \left\{ \frac{\gamma_2}{2} \sigma_2^- + \sqrt{\kappa_a \gamma_2 \epsilon_2}\, a + \sqrt{\gamma_2 \epsilon_2} f_{1a} + \sqrt{\gamma_2 (1-\epsilon_2)} h_2 \right\} \\
&\quad - conj \\
&\quad - \left[x, \sigma_3^+\right] \left\{ \frac{\gamma_3}{2} \sigma_3^- + \sqrt{\kappa_b \gamma_3 \epsilon_3}\, b + \sqrt{\gamma_3 \epsilon_3} f_{1b} + \sqrt{\gamma_3 (1-\epsilon_3)} h_3 \right\} \\
&\quad - conj. \qquad \text{(A.13)}
\end{aligned}$$

$$\begin{aligned}
\dot{x} &= -i\,[x, H_1] \\
&\quad - \left[x, a^\dagger\right] \left\{ \frac{\kappa_a}{2} a + \sqrt{\kappa_a} f_1 \right\} - conj \\
&\quad - \left[x, \sigma_2^+\right] \left\{ \frac{\gamma_2}{2} \sigma_2^- + \sqrt{\kappa_a \gamma_2 \epsilon_2}\, a \right. \\
&\qquad \left. + \sqrt{\frac{\gamma_2 \epsilon_2}{2}} f_1 + \sqrt{\frac{\gamma_2 \epsilon_2}{2}} h_1 + \sqrt{\gamma_2 (1-\epsilon_2)} h_2 \right\} - conj \\
&\quad - \left[x, \sigma_3^+\right] \left\{ \frac{\gamma_3}{2} \sigma_3^- + \sqrt{\kappa_a \gamma_3 \epsilon_3}\, a \right. \\
&\qquad \left. + \sqrt{\frac{\gamma_3 \epsilon_3}{2}} f_1 + \sqrt{\frac{\gamma_3 \epsilon_3}{2}} h_1 + \sqrt{\gamma_3 (1-\epsilon_3)} h_3 \right\} - conj. \qquad \text{(A.14)}
\end{aligned}$$

A.2 Conversion to a quantum Ito equation

Assume the input fields f_{1a}, f_{1b}, h_1, h_2 and h_3 (for the DPA f_1, h_1, h_2 and h_3) are describable as quantum white noise, in fact as vacuum fields. Define quantum Wiener processes (denoted by capital letters), corresponding to each input field, satisfying

$$\begin{aligned}
f_{1a}\,dt &= dF_{1a}, && \text{(A.15a)} \\
f_{1b}\,dt &= dF_{1b}, && \text{(A.15b)} \\
h_1\,dt &= dH_1, && \text{(A.15c)} \\
h_2\,dt &= dH_2, && \text{(A.15d)} \\
h_3\,dt &= dH_3. && \text{(A.15e)}
\end{aligned}$$

$$
\begin{aligned}
f_1\,dt &= dF_1, && \text{(A.16a)}\\
h_1\,dt &= dH_1, && \text{(A.16b)}\\
h_2\,dt &= dH_2, && \text{(A.16c)}\\
h_3\,dt &= dH_3. && \text{(A.16d)}
\end{aligned}
$$

The quantum Langevin equation may now be transformed into a Stratonovich quantum stochastic differential equation by direct substitution. We have

$$
\begin{aligned}
(S)\,dx &= -i\,[x, H_1]\,dt \\
&\quad - \left[x, a^\dagger\right]\left\{\frac{\kappa_a}{2}a\,dt + \sqrt{\kappa_a}\,dF_{1a}\right\} - conj \\
&\quad - \left[x, b^\dagger\right]\left\{\frac{\kappa_a}{2}b\,dt + \sqrt{\kappa_a}\,dF_{1b}\right\} - conj \\
&\quad - \left[x, \sigma_2^+\right]\left\{\frac{\gamma_2}{2}\sigma_2^-\,dt + \sqrt{\kappa_a\gamma_2\epsilon_2}a\,dt + \sqrt{\gamma_2\epsilon_2}\,dF_{1a}\right. \\
&\qquad \left. + \sqrt{\gamma_2(1-\epsilon_2)}\,dH_2\right\} - conj \\
&\quad - \left[x, \sigma_3^+\right]\left\{\frac{\gamma_3}{2}\sigma_3^-\,dt + \sqrt{\kappa_b\gamma_3\epsilon_3}b\,dt + \sqrt{\gamma_3\epsilon_3}\,dF_{1b}\right. \\
&\qquad \left. + \sqrt{\gamma_3(1-\epsilon_3)}\,dH_3\right\} - conj. \qquad \text{(A.17)}
\end{aligned}
$$

$$
\begin{aligned}
(S)\,dx &= -i\,[x, H_1]\,dt \\
&\quad - \left[x, a^\dagger\right]\left\{\frac{\kappa_a}{2}a\,dt + \sqrt{\kappa_a}\,dF_1\right\} - conj \\
&\quad - \left[x, \sigma_2^+\right]\left\{\frac{\gamma_2}{2}\sigma_2^-\,dt + \sqrt{\kappa_a\gamma_2\epsilon_2}a\,dt + \sqrt{\frac{\gamma_2\epsilon_2}{2}}(dF_1 + dH_1)\right. \\
&\qquad \left. + \sqrt{\gamma_2(1-\epsilon_2)}\,dH_2\right\} - conj \\
&\quad - \left[x, \sigma_3^+\right]\left\{\frac{\gamma}{2}\sigma_3^-\,dt + \sqrt{\kappa_a\gamma_3\epsilon_3}a\,dt + \sqrt{\frac{\gamma_3\epsilon_3}{2}}(dF_1 + dH_1)\right. \\
&\qquad \left. + \sqrt{\gamma_3(1-\epsilon_3)}\,dH_3\right\} - conj. \qquad \text{(A.18)}
\end{aligned}
$$

This equation may be converted to an Ito quantum stochastic differential equation using the substitution rules for a vacuum quantum Wiener pro-

cess [66]:

$$
\begin{aligned}
(S)\ g\,dW &\rightarrow (I)\ g\,dW, && \text{(A.19a)}\\
(S)\ dW\,g &\rightarrow (I)\ g\,dW + \frac{\sqrt{\gamma}}{2}\left[g,c\right], && \text{(A.19b)}\\
(S)\ g\,dW^\dagger &\rightarrow (I)\ g\,dW^\dagger - \frac{\sqrt{\gamma}}{2}\left[g,c^\dagger\right], && \text{(A.19c)}\\
(S)\ dW^\dagger\,g &\rightarrow (I)\ g\,dW^\dagger, && \text{(A.19d)}
\end{aligned}
$$

applicable to the quantum Langevin equation

$$
\dot{x} = -i\left[x,H_1\right] - \left[x,c^\dagger\right]\left\{\frac{\gamma}{2}c + \sqrt{\gamma}b_{in}(1,t)\right\} - conj. \qquad \text{(A.20)}
$$

The Ito equations are then found to be identical to the Stratonovich equations.

A.3 Conversion to master equation

Take the expectation value of Equation (A.17) and move to the Schrödinger picture to obtain a master equation. It is useful to first expand the commutators

$$
\begin{aligned}
(I)\ dx = {} & -i\left[x,H_1\right]\,dt\\
& +\frac{\kappa_a}{2}\left(2a^\dagger xa - xa^\dagger a - a^\dagger ax\right)dt\\
& +\frac{\kappa_b}{2}\left(2b^\dagger xb - xb^\dagger b - b^\dagger bx\right)dt\\
& +\frac{\gamma_2}{2}\left(2\sigma_2^+ x\sigma_2^- - x\sigma_2^+\sigma_2^- - \sigma_2^+\sigma_2^- x\right)dt\\
& +\frac{\gamma_3}{2}\left(2\sigma_3^+ x\sigma_3^- - x\sigma_3^+\sigma_3^- - \sigma_3^+\sigma_3^- x\right)dt\\
& -\sqrt{\kappa_a\gamma_2\epsilon_2}\left(xa\sigma_2^+ - \sigma_2^+ xa + \sigma_2^- a^\dagger x - a^\dagger x\sigma_2^-\right)dt\\
& -\sqrt{\kappa_b\gamma_3\epsilon_3}\left(xb\sigma_3^+ - \sigma_3^+ xb + \sigma_3^- b^\dagger x - b^\dagger x\sigma_3^-\right)dt\\
& +\text{Ito increments.} \qquad \text{(A.21)}
\end{aligned}
$$

$$
\begin{aligned}
(I)\ dx &= -i\left[x, H_1\right]\, dt \\
&\quad + \frac{\kappa_a}{2}\left(2a^\dagger x a - x a^\dagger a - a^\dagger a x\right) dt \\
&\quad + \frac{\gamma_2}{2}\left(2\sigma_2^+ x \sigma_2^- - x\sigma_2^+\sigma_2^- - \sigma_2^+\sigma_2^- x\right) dt \\
&\quad + \frac{\gamma_3}{2}\left(2\sigma_3^+ x \sigma_3^- - x\sigma_3^+\sigma_3^- - \sigma_3^+\sigma_3^- x\right) dt \\
&\quad - \sqrt{\kappa_a\gamma_2\epsilon_2}\left(xa\sigma_2^+ - \sigma_2^+ xa + \sigma_2^- a^\dagger x - a^\dagger x\sigma_2^-\right) dt \\
&\quad - \sqrt{\kappa_a\gamma_3\epsilon_3}\left(xa\sigma_3^+ - \sigma_3^+ xa + \sigma_3^- a^\dagger x - a^\dagger x\sigma_3^-\right) dt \\
&\quad + \text{Ito increments.}
\end{aligned}
\tag{A.22}
$$

Converting to a master equation, the Ito increments are discarded, and the sign of the first commutator is reversed to give

$$
\begin{aligned}
\frac{d\rho}{dt} &= i\left[\rho, H_1\right] \\
&\quad + \frac{\kappa_a}{2}\left(2a\rho a^\dagger - a^\dagger a\rho - \rho a^\dagger a\right) \\
&\quad + \frac{\kappa_b}{2}\left(2b\rho b^\dagger - b^\dagger b\rho - \rho b^\dagger b\right) \\
&\quad + \frac{\gamma_2}{2}\left(2\sigma_2^-\rho\sigma_2^+ - \sigma_2^+\sigma_2^-\rho - \rho\sigma_2^+\sigma_2^-\right) \\
&\quad + \frac{\gamma_3}{2}\left(2\sigma_3^-\rho\sigma_3^+ - \sigma_3^+\sigma_3^-\rho - \rho\sigma_3^+\sigma_3^-\right) \\
&\quad - \sqrt{\kappa_a\gamma_2\epsilon_2}\left(a\sigma_2^+\rho - a\rho\sigma_2^+ + \rho\sigma_2^- a^\dagger - \sigma_2^- \rho a^\dagger\right) \\
&\quad - \sqrt{\kappa_b\gamma_3\epsilon_3}\left(b\sigma_3^+\rho - b\rho\sigma_3^+ + \rho\sigma_3^- b^\dagger - \sigma_3^- \rho b^\dagger\right)
\end{aligned}
\tag{A.23}
$$

$$
\begin{aligned}
\frac{d\rho}{dt} &= i\left[\rho, H_1\right] \\
&\quad + \frac{\kappa_a}{2}\left(2a\rho a^\dagger - a^\dagger a\rho - \rho a^\dagger a\right) \\
&\quad + \frac{\gamma_2}{2}\left(2\sigma_2^-\rho\sigma_2^+ - \sigma_2^+\sigma_2^-\rho - \rho\sigma_2^+\sigma_2^-\right) \\
&\quad + \frac{\gamma_3}{2}\left(2\sigma_3^-\rho\sigma_3^+ - \sigma_3^+\sigma_3^-\rho - \rho\sigma_3^+\sigma_3^-\right) \\
&\quad - \sqrt{\kappa_a\gamma_2\epsilon_2}\left(a\sigma_2^+\rho - a\rho\sigma_2^+ + \rho\sigma_2^- a^\dagger - \sigma_2^- \rho a^\dagger\right) \\
&\quad - \sqrt{\kappa_a\gamma_3\epsilon_3}\left(a\sigma_3^+\rho - a\rho\sigma_3^+ + \rho\sigma_3^- a^\dagger - \sigma_3^- \rho a^\dagger\right)
\end{aligned}
\tag{A.24}
$$

A.4 Equivalent noise terms for system 1

The dynamics of system 1 can be reduced to a set of noise terms using a generalized P representation, leaving a master equation for systems 2 and 3 only. A positive P representation must be used to represent squeezed light owing to its non-classical nature. Define

$$\boldsymbol{\alpha} = (\alpha, \alpha^\dagger, \beta, \beta^\dagger), \tag{A.25}$$

$$\boldsymbol{\alpha} = (\alpha, \alpha^\dagger), \tag{A.26}$$

and $\rho(\boldsymbol{\alpha})$ to be an operator in the combined space of systems 2 and 3 so that

$$\rho = \int d^2\alpha \int d^2\alpha^\dagger \int d^2\beta \int d^2\beta^\dagger \frac{|\alpha\rangle \left\langle \alpha^{\dagger *}\right|_a}{\langle \alpha^{\dagger *}|\alpha\rangle_a} \frac{|\beta\rangle \left\langle \beta^{\dagger *}\right|_b}{\langle \beta^{\dagger *}|\beta\rangle_b} \rho(\boldsymbol{\alpha}). \tag{A.27}$$

$$\rho = \int d^2\alpha \int d^2\alpha^\dagger \frac{|\alpha\rangle \left\langle \alpha^{\dagger *}\right|_1}{\langle \alpha^{\dagger *}|\alpha\rangle_1} \rho(\boldsymbol{\alpha}). \tag{A.28}$$

We use the equivalences

$$a\rho \leftrightarrow \alpha\rho, \tag{A.29a}$$
$$\rho a^\dagger \leftrightarrow \alpha^\dagger \rho, \tag{A.29b}$$
$$a^\dagger \rho \leftrightarrow \left(\alpha^\dagger - \frac{\partial}{\partial \alpha}\right)\rho, \tag{A.29c}$$
$$\rho a \leftrightarrow \left(\alpha - \frac{\partial}{\partial \alpha^\dagger}\right)\rho. \tag{A.29d}$$

The reduced master equation becomes

$$\begin{aligned}
\frac{d\rho(\boldsymbol{\alpha})}{dt} &= -E\left\{\alpha^\dagger\beta^\dagger - \left(\alpha^\dagger - \frac{\partial}{\partial\alpha}\right)\left(\beta^\dagger - \frac{\partial}{\partial\beta}\right)\right\}\rho(\boldsymbol{\alpha}) \\
&\quad -E^*\left\{\alpha\beta - \left(\alpha - \frac{\partial}{\partial\alpha^\dagger}\right)\left(\beta - \frac{\partial}{\partial\beta^\dagger}\right)\right\}\rho(\boldsymbol{\alpha}) \\
&\quad +\frac{\kappa_a}{2}\left\{2\alpha\alpha^\dagger\rho(\boldsymbol{\alpha}) - \left(\alpha^\dagger - \frac{\partial}{\partial\alpha}\right)\alpha\rho(\boldsymbol{\alpha}) - \left(\alpha - \frac{\partial}{\partial\alpha^\dagger}\right)\alpha^\dagger\rho(\boldsymbol{\alpha})\right\} \\
&\quad +\frac{\kappa_b}{2}\left\{2\beta\beta^\dagger\rho(\boldsymbol{\alpha}) - \left(\beta^\dagger - \frac{\partial}{\partial\beta}\right)\beta\rho(\boldsymbol{\alpha}) - \left(\beta - \frac{\partial}{\partial\beta^\dagger}\right)\beta^\dagger\rho(\boldsymbol{\alpha})\right\} \\
&\quad +\frac{\gamma_2}{2}\left\{2\sigma_2^-\rho(\boldsymbol{\alpha})\sigma_2^+ - \sigma_2^+\sigma_2^-\rho(\boldsymbol{\alpha}) - \rho(\boldsymbol{\alpha})\sigma_2^+\sigma_2^-\right\} \\
&\quad +\frac{\gamma_3}{2}\left\{2\sigma_3^-\rho(\boldsymbol{\alpha})\sigma_3^+ - \sigma_3^+\sigma_3^-\rho(\boldsymbol{\alpha}) - \rho(\boldsymbol{\alpha})\sigma_3^+\sigma_3^-\right\} \\
&\quad -\sqrt{\kappa_a\gamma_2\epsilon_2}\left\{\alpha\sigma_2^+\rho(\boldsymbol{\alpha}) - \alpha\rho(\boldsymbol{\alpha})\sigma_2^+ + \rho(\boldsymbol{\alpha})\sigma_2^-\alpha^\dagger - \sigma_2^-\rho(\boldsymbol{\alpha})\alpha^\dagger\right\} \\
&\quad -\sqrt{\kappa_b\gamma_3\epsilon_3}\left\{\alpha\sigma_3^+\rho(\boldsymbol{\alpha}) - \alpha\rho(\boldsymbol{\alpha})\sigma_3^+ + \rho(\boldsymbol{\alpha})\sigma_3^-\beta^\dagger - \sigma_3^-\rho(\boldsymbol{\alpha})\beta^\dagger\right\}.
\end{aligned} \tag{A.30}$$

$$\begin{aligned}
\frac{d\rho(\boldsymbol{\alpha})}{dt} &= -\frac{1}{2}E\left\{\alpha^{\dagger 2} - \left(\alpha^\dagger - \frac{\partial}{\partial\alpha}\right)^2\right\}\rho(\boldsymbol{\alpha}) \\
&\quad -\frac{1}{2}E^*\left\{\alpha^2 - \left(\alpha - \frac{\partial}{\partial\alpha^\dagger}\right)^2\right\}\rho(\boldsymbol{\alpha}) \\
&\quad +\frac{\kappa_a}{2}\left\{2\alpha\alpha^\dagger\rho(\boldsymbol{\alpha})\right\} \\
&\quad -\frac{\kappa_a}{2}\left\{\left(\alpha^\dagger - \frac{\partial}{\partial\alpha}\right)\alpha\rho(\boldsymbol{\alpha}) + \left(\alpha - \frac{\partial}{\partial\alpha^\dagger}\right)\alpha^\dagger\rho(\boldsymbol{\alpha})\right\} \\
&\quad +\frac{\gamma_2}{2}\left\{2\sigma_2^-\rho(\boldsymbol{\alpha})\sigma_2^+ - \sigma_2^+\sigma_2^-\rho(\boldsymbol{\alpha}) - \rho(\boldsymbol{\alpha})\sigma_2^+\sigma_2^-\right\} \\
&\quad +\frac{\gamma_3}{2}\left\{2\sigma_3^-\rho(\boldsymbol{\alpha})\sigma_3^+ - \sigma_3^+\sigma_3^-\rho(\boldsymbol{\alpha}) - \rho(\boldsymbol{\alpha})\sigma_3^+\sigma_3^-\right\} \\
&\quad -\sqrt{\kappa_a\gamma_2\epsilon_2}\left\{\alpha\sigma_2^+\rho(\boldsymbol{\alpha}) - \alpha\rho(\boldsymbol{\alpha})\sigma_2^+ + \rho(\boldsymbol{\alpha})\sigma_2^-\alpha^\dagger - \sigma_2^-\rho(\boldsymbol{\alpha})\alpha^\dagger\right\} \\
&\quad -\sqrt{\kappa_a\gamma_3\epsilon_3}\left\{\alpha\sigma_3^+\rho(\boldsymbol{\alpha}) - \alpha\rho(\boldsymbol{\alpha})\sigma_3^+ + \rho(\boldsymbol{\alpha})\sigma_3^-\alpha^\dagger - \sigma_3^-\rho(\boldsymbol{\alpha})\alpha^\dagger\right\}.
\end{aligned} \tag{A.31}$$

This is equivalent to the master equation for systems 2 and 3

$$\begin{aligned}\frac{d\rho_a}{dt} &= -\sqrt{\kappa_a\gamma_2\epsilon_2}\left\{\alpha(t)\left[\sigma_2^+,\rho_a\right]+\alpha^\dagger(t)\left[\rho_a,\sigma_2^-\right]\right\}\\ &\quad -\sqrt{\kappa_b\gamma_3\epsilon_3}\left\{\beta(t)\left[\sigma_3^+,\rho_a\right]+\beta^\dagger(t)\left[\rho_a,\sigma_3^-\right]\right\}\\ &\quad +\frac{\gamma_2}{2}\left(2\sigma_2^-\rho_a\sigma_2^+-\sigma_2^+\sigma_2^-\rho_a-\rho_a\sigma_2^+\sigma_2^-\right)\\ &\quad +\frac{\gamma_3}{2}\left(2\sigma_3^-\rho_a\sigma_3^+-\sigma_3^+\sigma_3^-\rho_a-\rho_a\sigma_3^+\sigma_3^-\right), \qquad \text{(A.32)}\end{aligned}$$

$$\boxed{\begin{aligned}\frac{d\rho_a}{dt} &= -\sqrt{\kappa_a\gamma_2\epsilon_2}\left\{\alpha(t)\left[\sigma_2^+,\rho_a\right]+\alpha^\dagger(t)\left[\rho_a,\sigma_2^-\right]\right\}\\ &\quad -\sqrt{\kappa_a\gamma_3\epsilon_3}\left\{\alpha(t)\left[\sigma_3^+,\rho_a\right]+\alpha^\dagger(t)\left[\rho_a,\sigma_3^-\right]\right\}\\ &\quad +\frac{\gamma_2}{2}\left(2\sigma_2^-\rho_a\sigma_2^+-\sigma_2^+\sigma_2^-\rho_a-\rho_a\sigma_2^+\sigma_2^-\right)\\ &\quad +\frac{\gamma_3}{2}\left(2\sigma_3^-\rho_a\sigma_3^+-\sigma_3^+\sigma_3^-\rho_a-\rho_a\sigma_3^+\sigma_3^-\right), \qquad \text{(A.33)}\end{aligned}}$$

in which the phase space variables $\boldsymbol{\alpha}(t)$ satisfy the Fokker-Planck equation (FPE)

$$\begin{aligned}\frac{dP(\boldsymbol{\alpha})}{dt} &= \frac{\partial}{\partial\alpha}\left(\frac{\kappa_a}{2}\alpha-E\beta^\dagger\right)P(\boldsymbol{\alpha})+\frac{\partial}{\partial\alpha^\dagger}\left(\frac{\kappa_a}{2}\alpha^\dagger-E^*\beta\right)P(\boldsymbol{\alpha})\\ &\quad \frac{\partial}{\partial\beta}\left(\frac{\kappa_b}{2}\beta-E\alpha^\dagger\right)P(\boldsymbol{\alpha})+\frac{\partial}{\partial\beta^\dagger}\left(\frac{\kappa_b}{2}\beta^\dagger-E^*\alpha\right)P(\boldsymbol{\alpha})\\ &\quad +E\frac{\partial^2}{\partial\alpha\partial\beta}P(\boldsymbol{\alpha})+E^*\frac{\partial^2}{\partial\alpha^\dagger\partial\beta^\dagger}P(\boldsymbol{\alpha}). \qquad \text{(A.34)}\end{aligned}$$

$$\boxed{\begin{aligned}\frac{dP(\boldsymbol{\alpha})}{dt} &= \frac{\partial}{\partial\alpha}\left(\frac{\kappa_a}{2}\alpha-E\alpha^\dagger\right)P(\boldsymbol{\alpha})+\frac{\partial}{\partial\alpha^\dagger}\left(\frac{\kappa_a}{2}\alpha^\dagger-E^*\alpha\right)P(\boldsymbol{\alpha})\\ &\quad +\frac{1}{2}E\frac{\partial^2}{\partial\alpha^2}P(\boldsymbol{\alpha})+\frac{1}{2}E^*\frac{\partial^2}{\partial{\alpha^\dagger}^2}P(\boldsymbol{\alpha}). \qquad \text{(A.35)}\end{aligned}}$$

A.5 Conversion of FPE to SDEs

Assume the parametric amplifier driving term is real from the appropriate choice of phase. The Fokker-Planck equation is equivalent to the stochastic

differential equations (SDEs)

$$\frac{d}{dt}\begin{pmatrix}\alpha(t)\\ \alpha^\dagger(t)\\ \beta(t)\\ \beta^\dagger(t)\end{pmatrix} = \begin{pmatrix}-\frac{\kappa_a}{2} & 0 & 0 & E\\ 0 & -\frac{\kappa_a}{2} & E & 0\\ 0 & E & -\frac{\kappa_b}{2} & 0\\ E & 0 & 0 & -\frac{\kappa_b}{2}\end{pmatrix}\begin{pmatrix}\alpha(t)\\ \alpha^\dagger(t)\\ \beta(t)\\ \beta^\dagger(t)\end{pmatrix} + \sqrt{\frac{E}{2}}\begin{pmatrix}i & 0 & 1 & 0\\ 0 & i & 0 & 1\\ -i & 0 & 1 & 0\\ 0 & -i & 0 & 1\end{pmatrix}\begin{pmatrix}\eta_1(t)\\ \eta_2(t)\\ \eta_3(t)\\ \eta_4(t)\end{pmatrix}, \quad \text{(A.36)}$$

$$\frac{d}{dt}\begin{pmatrix}\alpha(t)\\ \alpha^\dagger(t)\end{pmatrix} = \begin{pmatrix}-\frac{\kappa_a}{2} & E\\ E & -\frac{\kappa_a}{2}\end{pmatrix}\begin{pmatrix}\alpha(t)\\ \alpha^\dagger(t)\end{pmatrix} + \sqrt{E}\begin{pmatrix}1 & 0\\ 0 & 1\end{pmatrix}\begin{pmatrix}\eta_1(t)\\ \eta_2(t)\end{pmatrix}, \quad \text{(A.37)}$$

where the $\eta_i(t)$ are real classical white noise terms obeying

$$\langle \eta_i(t)\rangle = 0, \quad \text{(A.38a)}$$
$$\langle \eta_i(t), \eta_j(t')\rangle = \delta_{ij}\delta(t-t'). \quad \text{(A.38b)}$$

The solution of this equation is

$$\begin{pmatrix}\alpha(t)\\ \beta^\dagger(t)\end{pmatrix} = \int_{-\infty}^{t} d\tau\, e^{A(t-\tau)}\begin{pmatrix}\xi_1(\tau)\\ \xi_2^\dagger(\tau)\end{pmatrix}, \quad \text{(A.39a)}$$
$$\begin{pmatrix}\alpha^\dagger(t)\\ \beta(t)\end{pmatrix} = \int_{-\infty}^{t} d\tau\, e^{A(t-\tau)}\begin{pmatrix}\xi_1^\dagger(\tau)\\ \xi_2(\tau)\end{pmatrix}, \quad \text{(A.39b)}$$

$$\begin{pmatrix}\alpha(t)\\ \alpha^\dagger(t)\end{pmatrix} = \int_{-\infty}^{t} d\tau\, e^{A(t-\tau)}\begin{pmatrix}\xi_1(\tau)\\ \xi_2(\tau)\end{pmatrix}, \quad \text{(A.39c)}$$

where

$$A = \begin{pmatrix}-\frac{\kappa_a}{2} & E\\ E & -\frac{\kappa_b}{2}\end{pmatrix}, \quad \text{(A.39d)}$$
$$\begin{pmatrix}\xi_1(t)\\ \xi_1^\dagger(t)\\ \xi_2(t)\\ \xi_2^\dagger(t)\end{pmatrix} = \sqrt{\frac{E}{2}}\begin{pmatrix}i & 0 & 1 & 0\\ 0 & i & 0 & 1\\ -i & 0 & 1 & 0\\ 0 & -i & 0 & 1\end{pmatrix}\begin{pmatrix}\eta_1(t)\\ \eta_2(t)\\ \eta_3(t)\\ \eta_4(t)\end{pmatrix}. \quad \text{(A.39e)}$$

$$A = \begin{pmatrix} -\frac{\kappa_a}{2} & E \\ E & -\frac{\kappa_a}{2} \end{pmatrix}, \tag{A.39f}$$

$$\begin{pmatrix} \xi_1(t) \\ \xi_2(t) \end{pmatrix} = \sqrt{E} \begin{pmatrix} \eta_1(t) \\ \eta_2(t) \end{pmatrix}. \tag{A.39g}$$

The non-zero correlations for ξ are

$$\langle \xi_1(0)\xi_2(\tau) \rangle = \left\langle \xi_1^\dagger(0)\xi_2^\dagger(\tau) \right\rangle = E\delta(\tau). \tag{A.40}$$

$$\langle \xi_1(0)\xi_1(\tau) \rangle = \langle \xi_2(0)\xi_2(\tau) \rangle = E\delta(\tau). \tag{A.41}$$

A.6 Solution of SDEs

Now solve for $\boldsymbol{\alpha}(t)$. The eigenvalues of A are

$$\lambda_{1,2} = \frac{1}{2}\left\{ -\frac{1}{2}(\kappa_a + \kappa_b) \pm \sqrt{\frac{1}{4}(\kappa_a - \kappa_b)^2 + 4E^2} \right\}. \tag{A.42}$$

$$\lambda_{1,2} = -\frac{\kappa_a}{2} \pm E. \tag{A.43}$$

The exponential evaluates to

$$e^{At} = \frac{1}{\lambda_1 - \lambda_2} \begin{pmatrix} B_1 & B_2 \\ B_2 & B_3 \end{pmatrix}, \tag{A.44a}$$

where

$$B_1 = \left(\lambda_1 + \frac{\kappa_a}{2}\right) e^{\lambda_2 t} - \left(\lambda_2 + \frac{\kappa_a}{2}\right) e^{\lambda_1 t}, \tag{A.44b}$$

$$B_2 = Ee^{\lambda_1 t} - Ee^{\lambda_2 t}, \tag{A.44c}$$

$$B_3 = \left(\lambda_1 + \frac{\kappa_a}{2}\right) e^{\lambda_1 t} + \left(\lambda_2 + \frac{\kappa_a}{2}\right) e^{\lambda_2 t}. \tag{A.44d}$$

$$e^{At} = \frac{1}{2} \begin{pmatrix} e^{\lambda_1 t} + e^{\lambda_2 t} & e^{\lambda_1 t} - e^{\lambda_2 t} \\ e^{\lambda_1 t} - e^{\lambda_2 t} & e^{\lambda_1 t} - e^{\lambda_2 t} \end{pmatrix}, \tag{A.45}$$

So we obtain

$$\alpha(t) = \frac{1}{\lambda_1-\lambda_2}\int_{-\infty}^{t} d\tau\,\left\{B_1\xi_1(\tau)+B_2\xi_2^\dagger(\tau)\right\}, \tag{A.46a}$$

$$\beta^\dagger(t) = \frac{1}{\lambda_1-\lambda_2}\int_{-\infty}^{t} d\tau\,\left\{B_2\xi_1(\tau)+B_3\xi_2^\dagger(\tau)\right\}. \tag{A.46b}$$

$$\begin{aligned}\alpha(t) &= +\frac{1}{2}\int_{-\infty}^{t} d\tau\,\left(e^{\lambda_1(t-\tau)}+e^{\lambda_2(t-\tau)}\right)\xi_1(\tau)\\ &\quad +\frac{1}{2}\int_{-\infty}^{t} d\tau\,\left(e^{\lambda_1(t-\tau)}-e^{\lambda_2(t-\tau)}\right)\xi_2(\tau), \qquad \text{(A.47a)}\\ \alpha^\dagger(t) &= +\frac{1}{2}\int_{-\infty}^{t} d\tau\,\left(e^{\lambda_1(t-\tau)}-e^{\lambda_2(t-\tau)}\right)\xi_1(\tau)\\ &\quad +\frac{1}{2}\int_{-\infty}^{t} d\tau\,\left(e^{\lambda_1(t-\tau)}+e^{\lambda_2(t-\tau)}\right)\xi_2(\tau). \qquad \text{(A.47b)}\end{aligned}$$

Now use the broad-bandwidth approximations

$$e^{\lambda_1(t-\tau)} \rightarrow \frac{2}{\lambda_1}\delta(t-\tau), \tag{A.48a}$$

$$e^{\lambda_2(t-\tau)} \rightarrow \frac{2}{\lambda_2}\delta(t-\tau). \tag{A.48b}$$

Hence, noting that the delta functions lie at the end of the range of integration we obtain

$$\begin{aligned}\alpha(t) &= \frac{1}{\lambda_1-\lambda 2}\left(\frac{\left(\lambda_1+\frac{\kappa_a}{2}\right)}{\lambda_2}-\frac{\left(\lambda_2+\frac{\kappa_a}{2}\right)}{\lambda_1}\right)\xi_1(t)\\ &\quad +\frac{1}{\lambda_1-\lambda 2}\left\{\frac{E}{\lambda_1}-\frac{E}{\lambda_2}\right\}\xi_2^\dagger(t)\\ &= \left(\frac{-1}{\lambda_1\lambda_2}\right)\left(\frac{\kappa_b}{2}\xi_1(t)+E\xi_2^\dagger(t)\right), \qquad \text{(A.49a)}\\ \beta^\dagger(t) &= \frac{1}{\lambda_1-\lambda 2}\left\{\frac{E}{\lambda_1}-\frac{E}{\lambda_2}\right\}\xi_1(t)\\ &\quad +\frac{1}{\lambda_1-\lambda 2}\left(\frac{\left(\lambda_1+\frac{\kappa_a}{2}\right)}{\lambda_1}-\frac{\left(\lambda_2+\frac{\kappa_a}{2}\right)}{\lambda_2}\right)\xi_2^\dagger(t)\\ &= \left(\frac{-1}{\lambda_1\lambda_2}\right)\left(E\xi_1(t)+\frac{\kappa_a}{2}\xi_2^\dagger(t)\right). \qquad \text{(A.49b)}\end{aligned}$$

Similarly, the other noise terms are

$$\alpha^\dagger(t) = \left(\frac{-1}{\lambda_1\lambda_2}\right)\left(\frac{\kappa_b}{2}\xi_1^\dagger(t) + E\xi_2(t)\right), \tag{A.49c}$$

$$\beta(t) = \left(\frac{-1}{\lambda_1\lambda_2}\right)\left(E\xi_1^\dagger(t) + \frac{\kappa_a}{2}\xi_2(t)\right). \tag{A.49d}$$

$$\alpha(t) = \frac{1}{2}\left(\frac{1}{\lambda_1}+\frac{1}{\lambda_2}\right)\xi_1(t) + \frac{1}{2}\left(\frac{1}{\lambda_1}-\frac{1}{\lambda_2}\right)\xi_2(t), \tag{A.50a}$$

$$\alpha^\dagger(t) = \frac{1}{2}\left(\frac{1}{\lambda_1}-\frac{1}{\lambda_2}\right)\xi_1(t) + \frac{1}{2}\left(\frac{1}{\lambda_1}+\frac{1}{\lambda_2}\right)\xi_2(t), \tag{A.50b}$$

A.7 Noise correlations

Define the parameters describing the squeezing in the parametric amplifier to be

$$N = \left(\frac{E^2\kappa_a\kappa_b}{{\lambda_1}^2{\lambda_2}^2}\right), \tag{A.51a}$$

$$M = \sqrt{\kappa_a\kappa_b}\,E\left(\frac{E^2+\frac{\kappa_a\kappa_b}{4}}{{\lambda_1}^2{\lambda_2}^2}\right). \tag{A.51b}$$

$$N = \left(\frac{E^2\kappa_a^2}{{\lambda_1}^2{\lambda_2}^2}\right), \tag{A.52a}$$

$$M = \kappa_a E\left(\frac{E^2+\frac{\kappa_a^2}{4}}{{\lambda_1}^2{\lambda_2}^2}\right). \tag{A.52b}$$

The non-zero correlations are then

$$\left\langle\alpha^\dagger(t)\alpha(0)\right\rangle = \frac{N}{\kappa_a}\delta(t), \tag{A.53a}$$

$$\left\langle\beta^\dagger(t)\beta(0)\right\rangle = \frac{N}{\kappa_b}\delta(t), \tag{A.53b}$$

$$\left\langle\alpha(t)\beta(0)\right\rangle = \frac{M}{\sqrt{\kappa_a\kappa_b}}\,\delta(t), \tag{A.53c}$$

$$\left\langle\alpha^\dagger(t)\beta^\dagger(0)\right\rangle = \frac{M}{\sqrt{\kappa_a\kappa_b}}\,\delta(t). \tag{A.53d}$$

$$\langle \alpha(t)\alpha(0)\rangle = \langle \alpha^\dagger(t)\alpha^\dagger(0)\rangle = \frac{M}{2\kappa_a}\delta(t), \tag{A.54a}$$

$$\langle \alpha(t)\alpha^\dagger(0)\rangle = \langle \alpha^\dagger(t)\alpha(0)\rangle = \frac{N}{2\kappa_a}\delta(t). \tag{A.54b}$$

A.8 Cumulant expansion

A cumulant expansion (taken to second order) may be used to transform the master equation by averaging over the noise terms. Write the master equation in the form

$$\frac{d\rho}{dt} = \left(A_0 + \alpha(t)A_1 + \alpha^\dagger(t)A_2 + \beta(t)B_1 + \beta^\dagger(t)B_2\right)\rho, \tag{A.55a}$$

where we have defined

$$\begin{aligned} A_0\rho &= +\frac{\gamma_2}{2}\left(2\sigma_2^-\rho\sigma_2^+ - \sigma_2^+\sigma_2^-\rho - \rho\sigma_2^+\sigma_2^-\right) \\ &\quad +\frac{\gamma_3}{2}\left(2\sigma_3^-\rho\sigma_3^+ - \sigma_3^+\sigma_3^-\rho - \rho\sigma_3^+\sigma_3^-\right), && \text{(A.55b)} \\ A_1\rho &= -\sqrt{\kappa_a\gamma_2\epsilon_2}\left[\sigma_2^+,\rho\right], && \text{(A.55c)} \\ A_2\rho &= -\sqrt{\kappa_a\gamma_2\epsilon_2}\left[\rho,\sigma_2^-\right], && \text{(A.55d)} \\ B_1\rho &= -\sqrt{\kappa_b\gamma_3\epsilon_3}\left[\sigma_3^+,\rho\right], && \text{(A.55e)} \\ B_2\rho &= -\sqrt{\kappa_b\gamma_3\epsilon_3}\left[\rho,\sigma_3^-\right]. && \text{(A.55f)} \end{aligned}$$

$$\frac{d\rho}{dt} = \left(A_0 + \alpha(t)A_1 + \alpha^\dagger(t)A_2\right)\rho, \tag{A.56a}$$

where we have defined

$$\begin{aligned} A_0\rho &= +\frac{\gamma_2}{2}\left(2\sigma_2^-\rho\sigma_2^+ - \sigma_2^+\sigma_2^-\rho - \rho\sigma_2^+\sigma_2^-\right) \\ &\quad +\frac{\gamma_3}{2}\left(2\sigma_3^-\rho\sigma_3^+ - \sigma_3^+\sigma_3^-\rho - \rho\sigma_3^+\sigma_3^-\right), && \text{(A.56b)} \\ A_1\rho &= -\sqrt{\kappa_a\gamma_2\epsilon_2}\left[\sigma_2^+,\rho\right] - \sqrt{\kappa_a\gamma_3\epsilon_3}\left[\sigma_3^+,\rho\right], && \text{(A.56c)} \\ A_2\rho &= -\sqrt{\kappa_a\gamma_2\epsilon_2}\left[\rho,\sigma_2^-\right] - \sqrt{\kappa_a\gamma_3\epsilon_3}\left[\rho,\sigma_3^-\right]. && \text{(A.56d)} \end{aligned}$$

Using the cumulant expansion to remove the noise terms results in the

transformed master equation

$$\begin{aligned}\frac{d\rho}{dt} &= A_0\rho \\ &\quad + \int_0^\infty d\tau \left\{\left\langle \alpha(\tau)\alpha^\dagger(0)\right\rangle (A_1A_2 + A_2A_1)\right\}\rho \\ &\quad + \int_0^\infty d\tau \left\{\left\langle \alpha(\tau)\beta(0)\right\rangle (A_1B_1 + B_1A_1)\right\}\rho \\ &\quad + \int_0^\infty d\tau \left\{\left\langle \alpha^\dagger(\tau)\beta^\dagger(0)\right\rangle (A_2B_2 + B_2A_2)\right\}\rho \\ &\quad + \int_0^\infty d\tau \left\{\left\langle \beta(\tau)\beta^\dagger(0)\right\rangle (B_1B_2 + B_2B_1)\right\}\rho. \end{aligned} \tag{A.57}$$

$$\begin{aligned}\frac{d\rho}{dt} &= A_0\rho \\ &\quad + \int_0^\infty d\tau \left\{\left\langle \alpha(\tau)\alpha(0)\right\rangle A_1A_1 + \left\langle \alpha(\tau)\alpha^\dagger(0)\right\rangle A_1A_2\right\}\rho \\ &\quad + \int_0^\infty d\tau \left\{\left\langle \alpha^\dagger(\tau)\alpha(0)\right\rangle A_2A_1 + \left\langle \alpha^\dagger(\tau)\alpha^\dagger(0)\right\rangle A_2A_2\right\}\rho. \end{aligned} \tag{A.58}$$

After integrating over the delta functions and substituting for A_0 we obtain

$$\begin{aligned}\frac{d\rho}{dt} &= +\frac{\gamma_2}{2}\left(2\sigma_2^-\rho\sigma_2^+ - \sigma_2^+\sigma_2^-\rho - \rho\sigma_2^+\sigma_2^-\right) \\ &\quad +\frac{\gamma_3}{2}\left(2\sigma_3^-\rho\sigma_3^+ - \sigma_3^+\sigma_3^-\rho - \rho\sigma_3^+\sigma_3^-\right) \\ &\quad +\frac{N}{2\kappa_a}\left(A_1A_2 + A_2A_1\right)\rho \\ &\quad +\frac{M}{2\sqrt{\kappa_a\kappa_b}}\left(A_1B_1 + B_1A_1\right)\rho \\ &\quad +\frac{M}{2\sqrt{\kappa_a\kappa_b}}\left(A_2B_2 + B_2A_2\right)\rho \\ &\quad +\frac{N}{2\kappa_b}\left(B_1B_2 + B_2B_1\right)\rho. \end{aligned} \tag{A.59}$$

$$\begin{aligned}\frac{d\rho}{dt} &= +\frac{\gamma_2}{2}\left(2\sigma_2^-\rho\sigma_2^+ - \sigma_2^+\sigma_2^-\rho - \rho\sigma_2^+\sigma_2^-\right) \\ &\quad +\frac{\gamma_3}{2}\left(2\sigma_3^-\rho\sigma_3^+ - \sigma_3^+\sigma_3^-\rho - \rho\sigma_3^+\sigma_3^-\right) \\ &\quad +\frac{M}{4\kappa_a}\left(A_1A_1 + A_2A_2\right)\rho \\ &\quad +\frac{N}{4\kappa_a}\left(A_1A_2 + A_2A_1\right)\rho. \end{aligned} \tag{A.60}$$

A.9 Reduced master equation

Substituting Equations (A.55c-A.55f), we obtain the reduced master equation for the atoms alone

$$\begin{aligned}\frac{d\rho}{dt} &= +\frac{1}{2}\gamma_2\left(2\sigma_2^-\rho\sigma_2^+ - \sigma_2^+\sigma_2^-\rho - \rho\sigma_2^+\sigma_2^-\right) \\ &\quad +\frac{1}{2}\gamma_3\left(2\sigma_3^-\rho\sigma_3^+ - \sigma_3^+\sigma_3^-\rho - \rho\sigma_3^+\sigma_3^-\right) \\ &\quad +\frac{1}{2}\gamma_2\epsilon_2 N\left(2\sigma_2^-\rho\sigma_2^+ - \sigma_2^+\sigma_2^-\rho - \rho\sigma_2^+\sigma_2^-\right) \\ &\quad +\frac{1}{2}\gamma_2\epsilon_2 N\left(2\sigma_2^+\rho\sigma_2^- - \sigma_2^-\sigma_2^+\rho - \rho\sigma_2^-\sigma_2^+\right) \\ &\quad +\frac{1}{2}\gamma_3\epsilon_3 N\left(2\sigma_3^-\rho\sigma_3^+ - \sigma_3^+\sigma_3^-\rho - \rho\sigma_3^+\sigma_3^-\right) \\ &\quad +\frac{1}{2}\gamma_3\epsilon_3 N\left(2\sigma_3^+\rho\sigma_3^- - \sigma_3^-\sigma_3^+\rho - \rho\sigma_3^-\sigma_3^+\right) \\ &\quad -\frac{1}{2}\sqrt{\gamma_2\gamma_3\epsilon_2\epsilon_3}M\left(2\sigma_2^+\rho\sigma_3^+ - \sigma_3^+\sigma_2^+\rho - \rho\sigma_3^+\sigma_2^+\right) \\ &\quad -\frac{1}{2}\sqrt{\gamma_2\gamma_3\epsilon_2\epsilon_3}M\left(2\sigma_3^+\rho\sigma_2^+ - \sigma_2^+\sigma_3^+\rho - \rho\sigma_2^+\sigma_3^+\right) \\ &\quad -\frac{1}{2}\sqrt{\gamma_2\gamma_3\epsilon_2\epsilon_3}M\left(2\sigma_2^-\rho\sigma_3^- - \sigma_3^-\sigma_2^-\rho - \rho\sigma_3^-\sigma_2^-\right) \\ &\quad -\frac{1}{2}\sqrt{\gamma_2\gamma_3\epsilon_2\epsilon_3}M\left(2\sigma_3^-\rho\sigma_2^- - \sigma_2^-\sigma_3^-\rho - \rho\sigma_2^-\sigma_3^-\right). \end{aligned} \tag{A.61}$$

Substituting Equations (A.56c) and (A.56d), we obtain the reduced master equation for the atoms alone

$$\begin{aligned}
\frac{d\rho}{dt} &= +\frac{1}{2}\gamma_2\left(2\sigma_2^-\rho\sigma_2^+ - \sigma_2^+\sigma_2^-\rho - \rho\sigma_2^+\sigma_2^-\right) \\
&\quad +\frac{1}{2}\gamma_3\left(2\sigma_3^-\rho\sigma_3^+ - \sigma_3^+\sigma_3^-\rho - \rho\sigma_3^+\sigma_3^-\right) \\
&\quad +\frac{1}{4}\gamma_2\epsilon_2 N\left(2\sigma_2^-\rho\sigma_2^+ - \sigma_2^+\sigma_2^-\rho - \rho\sigma_2^+\sigma_2^-\right) \\
&\quad +\frac{1}{4}\gamma_2\epsilon_2 N\left(2\sigma_2^+\rho\sigma_2^- - \sigma_2^-\sigma_2^+\rho - \rho\sigma_2^-\sigma_2^+\right) \\
&\quad +\frac{1}{4}\gamma_3\epsilon_3 N\left(2\sigma_3^-\rho\sigma_3^+ - \sigma_3^+\sigma_3^-\rho - \rho\sigma_3^+\sigma_3^-\right) \\
&\quad +\frac{1}{4}\gamma_3\epsilon_3 N\left(2\sigma_3^+\rho\sigma_3^- - \sigma_3^-\sigma_3^+\rho - \rho\sigma_3^-\sigma_3^+\right) \\
&\quad +\frac{1}{4}\sqrt{\gamma_2\gamma_3\epsilon_2\epsilon_3}N\left(2\sigma_2^-\rho\sigma_3^+ - \sigma_3^+\sigma_2^-\rho - \rho\sigma_3^+\sigma_2^-\right) \\
&\quad +\frac{1}{4}\sqrt{\gamma_2\gamma_3\epsilon_2\epsilon_3}N\left(2\sigma_2^+\rho\sigma_3^- - \sigma_3^-\sigma_2^+\rho - \rho\sigma_3^-\sigma_2^+\right) \\
&\quad +\frac{1}{4}\sqrt{\gamma_2\gamma_3\epsilon_2\epsilon_3}N\left(2\sigma_3^-\rho\sigma_2^+ - \sigma_2^+\sigma_3^-\rho - \rho\sigma_2^+\sigma_3^-\right) \\
&\quad +\frac{1}{4}\sqrt{\gamma_2\gamma_3\epsilon_2\epsilon_3}N\left(2\sigma_3^+\rho\sigma_2^- - \sigma_2^-\sigma_3^+\rho - \rho\sigma_2^-\sigma_3^+\right) \\
&\quad -\frac{1}{4}\gamma_2\epsilon_2 M\left(2\sigma_2^+\rho\sigma_2^+ - \sigma_2^+\sigma_2^+\rho - \rho\sigma_2^+\sigma_2^+\right) \\
&\quad -\frac{1}{4}\gamma_2\epsilon_2 M\left(2\sigma_2^-\rho\sigma_2^- - \sigma_2^-\sigma_2^-\rho - \rho\sigma_2^-\sigma_2^-\right) \\
&\quad -\frac{1}{4}\gamma_3\epsilon_3 M\left(2\sigma_3^+\rho\sigma_3^+ - \sigma_3^+\sigma_3^+\rho - \rho\sigma_3^+\sigma_3^+\right) \\
&\quad -\frac{1}{4}\gamma_3\epsilon_3 M\left(2\sigma_3^-\rho\sigma_3^- - \sigma_3^-\sigma_3^-\rho - \rho\sigma_3^-\sigma_3^-\right) \\
&\quad -\frac{1}{4}\sqrt{\gamma_2\gamma_3\epsilon_2\epsilon_3}M\left(2\sigma_2^+\rho\sigma_3^+ - \sigma_3^+\sigma_2^+\rho - \rho\sigma_3^+\sigma_2^+\right) \\
&\quad -\frac{1}{4}\sqrt{\gamma_2\gamma_3\epsilon_2\epsilon_3}M\left(2\sigma_3^+\rho\sigma_2^+ - \sigma_2^+\sigma_3^+\rho - \rho\sigma_2^+\sigma_3^+\right) \\
&\quad -\frac{1}{4}\sqrt{\gamma_2\gamma_3\epsilon_2\epsilon_3}M\left(2\sigma_2^-\rho\sigma_3^- - \sigma_3^-\sigma_2^-\rho - \rho\sigma_3^-\sigma_2^-\right) \\
&\quad -\frac{1}{4}\sqrt{\gamma_2\gamma_3\epsilon_2\epsilon_3}M\left(2\sigma_3^-\rho\sigma_2^- - \sigma_2^-\sigma_3^-\rho - \rho\sigma_2^-\sigma_3^-\right). \qquad \text{(A.62)}
\end{aligned}$$

Appendix B

Calculation of steady states

In this Appendix we present details of the method used to automate the calculation of the steady state solution of a given master equation.

In this Thesis we commonly wish to calculate the steady state solutions for master equations in $2 \otimes 2$ systems. Density matrices for these systems have 15 degrees of freedom and it is a tedious exercise to calculate the steady state by hand. For this reason, the process has been automated by writing a computer program to run in the mathematics package MATLAB©.

The computer program represents the master equation symbolically. The stored symbolic representation of the master equation is then manipulated in the computer in a manner equivalent to the steps used when solving a master equation by hand. The process of solving the master equation is as follows:

1. Define the constants and operators that occur in the master equation. Each constant and operator is represented by a unique integer and has an associated human-readable string.

2. Define the commutation relations between the operators, and other relevant operator identities (e.g., $\sigma^+\sigma^+ = 0$), that are needed to calculate the differential equations governing each element of the density matrix.

3. Define the Liouvillian, in a symbolic manner, using the constants and operators previously defined.

4. The computer then finds the Bloch equations for the master equation. It calculates a 16×16 matrix of symbolic expressions that describes the evolution of the 16 density matrix elements in a $2 \otimes 2$ system.

5. The symbolic evolution matrix is block-diagonalized and subblocks of interest may be selectively processed.

6. Constraints are added to handle the trace condition (and any decoupled dark states) so that a unique steady state solution is calculable.

7. A text file of the evolution matrix (with constraints) is written to disk in a suitable format to be readable by the symbolic mathematics package Mathematica©. This matrix may then be imported into a simple Mathematica program which inverts the matrix to find an analytic formula for the steady state solution to the master equation.

Appendix C

Adiabatic elimination of excited states

In this Appendix we provide details of the projector technique that is used to eliminate the excited states of the atoms in Chapter 7. The adiabatic elimination is performed in two ways, depending on whether spontaneous emission from the excited atomic states can be neglected.

Contents

A projector technique may be used to eliminate the excited states of the atoms. Here we employ the technique used in [78] and apply it to the master equation (7.2). This method for the adiabatic elimination deals exclusively with the master equation and avoids the difficulties that can arise due to operator ordering when working with the Heisenberg equations of motion [83].

In this Appendix we commonly use notation for operators where only the atomic spaces are explicitly stated. The space of the cavity is assumed. Thus the operator $Q_1 \otimes \mathbf{1}$ is a notational shortcut for $\mathbf{1}_{cav} \otimes Q_1 \otimes \mathbf{1}_2$.

C.1 Interaction picture

To begin we move the master equation (7.2) into the interaction picture. The frame we choose has the excited states stopped with respect to the rotation of their respective virtual transitions (shown as dotted lines in Figure 7.2). The rotation of state $|1\rangle$ is also stopped. We obtain

$$\dot{\rho} = -i\left[Q + Q^\dagger + Z, \rho\right] + \mathcal{L}_{cav}\rho + \mathcal{L}_{spon}\rho, \tag{C.1a}$$

where we have defined

$$\begin{aligned} Q_1^\dagger &= g_r a \left|r\right\rangle\left\langle 0\right|_1 + g_s a \left|s\right\rangle\left\langle 1\right|_1 \\ &\quad + \frac{\Omega_r}{2}\left|r\right\rangle\left\langle 1\right|_1 + \frac{\Omega_s}{2}e^{-i\phi}\left|s\right\rangle\left\langle 0\right|_1 + \frac{\Omega_t}{2}\left|t\right\rangle\left\langle 1\right|_1, && \text{(C.1b)} \\ Q_2^\dagger &= g_r a \left|r\right\rangle\left\langle 0\right|_2 + g_s a \left|s\right\rangle\left\langle 1\right|_2 \\ &\quad + \frac{\Omega_r}{2}\left|r\right\rangle\left\langle 1\right|_2 + \frac{\Omega_s}{2}e^{-i\phi}\left|s\right\rangle\left\langle 0\right|_2 + \frac{\Omega_t}{2}\left|t\right\rangle\left\langle 1\right|_2, && \text{(C.1c)} \\ Q^\dagger &= Q_1^\dagger \otimes \mathbf{1} + \mathbf{1} \otimes Q_2^\dagger, && \text{(C.1d)} \end{aligned}$$

and

$$\begin{aligned} Z_1 &= -\Delta_r \left|r\right\rangle\left\langle r\right|_1 - \Delta_s \left|s\right\rangle\left\langle s\right|_1 - \Delta_t \left|t\right\rangle\left\langle t\right|_1, && \text{(C.1e)} \\ Z_2 &= -\Delta_r \left|r\right\rangle\left\langle r\right|_2 - \Delta_s \left|s\right\rangle\left\langle s\right|_2 - \Delta_t \left|t\right\rangle\left\langle t\right|_2, && \text{(C.1f)} \\ Z &= Z_1 \otimes \mathbf{1} + \mathbf{1} \otimes Z_2. && \text{(C.1g)} \end{aligned}$$

The forms of $\mathcal{L}_{cav}\rho$ and $\mathcal{L}_{spon}\rho$ remain unchanged from Equation (7.2c) and Equation (7.3a). The operators Q and $Q^\dagger$ are lowering and raising operators that describe the action of the driving lasers and the cavity mode in moving the system between the ground and excited states. The operator Z gives the residual rotation of the excited states.

C.2 Projectors

We define projectors onto the excited and the ground states of the atoms as

$$\begin{aligned} P_1^+ &= \left|r\right\rangle\left\langle r\right|_1 + \left|s\right\rangle\left\langle s\right|_1 + \left|t\right\rangle\left\langle t\right|_1, && \text{(C.2a)} \\ P_2^+ &= \left|r\right\rangle\left\langle r\right|_2 + \left|s\right\rangle\left\langle s\right|_2 + \left|t\right\rangle\left\langle t\right|_2, && \text{(C.2b)} \\ P_1^- &= \left|1\right\rangle\left\langle 1\right|_1 + \left|0\right\rangle\left\langle 0\right|_1, && \text{(C.2c)} \\ P_2^- &= \left|1\right\rangle\left\langle 1\right|_2 + \left|0\right\rangle\left\langle 0\right|_2, && \text{(C.2d)} \end{aligned}$$

so that the projectors in the full Hilbert space may be written

$$P^{++} = P_1^+ \otimes P_2^+, \tag{C.2e}$$
$$P^{+-} = P_1^+ \otimes P_2^-, \tag{C.2f}$$
$$P^{-+} = P_1^- \otimes P_2^+, \tag{C.2g}$$
$$P^{--} = P_1^- \otimes P_2^-. \tag{C.2h}$$

We need to commute the projectors and the Q operators. This can be done using

$$P^{++}Q = 0, \tag{C.3a}$$
$$P^{+-}Q = (\mathbf{1} \otimes Q_2)\, P^{++}, \tag{C.3b}$$
$$P^{-+}Q = (Q_1 \otimes \mathbf{1})\, P^{++}, \tag{C.3c}$$
$$P^{--}Q = (Q_1 \otimes \mathbf{1})\, P^{+-} + (\mathbf{1} \otimes Q_2)\, P^{-+}. \tag{C.3d}$$
$$P^{++}Q^\dagger = \left(Q_1^\dagger \otimes \mathbf{1}\right) P^{+-} + \left(\mathbf{1} \otimes Q_2^\dagger\right) P^{-+}, \tag{C.3e}$$
$$P^{+-}Q^\dagger = \left(Q_1^\dagger \otimes \mathbf{1}\right) P^{--}, \tag{C.3f}$$
$$P^{-+}Q^\dagger = \left(\mathbf{1} \otimes Q_2^\dagger\right) P^{--}, \tag{C.3g}$$
$$P^{--}Q^\dagger = 0. \tag{C.3h}$$

C.3 Neglecting spontaneous emission

We perform the adiabatic elimination in two ways, depending on whether spontaneous emission from the atoms is being considered or not. In this Section we consider the case where spontaneous emission may be neglected. The adiabatic elimination in the presence of spontaneous emission is covered in Section C.4.

Define partial density matrices

$$\rho^{----} = P^{--}\rho P^{--}, \tag{C.4a}$$
$$\rho^{+---} = P^{+-}\rho P^{--}, \tag{C.4b}$$
$$\rho^{-+--} = P^{-+}\rho P^{--} \ldots \text{etc.} \tag{C.4c}$$

Then partial master equations can be obtained

$$\frac{d}{dt}\rho^{----} = -i\,(Q_1 \otimes \mathbf{1})\,\rho^{+---} - i\,(\mathbf{1} \otimes Q_2)\,\rho^{-+--} + \text{H.c.}, \tag{C.5a}$$
$$\frac{d}{dt}\rho^{+---} = -iZ\rho^{+---} - i\left(Q_1^\dagger \otimes \mathbf{1}\right)\rho^{----}, \tag{C.5b}$$
$$\frac{d}{dt}\rho^{-+--} = -iZ\rho^{-+--} - i\left(\mathbf{1} \otimes Q_2^\dagger\right)\rho^{----}. \tag{C.5c}$$

Now the adiabatic elimination may be performed by assuming that the coherence terms ρ^{+---} and ρ^{-+--} follow adiabatically the population ρ^{----} in the ground states. Setting the derivatives in Equations (C.5b,C.5c) to zero and substituting into (C.5a) we obtain the following master equation

$$\frac{d}{dt}\rho = -i\left(H_{eff}\rho - \rho H_{eff}^{\dagger}\right), \tag{C.6a}$$

where

$$H_{eff} = -\left(Q_1 Z_1^{-1} Q_1^{\dagger} \otimes \mathbf{1} + \mathbf{1} \otimes Q_2 Z_2^{-1} Q_2^{\dagger}\right), \tag{C.6b}$$

and where we take

$$Z_1^{-1} = -\frac{1}{\Delta_r}|r\rangle\langle r|_1 - \frac{1}{\Delta_s}|s\rangle\langle s|_1 - \frac{1}{\Delta_t}|t\rangle\langle t|_1, \tag{C.6c}$$

$$Z_2^{-1} = -\frac{1}{\Delta_r}|r\rangle\langle r|_2 - \frac{1}{\Delta_s}|s\rangle\langle s|_2 - \frac{1}{\Delta_t}|t\rangle\langle t|_2. \tag{C.6d}$$

This master equation is for the reduced density matrix in the space $\mathcal{H}^{cav} \otimes \mathcal{H}^2 \otimes \mathcal{H}^2$.

C.4 Including spontaneous emission

In this Section we consider the adiabatic elimination in the presence of spontaneous emission. The definitions of the spontaneous emission terms used are those of Equation 7.3a, i.e. the case where $\delta \neq 0$ and each decay from each excited state is effectively into a different reservoir. We assume in this Section that the detunings are all the same (i.e., $\Delta_r = \Delta_s = \Delta_t = \Delta$) and that the spontaneous emission rates from the excited states are all the same (i.e., $\gamma_r = \gamma_s = \gamma_t = \gamma$).

By neglecting all terms that are second order or more (i.e., more than

two '+'s) we obtain the partial master equations

$$\begin{aligned}
\frac{d}{dt}\rho^{----} &= -i\left(Q_1 \otimes \mathbf{1}\right)\rho^{+---} - i\left(\mathbf{1} \otimes Q_2\right)\rho^{-+--} + \text{H.c.} \\
&\quad +\gamma \sum_{Y_1} \left(Y_1 \otimes \mathbf{1}\right)\rho^{+-+-}\left(Y_1^\dagger \otimes \mathbf{1}\right) \\
&\quad +\gamma \sum_{Y_2} \left(\mathbf{1} \otimes Y_2\right)\rho^{-+-+}\left(\mathbf{1} \otimes Y_2^\dagger\right) \qquad \text{(C.7a)} \\
\frac{d}{dt}\rho^{+---} &= \left(i\Delta - \frac{\gamma}{2}\right)\rho^{+---} - i\left(Q_1^\dagger \otimes \mathbf{1}\right)\rho^{----}, \qquad \text{(C.7b)} \\
\frac{d}{dt}\rho^{-+--} &= \left(i\Delta - \frac{\gamma}{2}\right)\rho^{-+--} - i\left(\mathbf{1} \otimes Q_2^\dagger\right)\rho^{----}. \qquad \text{(C.7c)} \\
\frac{d}{dt}\rho^{+-+-} &= \frac{1}{\Delta^2 + \frac{\gamma^2}{4}}\left(Q_1^\dagger \otimes \mathbf{1}\right)\rho^{----}\left(Q_1 \otimes \mathbf{1}\right), \qquad \text{(C.7d)} \\
\frac{d}{dt}\rho^{-+-+} &= \frac{1}{\Delta^2 + \frac{\gamma^2}{4}}\left(\mathbf{1} \otimes Q_2^\dagger\right)\rho^{----}\left(\mathbf{1} \otimes Q_2\right), \qquad \text{(C.7e)}
\end{aligned}$$

For clarity, we use a shorthand notation where summation over Y_i means the summation over all decay channels for atom i, i.e.,

$$\sum_{Y_i} Y_i \equiv \sum_{j\in\{r,s,t\}} \sum_{k\in\{0,1\}} Y_{ijk}. \qquad \text{(C.8)}$$

We perform the adiabatic elimination by taking the derivatives to be zero in Equations (C.7b-C.7e) and substituting into Equation (C.7a). The final master equation we obtain is

$$\begin{aligned}
\frac{d}{dt}\rho &= -i\left(H_{eff}\rho - \rho H_{eff}^\dagger\right) \\
&\quad +\sum_{Y_1} \frac{\gamma}{\Delta^2 + \frac{\gamma^2}{4}}\left(Y_1 Q_1^\dagger \otimes \mathbf{1}\right)\rho\left(Q_1 Y_1^\dagger \otimes \mathbf{1}\right) \\
&\quad +\sum_{Y_2} \frac{\gamma}{\Delta^2 + \frac{\gamma^2}{4}}\left(\mathbf{1} \otimes Y_2 Q_2^\dagger\right)\rho\left(\mathbf{1} \otimes Q_2 Y_2^\dagger\right), \qquad \text{(C.9a)}
\end{aligned}$$

where

$$H_{eff} = \frac{1}{\Delta + i\frac{\gamma}{2}}\left(Q_1 Q_1^\dagger \otimes \mathbf{1} + \mathbf{1} \otimes Q_2 Q_2^\dagger\right). \qquad \text{(C.9b)}$$

Bibliography

[1] J. F. Poyatos, J. I. Cirac, and P. Zoller. Quantum reservoir engineering with laser cooled trapped ions. *Physical Review Letters*, 77:4728, 1996.

[2] G. M. Palma and P. L. Knight. Phase-sensitive population decay: The two-atom Dicke model in a broadband squeezed vacuum. *Physical Review A*, 39:1962, 1989.

[3] David Deutsch. Quantum theory, the Church-Turing principle and the universal quantum computer. *Proceedings of the Royal Society of London A 400*, page 97, 1985.

[4] Peter W. Shor. Algorithms for quantum computation: discrete log and factoring. *Proceedings of the 35th Annual IEEE Symposium on Foundations of Computer Science*, 1994.

[5] L. Grover. A fast quantum-mechanical algorithm for database search. *Proceedings of the 28th Annual Symposium on the Theory of Computing*, 1996.

[6] William K. Wootters and Wojciech H. Zurek. A single quantum cannot be cloned. *Nature*, 299:802, 1982.

[7] J. S. Bell. On the Einstein Podolsky Rosen paradox. *Physics*, 1:195, 1964.

[8] Benjamin Schumacher. Quantum coding. *Physical Review A*, 51:2738, 1995.

[9] Paul G. Kwiat, Edo Waks, Andrew G. White, Ian Appelbaum, and Philippe H. Eberhard. Ultrabright source of polarization-entangled photons. *Physical Review A*, 60:R773, 1999.

[10] Jian-Wei Pan, Matthew Daniell, Sara Gasparoni, Gregor Wells, and Anton Zeilinger. Experimental demonstration of four-photon entanglement and high-fidelity teleportation. *Physical Review Letters*, 86:4435, 2001.

[11] A. Rauschenbeutel, P. Bertet, S. Osnaghi, G. Nogues, M. Brune, J. M. Raimond, and S. Haroche. Controlled entanglement of two field modes in a cavity quantum electrodynamics experiment. *Physical Review A*, 64:050301(R), 2001.

[12] R. Scheunemann, F. S. Cataliotti, T. W. Hansch, and M. Weitz. Resolving and addressing atoms in individual sites of a CO_2-laser optical lattice. *Physical Review A*, 62:051801(R), 2000.

[13] Nicolas Schlosser, Georges Reymond, Igor Protsenko, and Philippe Grangier. Sub-poissonian loading of single atoms in a microscopic dipole trap. *Nature*, 411:1024, 2001.

[14] J. Ye, D.W. Vernooy, and H.J. Kimble. Trapping of single atoms in cavity QED. *Physical Review Letters*, 83:4987, 1999.

[15] C. J. Hood, T. W. Lynn, A. C. Doherty, A. S. Parkins, and H. J. Kimble. The atom-cavity microscope: single atoms bound in orbit by single photons. *Science*, 287:1447, 2000.

[16] P. W. H. Pinkse, T. Fischer, P. Maunz, and G. Rempe. Trapping an atom with single photons. *Nature*, 404:365, 2000.

[17] P. W. H. Pinkse, T. Fischer, P. Maunz, T. Puppe, and G. Rempe. How to catch an atom with single photons. *Journal of Modern Optics*, 47:2769, 2000.

[18] G. R. Guthöhrlein, M. Keller, K. Hayasaka, W. Lange, and H. Walther. A single ion as a nanoscopic probe of an optical field. *Nature*, 414:49, 2001.

[19] M. B. Plenio, S. F. Huelga, A. Beige, and P. L. Knight. Cavity-loss-induced generation of entangled atoms. *Physical Review A*, 59:2468, 1999.

[20] Almut Beige, William J. Munro, and Peter L. Knight. Bell's inequality test with entangled atoms. *Physical Review A*, 62:052101, 2000.

[21] E. Hagley, X. Maître, G. Nogues, C. Wunderlich, M. Brune, J. M. Raimond, and S. Haroche. Generation of Einstein-Podolsky-Rosen pairs of atoms. *Physical Review Letters*, 79:1, 1997.

[22] Arno Rauschenbeutel, Gilles Nogues, Stefano Osnaghi, Patrice Bertet, Michel Brune, Jean-Michel Raimond, and Serge Haroche. Step-by-step engineered multiparticle entanglement. *Science*, 288:2024, 2000.

[23] S. Osnagi, P. Bertet, A. Auffeves, P. Maioli, M. Brune, J. M. Raimond, and S. Haroche. Coherent control of an atomic collision in a cavity. *Physical Review Letters*, 87:037902, 2001.

[24] C. A. Sackett, D. Kielpinski, B. E. King, C. Langer, V. Meyer, C. J. Myatt, M. Rowe, Q. A. Turchette, W. M. Itano, D. J. Wineland, and C. Monroe. Experimental entanglement of four particles. *Nature*, 404:256, 2000.

[25] Q. A. Turchette, C. S. Wood, B. E. King, C. J. Myatt, D. Leibfried, W. M. Itano, C. Monroe, and D. J. Wineland. Deterministic entanglement of two trapped ions. *Physical Review Letters*, 81:3631, 1998.

[26] M. A. Rowe, D. Kielpinski, V. Meyer, C. A. Sackett, W. M. Itano, C. Monroe, and D. J. Wineland. Experimental violation of a Bell's inequality with efficient detection. *Nature*, 409:791, 2001.

[27] Nielson and Chuang. *Quantum Computation and Quantum Information*. Cambridge University Press, 2000.

[28] Charles H. Bennett, Giles Brassard, Claude Crépeau, Richard Jozsa, Asher Peres, and William K. Wootters. Teleporting an unknown quantum state via dual classical and Einstein-Podolsky-Rosen channels. *Physical Review Letters*, 70:1895, 1993.

[29] Charles H. Bennett, Herbert J. Bernstein, Sandu Popescu, and Benjamin Schumacher. Concentrating partial entanglement by local operations. *Physical Review A*, 53:2046, 1996.

[30] William K. Wootters. Entanglement of formation of an arbitrary state of two qubits. *Physical Review Letters*, 80:2245, 1998.

[31] Sze M. Tan. A computational toolbox for quantum and atomic optics. *Journal of Optics B*, 1:424, 1999.

[32] G. Alber, T. Beth, M. Horodecki, P. Horodecki, R. Horodecki, M. Rötteler, H. Weinfurter, R. Werner, and A. Zeilinger. *Quantum Information*. Springer, 2001.

[33] Martin B. Plenio and Vlatko Vedral. Teleportation, entanglement and thermodynamics in the quantum world. *Contemporary Physics*, 39:431, 1998.

[34] R. Horodecki, M. Horodecki, and P. Horodecki. Balance of information in bipartite quantum-communication systems: Entanglement-energy analogy. *Physical Review A*, 63:022310, 2001.

[35] Sandu Popescu and Daniel Rohrlich. Thermodynamics and the measure of entanglement. *Physical Review A*, 56:R3319, 1997.

[36] L. Henderson and V. Vedral. Information, relative entropy of entanglement, and irreversibility. *Physical Review Letters*, 84:2263, 2000.

[37] Reinhard F. Werner. Quantum states with Einstein-Podolsky-Rosen correlations admitting a hidden-variable model. *Physical Review A*, 40:4277, 1989.

[38] M. Lewenstein, D. Brub, J. I. Cirac, B. Kraus, M. Kus, J. Samsonowicz, A. Sanpera, and R. Tarrach. Separability and distillability in composite quantum systems - a primer. *Journal of Modern Optics*, 47:2481, 2000.

[39] Asher Peres. Separability criterion for density matrices. *Physical Review Letters*, 77:1413, 1996.

[40] Michal Horodecki, Pawel Horodecki, and Ryszard Horodecki. Separability of mixed states: Necessary and sufficient conditions. *Physics Letters A*, 223:1, 1996.

[41] Charles H. Bennett, David P. DiVincenzo, John A. Smolin, and William K. Wootters. Mixed-state entanglement and quantum error correction. *Physical Review A*, 54:3824, 1996.

[42] Michal Horodecki, Pawel Horodecki, and Ryszard Horodecki. Mixed-state entanglement and distillation: Is there a "bound" entanglement in Nature. *Physical Review Letters*, 80:5239, 1998.

[43] Michal Horodecki, Pawel Horodecki, and Ryszard Horodecki. Inseparable two spin-$\frac{1}{2}$ density matrices can be distilled to a singlet form. *Physical Review Letters*, 78:574, 1997.

[44] V. Vedral, M. B. Plenio, M. A. Rippin, and P. L. Knight. Quantifying entanglement. *Physical Review Letters*, 78:2275, 1997.

[45] V. Vedral and M. B. Plenio. Entanglement measures and purification procedures. *Physical Review A*, 57:1619, 1998.

[46] G. Vidal and R. F. Werner. A computable measure of entanglement. *quant-ph/0102117*, 2001.

[47] F. Verstraete, K. Audenaert, J. Dehaene, and Bart De Moor. A comparison of the entanglement measures negativity and concurrence. *quant-ph/0108021*, 2001.

[48] Clauser, Horne, Shimony, and Holt. Proposed experiment to test hidden variable theories. *Physical Review Letters*, 23:880, 1969.

[49] Samuel L. Braunstein and Carlton M. Caves. Information-theoretic Bell inequalities. *Physical Review Letters*, 61:662, 1988.

[50] Itamar Pitowsky. Optimal tests of quantum nonlocality. *Physical Review A*, 64:014102, 2001.

[51] N. David Mermin. Extreme quantum entanglement in a superposition of macroscopically distinct states. *Physical Review Letters*, 64:1838, 1990.

[52] A. Aspect, J. Dalibard, and G. Roger. Experimental test of Bell's inequalities using time-varying analyzers. *Physical Review Letters*, 49:1804, 1982.

[53] Z. Y. Ou, S. F. Pereira, H. J. Kimble, and K. C. Peng. Realization of the Einstein-Podolsky-Rosen paradox for continuous variables. *Physical Review Letters*, 68:3663, 1992.

[54] R. Horodecki, P. Horodecki, and M. Horodecki. Violating Bell inequality by mixed spin-1/2 states: Necessary and sufficient condition. *Physics Letters A*, page 340, 1995.

[55] Sandu Popescu. Bell's inequalities versus teleportation: What is nonlocality? *Physical Review Letters*, 72:797, 1994.

[56] W. J. Munro, K. Nemoto, and A. G. White. The Bell inequality: A measure of entanglement. *Journal of Modern Optics*, 28:1239, 2001.

[57] Sandu Popescu. Bell's inequalities and density matrices: Revealing "hidden" nonlocality. *Physical Review Letters*, 74:2619, 1995.

[58] John F. Clauser and Abner Shimony. Bell's theorem: Experimental tests and implications. *Reports on Progress in Physics*, 41:1881, 1978.

[59] W. J. Munro, D. F. V. James, A. G. White, and P. G. Kwiat. Maximizing the entanglement of two mixed qubits. *Physical Review A*, 64:030302, 2001.

[60] S. Bose and V. Vedral. Mixedness and teleportation. *Physical Review A*, 61:040101, 2000.

[61] Satoshi Ishizaka and Tohya Hiroshima. Maximally entangled mixed states under nonlocal unitary operations in two qubits. *Physical Review A*, 62:022310, 2000.

[62] D. F. Walls and G. J. Milburn. *Quantum Optics*. Springer-Verlag, Berlin, 2nd edition, 1994.

[63] M. Orszag. *Quantum Optics*. Springer, 2000.

[64] Marlan O. Scully and M. Suhail Zubairy. *Quantum Optics*. Cambridge University Press, 1997.

[65] Roy J. Glauber. Coherent and incoherent states of the radiation field. *Physical Review*, 131:2766, 1963.

[66] C. W. Gardiner and P. Zoller. *Quantum Noise*. Springer, 2nd edition, 2000.

[67] Philippe Grangier, Georges Raymond, and Nicolas Schlosser. Implementations of quantum computing using cavity quantum electrodynamics. *Fortschritte der Physik*, 48:859, 2000.

[68] Z. Ficek and P. D. Drummond. Comment on "phase-sensitive population decay: The two-atom Dicke model in a broadband squeezed vacuum". *Physical Review A*, 42:1826, 1990.

[69] A. K. Ekert, G. M. Palma, S. M. Barnett, and P. L. Knight. Establishment of correlated pure states through decay in a squeezed reservoir. *Physical Review A*, 39:6026, 1989.

[70] G. S. Agarwal and R. R. Puri. Cooperative behavior of atoms irradiated by broadband squeezed light. *Physical Review A*, 41:3782, 1990.

[71] P. van Loock and Samuel L. Braunstein. Multipartite entanglement for continuous variables: A quantum teleportation network. *Physical Review Letters*, 84:3482, 2000.

[72] J. I. Cirac, P. Zoller, H. J. Kimble, and H. Mabuchi. Quantum state transfer and entanglement distribution among distant nodes in a quantum network. *Physical Review Letters*, 78:3221, 1997.

[73] Q. A. Turchette, N. Ph. Georgiades, C. J. Hood, H. J. Kimble, and A. S. Parkins. Squeezed excitation in cavity QED: Experiment and theory. *Physical Review A*, 58:4056, 1998.

[74] A. S. Parkins and H. J. Kimble. Quantum state transfer between motion and light. *Journal of Optics B*, 1:496, 1999.

[75] C. W. Gardiner and M. J. Collett. Input and output in damped quantum systems: Quantum stochastic differential equations and the master equation. *Physical Review A*, 31:3761, 1985.

[76] Arup Banerjee. Generation of atomic-squeezed states in an optical cavity with an injected squeezed vacuum. *Physical Review A*, 54:5327, 1996.

[77] A. R. R. Carvalho, P. Milman, R. L. de Matos Filho, and L. Davidovich. Decoherence, pointer engineering and quantum state protection. *Physical Review Letters*, 86:4988, 2001.

[78] N. Lütkenhaus, J. I. Cirac, and P. Zoller. Mimicking a squeezed-bath interaction: Quantum-reservoir engineering with atoms. *Physical Review A*, 57:548, 1998.

[79] C. W. Gardiner. Inihibition of atomic phase decays by squeezed light: A direct effect of squeezing. *Physical Review Letters*, 56:1917, 1986.

[80] D. Frese, B. Ueberholz, S. Kuhr, W. Alt, D. Schrader, V. Gomer, and D. Merschede. Single atoms in an optical dipole trap: Towards a deterministic source of cold atoms. *Physical Review Letters*, 85:3777, 2000.

[81] S. M. Barnett and M.-A. Dupertuis. Multiatom squeezed states: a new class of collective atomic states. *Journal of the Optical Society of America B*, 4:505, 1987.

[82] C. W. Gardiner and A. S. Parkins. Driving atoms with light of arbitrary statistics. *Physical Review A*, 50:1792, 1994.

[83] Stephen M. Barnett and Paul M. Radmore. *Methods in Theoretical Quantum Optics*. Oxford Series in Optical and Imaging Sciences. Oxford University Press, 1997.